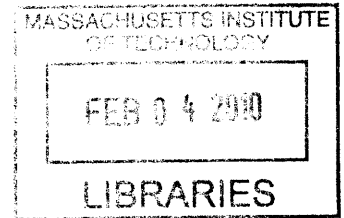


TARGETING THE TIGHT JUNCTION: IMMUNOTHERAPY OF COLON CANCER

by

Margaret E. Ackerman

B.S. and M.S. Biochemistry  
Brandeis University, 2003



Submitted to the Department of Biology in  
Partial Fulfillment of the Requirements for the Degree of

**ARCHIVES**

Doctor of Philosophy in Biology

at the

Massachusetts Institute of Technology

February 2010

© 2009 Margaret E. Ackerman. All rights reserved.

The author hereby grants to MIT permission to reproduce and to distribute publicly paper and electronic copies of this thesis document in whole or in part in any medium now known or hereafter created.

Signature of Author: \_\_\_\_\_

Department of Biology  
September 25, 2009

Certified by: \_\_\_\_\_

K. Dane Wittrup  
Professor of Chemical Engineering & Biological Engineering  
Thesis Supervisor

Accepted by: \_\_\_\_\_

Stephen Bell or Tania Baker  
Biology Graduate Committee Chair

# TARGETING THE TIGHT JUNCTION: IMMUNOTHERAPY OF COLON CANCER

by  
Margaret E. Ackerman

Submitted to the Department of Biology on September 25, 2009 in partial fulfillment of the requirements for the degree of Doctor of Philosophy in Biology

## ABSTRACT:

A33 is a cell surface glycoprotein of colon epithelium with a long clinical history as a target in antibody-based cancer therapy. Despite being present in normal colon, radiolabeled antibodies against A33 are selectively retained by tumors at long time points. Accordingly, we have studied the trafficking and kinetic properties of the antigen to determine its promise in multi-step, pretargeted immunotherapy.

*In vitro*, the localization, mobility, and persistence of the antigen were investigated, and this work has demonstrated that the antigen is both highly immobile and extremely persistent, properties which may contribute to the prolonged retention of the clinically administered antibodies, and their uncommon ability to penetrate solid tumors.

Secondly, because poor tissue penetration is a significant obstacle to the development of successful antibody drugs for immunotherapy of solid tumors, we assess the contribution of antigen density and turnover rate by evaluating the distance to which antibodies penetrate spheroids when these properties are systematically varied. The results agree well with the quantitative modeling predictions, and demonstrate that dosing distal regions of tumors is best achieved by selecting slowly internalized targets that are not expressed above the level necessary for recruiting a toxic dose of therapeutic.

Lastly, we describe the *in vitro* characteristics and report the promising *in vivo* biodistribution of a multi-step tumor targeting therapy utilizing a novel bispecific antibody which recognizes both the A33 antigen and a small molecule radiometal chelate.

Following these studies, several protein engineering techniques are presented. First, a new method of conducting *de novo* protein engineering utilizing highly avid magnetic beads is described, in which extremely weak interactions can be captured from large library populations. Secondly, an *in vitro* assay which utilizes these highly avid magnetic beads is used to score the clinical immunogenicity of therapeutic protein drugs is presented. Finally, the use of sortase A as a means to generate fusion proteins post-translationally is described. Taken together, this additional work demonstrates a productive intersection of basic research and protein engineering methods.

Thesis Advisor: K. Dane Wittrup

Title: C.P. Dubbs Professor of Chemical Engineering & Biological Engineering

## Table of Contents

### Chapter 1: Introduction

1.1 Abstract.....	6
1.2 Immunotherapy.....	6
1.3 Mechanisms of antibody action.....	8
1.4 Limitations to antibody therapy.....	10
1.5 Pre-targeted radioimmunotherapy.....	12
1.6 A33 antigen as a tumor target.....	13
1.7 Thesis overview.....	15
1.8 Works Cited.....	18

### Chapter 2: A33 antigen displays persistent surface expression

2.1 Abstract.....	21
2.2 Background.....	22
2.3 Materials and methods.....	25
2.4 Results.....	29
2.4.1 Homeostatic and kinetic localization of A33 antigen.....	29
2.4.2 Colocalization profile.....	31
2.4.3 Investigation of A33 as a tight junction-associated protein.....	33
2.4.4 Determination of the role of cytoskeleton in A33 localization.....	36
2.4.5 Determination of mobility and persistence of A33.....	39
2.5 Discussion.....	43
2.6 Works cited.....	46

### Chapter 3: Effect of antigen turnover rate and expression level on antibody penetration into tumor spheroids

3.1 Abstract.....	49
3.2 Background.....	50
3.3 Materials and methods.....	52
3.4 Results.....	57
3.4.1 Processing of spheroid images.....	57
3.4.2 Antigen density affects spheroid penetration.....	59
3.4.3 Penetration studies utilizing different cell lines.....	62
3.4.4 Antigen internalization and turnover affects penetration.....	64
3.4.5 Antigen internalization reaches a steady state with diffusion.....	66
3.4.6 Differential turnover and accessibility of CEA and A33.....	68
3.5 Discussion.....	70
3.6 Works cited.....	74

### Chapter 4: Multi-step tumor targeting with a bispecific A33 antibody

4.1 Abstract.....	76
4.2 Background.....	77
4.3 Materials and methods.....	81
4.4 Results.....	86

4.4.1 Bifunctionality tests.....	86
4.4.2 Kd measurements and FcRn binding.....	88
4.4.3 Clearing agent characterization.....	90
4.4.4 <i>In vivo</i> biodistribution of ALDO.....	92
4.4.5 Impact of clearing step.....	93
4.4.6 <i>In vivo</i> biodistribution of DOTA.....	94
4.5 Discussion.....	96
4.6 Works cited.....	98

**Chapter 5: Highly avid magnetic bead capture: an efficient selection method for *de novo* protein engineering utilizing yeast surface display**

5.1 Abstract.....	101
5.2 Background.....	102
5.3 Materials and methods.....	107
5.4 Results.....	112
5.4.1 Profile of multivalent selection methods.....	112
5.4.2 FACS profile of multivalent selection methods.....	116
5.4.3 Efficiency of magnetic bead sorting.....	118
5.4.4 Yield of magnetic bead sorting.....	122
5.4.5 Dependencies of magnetic bead sorting.....	124
5.4.6 Demonstration of method utility in <i>de novo</i> isolation.....	126
5.4.7 Recommended quality control steps for <i>de novo</i> selections.....	130
5.5 Discussion.....	133
5.6 Works cited.....	137

**Chapter 6: An *in vitro* assay to predict clinical B-cell immunogenicity of therapeutic proteins**

6.1 Abstract.....	139
6.2 Background.....	140
6.3 Materials and methods.....	145
6.4 Results.....	150
6.4.1 Assay process.....	150
6.4.2 Assay quality control.....	152
6.4.3 Panels of human and orthologous proteins.....	155
6.4.4 Fine discrimination between protein variants.....	157
6.4.5 Diversity and specificity of selected clones.....	160
6.4.6 Cross-reactivity of selected clones and populations.....	162
6.5 Discussion.....	164
6.6 Works cited.....	167

**Chapter 7: *In vitro* protein-protein fusion catalyzed by sortase A**

7.1 Abstract.....	169
7.2 Background.....	170
7.3 Materials and methods.....	172

7.4 Results.....	177
7.4.1 and 7.4.2 Sortassembly reaction and optimization.....	177
7.4.3 Optimization of sortase concentration.....	180
7.4.4 Separation of product and reactants.....	181
7.4.5 and 7.4.6 Assembled domains, reactions, and functional testing.....	182
7.5 Discussion.....	185
7.6 Works cited.....	186
CV.....	187

## **Chapter 1: Background and Introduction**

### **1.1 Abstract**

Immunotherapy is a promising mode of cancer treatment which utilizes antibodies to achieve the twin goals of systemic exposure and specific action. Here, we present a case study of immunotherapy, in which we have selected a tumor antigen, examined its clinical history and *in vitro* properties, used this information to determine an appropriate targeting strategy, and investigated this altered protocol in a mouse model. This rational approach to improving cancer therapy has led to significant gains in *in vivo* studies.

### **1.2 Immunotherapy**

Traditional cancer therapies are limited to highly specific treatments such as surgery and external beam radiation, which have excellent ability to ablate primary tumors; and systemic therapies such as chemotherapeutic drugs, which allow treatment of metastatic and residual disease. However, chemotherapy has limited specificity, causing significant toxicity to normal tissue, and surgery does not provide systemic exposure, leaving a high probability of recurrence; whereas, the ideal treatment would offer systemic exposure but possess highly specific action to eliminate the pathologic state of cancer. When framing the design criteria for novel therapies in this way, it becomes apparent that improved cancer therapies would mimic the function of the immune system, which functions to differentiate self from sinister with a remarkable capacity to detect and destroy pathogenic states.

However, when compared to the role of the immune system in combating infectious disease, the problem with cancer is one of detection limits—how is

differentiation of self from sinister possible when the sinister cells are of self origin, and consequently bear much antigenic similarity to normal tissue. Interestingly, there is evidence that our immune systems do have an existing capacity to provide tumor surveillance in that individuals with autoimmune diseases have a lower incidence of cancer, but when such individuals get cancer, their autoimmune disease tends to subside—that is, individuals with more sensitive or reactive immune systems do a better job at detecting cancer and destroying these misregulated self cells.

Though the bar for detection is set higher, it is perhaps similar to the immune system's ability to detect the altered behavior of cells infected by a pathogen. Changes in cellular behavior and expression patterns, even subtle changes in normal phenotypes can function as molecular markers of disease. In this way, at this molecular level, each transformative mutation allowing the altered growth profile of the cancer cell is a distinct difference between tumor and normal tissue, and can function as a molecular marker of cancer.

The premise behind immunotherapy is that these molecular markers of cancer can be exploited as therapeutic targets. In fact, there are two general ways to use the immune system to treat cancer. The first is antigen, or target driven, and includes cancer vaccine strategies, which consist of training the immune system to recognize and eliminate tumors. While promising, there are no approved therapies utilizing this cancer vaccine strategy. The second type of immunotherapy is antibody driven, and relies on the superior molecular recognition properties of antibodies to detect and treat cancer. Antibodies have a long history as drugs dating back to the use of antiserums against snake venoms, and antibody driven immunotherapy of cancer has been particularly

fruitful. There are currently 9 FDA approved antibodies for cancer therapy—and many other antibodies approved for the treatment of other diseases.

The differential success between antigen and antibody driven immunotherapy may be partially explained by advances in antibody technology. These advances include: hybridoma technology, which allows a single antibody specificity to be isolated and produced—in stark contrast to the horse serum antibody products used previously; new production systems that allow large yields of protein; and lastly, due to protein evolution technologies such as yeast display, which allow the binding interaction between the cancer target and the antibody to be engineered *in vitro*. The ability to evolve protein drugs is particularly important because it means that therapy is not limited to use of antibodies naturally generated by the immune system, but the binding properties of these antibodies can be improved one-million-fold quite easily. Combined, these technologies have made possible what Paul Ehrlich hoped some 100 years ago, that antibodies may be used as “magic bullets” to specifically treat cancer. They may be administered intravenously to achieve systemic circulation, but have specific action on tumors where they bind their target antigen, decorate the surface of these cells, and interact with immune system to trigger a cytotoxic response.

### **1.3 Mechanisms of antibody action**

Interestingly, the ability to manipulate antibody properties *in vitro* has not only allowed their binding, or detection functions to be improved, but also their destructive properties. Naturally, antibodies act by two mechanisms. First, their conserved Fc domains interact with complement proteins in the blood in what has been termed the



complement cascade. Activation of complement factors results in formation of pores in the cell membrane, resulting in cellular rupture. Second, the Fc interacts with receptors on immune effector cells such as natural killer cells, which can likewise trigger destruction of the antibody-coated cell. Much effort has gone into engineering Fc variants that have improved abilities to initiate the complement cascade or activate effector cells via improved interactions with activating Fcγ receptors<sup>1-4</sup>.

However, antibodies can also utilize modes of action that are independent of interactions with complement or effector cells. Such independence can be achieved by utilizing an antibody which targets a cell surface marker and disrupts cellular signaling, such as antibodies against some growth receptors do<sup>5-9</sup>. However, because this mechanism requires the tumor marker to be necessary for growth, a simpler strategy is to design the antibody to carry a toxin. Numerous approaches to incorporating a toxic component to an antibody have been explored, including fusion to radionuclides, nanoparticles that can be heat activated, toxic enzymes, enzymes which convert pro-drugs into active drug, and even DNA encoding cell-killing proteins<sup>10-15</sup>.

The appeal of these approaches is that they do not require activation of the patient's own immune system in order to kill tumor cells because both targeting and toxic functions are fully incorporated into a single molecule. While each of the different toxins claims certain advantages over the others, enzyme fusions alter the pharmacokinetic behavior of the antibody by increasing its size, the use of a foreign, generally bacterial enzyme can lead to an immune response against the therapeutic, and some toxins require not only internalization but also escape from the endosome to cause toxicity. Similarly, fusion to nanoparticles, or liposomes encapsulating DNA increases size dramatically, and

the specificity derived from the antibody may be dominated by passive size effects. Radioactive antibodies, however, have a number of appealing attributes.

First, radiation is a well-established mode of cell killing. Secondly, radioactive conjugation is a small perturbation to antibody size and structure, allowing the pharmacokinetic behavior of the antibody to remain unaltered. Third, numerous radioactive isotopes are available, ranging from alpha emitters which can achieve cell killing with a single particle decay, to long range beta emitters which possess the ability to kill cells at a distance by depositing their decay energy as much as a centimeter away, allowing tumors to be fully irradiated without requiring that each cell be coated with antibody. Given certain characteristics of the tumor microenvironment that disfavor the penetration of antibody throughout solid tumors as will be discussed later, this cross-fire, or bystander effect can be a significant advantage. Lastly, the specific localization of the radioactive particle, whether intracellular or surface localized has less of an impact on therapy. Accordingly, this work will focus on the use of radiation as the mode of cell killing.

#### **1.4 Limitations to antibody therapies**

However, there are some drawbacks to antibody-based therapies. The first is the strict requirement for a cancer-specific tumor antigen—a cell surface protein that is the target of the antibody drug. Additionally, beyond simple tumor specificity, the cellular target antigen must have the right profile in terms of other properties for the mode of toxicity being used. For example, the cancer antigen must be expressed at a sufficient level to recruit a toxic dose of therapeutic. For toxins that act intracellularly, it must be

internalized at a sufficient rate, whereas for some more complicated treatment regimens such as multi-step therapies, it must remain surface accessible. Here, however, the number of different toxins or radionuclides that can be used is an advantage, and allows thoughtfully pairing of the mode of toxicity or decay properties given the properties of the target antigen. This flexibility provides room for significant improvement in efficacy given proper study of tumor susceptibility and target antigen properties. In fact, the first line therapy for non-Hodgkin's lymphoma (NHL) is a radiolabeled antibody, which performs significantly better than its non-radioactive variant—suggesting that *in vitro* improvements to the natural binding (detection) and toxic (destruction) properties of antibodies can allow substantial improvements in the clinic.

Unfortunately, there are a number of barriers to access in terms of localizing antibody drugs to tumors. Of the antibody drugs currently approved for cancer, almost all treat blood cancers while very few treat solid tumors, and those that are approved for solid tumors have had disappointingly limited efficacy. Perhaps the most influential barriers in localization are the transport phenomenon related to antibody access to solid tumors. First, the antibody must extravasate from the blood through the vasculature. The rate of vascular escape is highly unfavorable and can lead to a thousand fold decrease in antibody concentration in solid tissue relative to the blood. For a directly radiolabeled antibody this leads to a huge dose of radiation to the blood and bone marrow. Beyond this barrier, the interstitial pressure in solid tumors is high, and the extracellular matrix is dense, disfavoring flow through the tumor, and leaving diffusion down a concentration gradient as the predominant mode of transport.

The effect of these barriers is strikingly apparent when the typical antibody distribution within a solid tumor is observed. Generally, the antibody only penetrates the tumor for a few cell layers—leaving whole regions of the tumor completely untargeted and unexposed to antibody drug. Quantitative models of the relevant transport and kinetic processes, which capture these effects have been developed and are highly useful in terms of identifying the best ways to improve therapy<sup>16-21</sup>. The success of radioactive antibodies in treating NHL suggests that if we can identify and rationally engineer our way around some of these limits we could generate successful therapies for solid tumors as well. Short of these strategies, which include increasing vascular permeability, and altering the affinity and valency of the antibodies used, selecting the right tumor target and using an appropriate targeting strategy can circumvent some of these tumor physiology-based limits.

### **1.5 Pre-targeted radioimmunotherapy**

The recent success of several radioimmunotherapeutics has demonstrated proof of principle for this type of targeted cancer therapy<sup>22</sup>. Unfortunately, in many potential applications, bone marrow toxicity limits therapy. In order to circumvent this toxicity, a two-step strategy, known as pretargeted immunotherapy (PRIT) has been proposed, in which the targeting construct and radionuclide are separated into two distinct dosing steps. In this way, one preserves the specificity of antibody binding in tumor targeting, but eliminates the toxic effects of long-lived, directly labeled antibodies. When compared to single step therapies using directly labeled antibodies, PRIT has generally lead to lower toxicity and better efficacy<sup>23-25</sup>. However, the addition of a separate step constrains

the desirable kinetic attributes of the cellular target in comparison with direct RIT, immunotoxin therapy, or approaches relying on effector functions. In PRIT, the competing interests of target saturation, clearance of unbound construct from circulation, availability of the construct to chelated radionuclide, sufficient proximity to the nucleus relative to decay pathlength, and the half-life of the radionuclide must all be taken into consideration. This study seeks to determine if the A33 antigen, a member of the immunoglobulin superfamily (IGSF) with homology to cell adhesion<sup>26</sup> and tight junction-associated (TJ) proteins, possesses the properties particularly suited for PRIT.

#### **1.6 A33 antigen as a tumor target**

The A33 antigen is an abundant cell surface protein expressed in 95% of colon tumors, but not in other organs<sup>27</sup>. This restricted expression pattern led to interest in use of the A33 antigen in radioimmunotherapy, and directly <sup>125/131</sup>I radiolabeled A33 antibodies were administered to patients with colon cancer in a series of phase I and II clinical trials<sup>28-33</sup>. The results of these trials were mixed from a therapeutic perspective, as some patients developed an anti-antibody response<sup>34</sup>, and there was dose-limiting bone marrow toxicity. Alternatively, they were also quite promising in that they exhibited a startlingly localized persistence of radiolabel. A33 was constitutively expressed in the entire colon, and evenly throughout the entire crypt<sup>35</sup>. Provocatively, however, it was found that after an initial period of time in which the therapeutic conjugate bound the entire colon, after a period of a week, staining was present only in tumors<sup>28</sup> and whole body scans revealed labeling even 6 weeks after antibody administration<sup>30</sup>.

Significant work has gone into investigation of the tissue specific expression of A33<sup>35-37</sup>, whose promoter has now been used to drive colon-specific expression of transgenes<sup>38</sup>; the glycosylation pattern of the antigen<sup>39,40</sup>, and its regulation by PPARgamma<sup>41</sup>. Despite homology to proteins of the tight junction, the cellular role of A33 is unclear. Nonetheless, in addition to the human clinical studies cited already, investigation into a number of novel formats including layer-by-layer polymer particles and capsules, polyethylene glycol fusions, carboxypeptidase and cytosine deaminase enzyme fusions, trivalent antibody fragments, and scFv<sup>42-47</sup> have been utilized *in vitro* and in mouse models. Similarly, the use of numerous radiologic agents have been investigated<sup>45,48-51</sup>, including lutetium, astatine, yttrium, bromine, and various iodine isotopes.

## 1.7 Thesis overview

A33 is a cell surface glycoprotein of colon epithelium with homology to tight junction-associated proteins of the immunoglobulin superfamily, including CAR and JAM. Its restricted tissue localization and high level of expression have led to its use as a target in colon cancer immunotherapy. Although the antigen is also present in normal colon, radiolabeled antibodies against A33 are selectively retained by tumors in the gut as well as in metastatic lesions for as long as 6 weeks<sup>30</sup>. Accordingly, we have studied the trafficking and kinetic properties of the antigen to determine its promise in two-step, pretargeted therapies, and have considered this target at 3 different levels: at cells cultured *in vitro*—allowing study of the basic biology of A33; at spheroids, an *in vitro* tumor models—allowing higher order study of antibody diffusion and binding; and *in vivo* in a mouse tumor model where we can fully explore this 2 step strategy.

*In vitro*, the localization, mobility, and persistence of the antigen were investigated, and this work has demonstrated that the antigen is both highly immobile and extremely persistent—retaining its surface localization for a turnover half-life of greater than 2 days. In order to explain these unusual properties, we explored the possibility that A33 is a component of the tight junction. The simple property of surface persistence, described here, may contribute to the prolonged retention of the clinically administered antibodies, and their uncommon ability to penetrate solid tumors<sup>52</sup>.

Poor tissue penetration is a significant obstacle to the development of successful antibody drugs for immunotherapy of solid tumors, and diverse alterations to the properties of antibody drugs have been made to improve penetration and homogeneity of exposure. However, in addition to properties of the antibody drug, mathematical models

of antibody transport<sup>17,53</sup> predict that the antigen expression level and turnover rate significantly influence penetration. As intrinsic antigen properties are likely to be difficult to modify, they may set inherent limits to penetration. Accordingly, in our spheroid studies we assess their contribution by evaluating the distance to which antibodies penetrate spheroids when these antigen properties are systematically varied. Additionally, the penetration profiles of antibodies against CEA and A33, two targets of clinical interest, are compared. The results agree well with the quantitative predictions of the model, and demonstrate that dosing distal regions of tumors is best achieved by selecting slowly internalized targets that are not expressed above the level necessary for recruiting a toxic dose of therapeutic. Each antibody-bound antigen molecule that is turned over or present in excess incurs a real cost in terms of penetration depth—a limiting factor in the development of effective therapies for treating solid tumors<sup>54</sup>.

Lastly, we describe the *in vitro* characterization and *in vivo* biodistribution of a multi-step tumor targeting therapy utilizing a novel bispecific antibody which recognizes both the A33 antigen and a small molecule radiometal chelate. This bispecific antibody consists of a typical IgG molecule with an additional scFv domain fused to the C terminus of the IgG light chain, generating a tetravalent molecule capable of recognizing 2 copies of the A33 tumor antigen, and 2 small molecule radiometal chelates. Following *in vitro* testing, the A33 bispecific was administered to mice bearing SW1222 xenograft tumors and its biodistribution was determined. Subsequent preliminary experiments have characterized the effect of a clearing step utilized to block and eliminate the remaining blood pool fraction of bispecific prior to administration of a radioactive DOTA chelate



and determinations of its biodistribution and tumor uptake. These studies strongly support further investigation of the A33 antigen as a target in multi-step immunotherapy.

Following these studies of the A33 antigen in terms of its basic cell biology, its characteristics in a spheroid tumor model, and its use in a multistep strategy in a mouse xenograft model, several protein engineering techniques are presented. First, a new method of conducting *de novo* protein engineering utilizing highly avid magnetic beads is described, in which even very weak interactions can be captured from large library populations<sup>55</sup>. Secondly, an *in vitro* assay which utilizes these highly avid magnetic beads is used to predict the clinical immunogenicity of therapeutic protein drugs is presented. And finally, the use of sortase A as a means to generate fusion proteins post-translationally is described. Taken together, this additional work demonstrates a productive intersection of basic research and protein engineering methods.

## 1.8 Works Cited

1. Kubota, T. et al. Engineered therapeutic antibodies with improved effector functions. *Cancer Sci* **100**, 1566-72 (2009).
2. Oganessian, V., Gao, C., Shirinian, L., Wu, H. & Dall'Acqua, W.F. Structural characterization of a human Fc fragment engineered for lack of effector functions. *Acta Crystallogr D Biol Crystallogr* **64**, 700-4 (2008).
3. Natsume, A. et al. Engineered antibodies of IgG1/IgG3 mixed isotype with enhanced cytotoxic activities. *Cancer Res* **68**, 3863-72 (2008).
4. Lazar, G.A. et al. Engineered antibody Fc variants with enhanced effector function. *Proc Natl Acad Sci U S A* **103**, 4005-10 (2006).
5. Patel, D. et al. Anti-epidermal growth factor receptor monoclonal antibody cetuximab inhibits EGFR/HER-2 heterodimerization and activation. *Int J Oncol* **34**, 25-32 (2009).
6. Ciardiello, F. & Tortora, G. Anti-epidermal growth factor receptor drugs in cancer therapy. *Expert Opin Investig Drugs* **11**, 755-68 (2002).
7. Lincoln, D.T., Singal, P.K. & Al-Banaw, A. Growth hormone in vascular pathology: neovascularization and expression of receptors is associated with cellular proliferation. *Anticancer Res* **27**, 4201-18 (2007).
8. Riedemann, J. & Macaulay, V.M. IGF1R signalling and its inhibition. *Endocr Relat Cancer* **13 Suppl 1**, S33-43 (2006).
9. Bianco, A.R. Targeting c-erbB2 and other receptors of the c-erbB family: rationale and clinical applications. *J Chemother* **16 Suppl 4**, 52-4 (2004).
10. Witlox, M.A. et al. Epidermal growth factor receptor targeting enhances adenoviral vector based suicide gene therapy of osteosarcoma. *J Gene Med* **4**, 510-6 (2002).
11. Bagshawe, K.D. Targeting: the ADEPT story so far. *Curr Drug Targets* **10**, 152-7 (2009).
12. Bagshawe, K.D. Antibody-directed enzyme prodrug therapy (ADEPT) for cancer. *Expert Rev Anticancer Ther* **6**, 1421-31 (2006).
13. Pastan, I., Hassan, R., FitzGerald, D.J. & Kreitman, R.J. Immunotoxin treatment of cancer. *Annu Rev Med* **58**, 221-37 (2007).
14. Wang, A.Z. et al. Biofunctionalized targeted nanoparticles for therapeutic applications. *Expert Opin Biol Ther* **8**, 1063-70 (2008).
15. McCarthy, J.R. & Weissleder, R. Multifunctional magnetic nanoparticles for targeted imaging and therapy. *Adv Drug Deliv Rev* **60**, 1241-51 (2008).
16. Thurber, G.M., Schmidt, M.M. & Wittrup, K.D. Antibody tumor penetration: transport opposed by systemic and antigen-mediated clearance. *Adv Drug Deliv Rev* **60**, 1421-34 (2008).
17. Thurber, G.M., Zajic, S.C. & Wittrup, K.D. Theoretic criteria for antibody penetration into solid tumors and micrometastases. *J Nucl Med* **48**, 995-9 (2007).
18. Baxter, L.T., Zhu, H., Mackensen, D.G., Butler, W.F. & Jain, R.K. Biodistribution of monoclonal antibodies: scale-up from mouse to human using a physiologically based pharmacokinetic model. *Cancer Res* **55**, 4611-22 (1995).
19. Baxter, L.T., Zhu, H., Mackensen, D.G. & Jain, R.K. Physiologically based pharmacokinetic model for specific and nonspecific monoclonal antibodies and fragments in normal tissues and human tumor xenografts in nude mice. *Cancer Res* **54**, 1517-28 (1994).
20. Baxter, L.T. & Jain, R.K. Vascular permeability and interstitial diffusion in superfused tissues: a two-dimensional model. *Microvasc Res* **36**, 108-15 (1988).

21. Nugent, L.J. & Jain, R.K. Two-compartment model for plasma pharmacokinetics in individual blood vessels. *J Pharmacokinet Biopharm* **12**, 451-61 (1984).
22. DeNardo, G.L. Treatment of non-Hodgkin's lymphoma (NHL) with radiolabeled antibodies (mAbs). *Semin Nucl Med* **35**, 202-11 (2005).
23. Pagel, J.M. et al. Comparison of anti-CD20 and anti-CD45 antibodies for conventional and pretargeted radioimmunotherapy of B-cell lymphomas. *Blood* **101**, 2340-8 (2003).
24. Gruaz-Guyon, A., Raguin, O. & Barbet, J. Recent advances in pretargeted radioimmunotherapy. *Curr Med Chem* **12**, 319-38 (2005).
25. Boerman, O.C., van Schaijk, F.G., Oyen, W.J. & Corstens, F.H. Pretargeted radioimmunotherapy of cancer: progress step by step. *J Nucl Med* **44**, 400-11 (2003).
26. Johnstone, C.N. et al. Characterization of mouse A33 antigen, a definitive marker for basolateral surfaces of intestinal epithelial cells. *Am J Physiol Gastrointest Liver Physiol* **279**, G500-10 (2000).
27. Garin-Chesa, P., Junichi Sakamoto, Sydney Welk, Francisco X. Real, Wolfgang J. Rettig, Lloyd J. Old. Organ-specific expression of the colon cancer antigen A33, a cell surface target for antibody-based therapy. *International Journal of Oncology* **9**, 465-471 (1996).
28. Welt, S. et al. Quantitative analysis of antibody localization in human metastatic colon cancer: a phase I study of monoclonal antibody A33. *J Clin Oncol* **8**, 1894-906 (1990).
29. Welt, S. et al. Phase I/II study of iodine 131-labeled monoclonal antibody A33 in patients with advanced colon cancer. *J Clin Oncol* **12**, 1561-71 (1994).
30. Welt, S. et al. Phase I/II study of iodine 125-labeled monoclonal antibody A33 in patients with advanced colon cancer. *J Clin Oncol* **14**, 1787-97 (1996).
31. Welt, S. et al. Phase I study of anticolon cancer humanized antibody A33. *Clin Cancer Res* **9**, 1338-46 (2003).
32. Scott, A.M. et al. A phase I trial of humanized monoclonal antibody A33 in patients with colorectal carcinoma: biodistribution, pharmacokinetics, and quantitative tumor uptake. *Clin Cancer Res* **11**, 4810-7 (2005).
33. Chong, G. et al. Phase I trial of 131I-huA33 in patients with advanced colorectal carcinoma. *Clin Cancer Res* **11**, 4818-26 (2005).
34. Ritter, G. et al. Serological analysis of human anti-human antibody responses in colon cancer patients treated with repeated doses of humanized monoclonal antibody A33. *Cancer Res* **61**, 6851-9 (2001).
35. Johnstone, C.N. et al. Analysis of the regulation of the A33 antigen gene reveals intestine-specific mechanisms of gene expression. *J Biol Chem* **277**, 34531-9 (2002).
36. Heath, J.K. et al. The human A33 antigen is a transmembrane glycoprotein and a novel member of the immunoglobulin superfamily. *Proc Natl Acad Sci U S A* **94**, 469-74 (1997).
37. Mao, Z. et al. Transcriptional regulation of A33 antigen expression by gut-enriched Kruppel-like factor. *Oncogene* **22**, 4434-43 (2003).
38. Cafferata, E.G. et al. A novel A33 promoter-based conditionally replicative adenovirus suppresses tumor growth and eradicates hepatic metastases in human colon cancer models. *Clin Cancer Res* **15**, 3037-49 (2009).
39. Joosten, C.E., Cohen, L.S., Ritter, G., Batt, C.A. & Shuler, M.L. Glycosylation profiles of the human colorectal cancer A33 antigen naturally expressed in the human colorectal cancer cell line SW1222 and expressed as recombinant protein in different insect cell lines. *Biotechnol Prog* **20**, 1273-9 (2004).
40. Ritter, G. et al. Characterization of posttranslational modifications of human A33 antigen, a novel palmitoylated surface glycoprotein of human gastrointestinal epithelium. *Biochem Biophys Res Commun* **236**, 682-6 (1997).

41. Rageul, J. et al. KLF4-dependent, PPAR $\gamma$ -induced expression of GPA33 in colon cancer cell lines. *Int J Cancer* (2009).
42. Deckert, P.M. et al. Pharmacokinetics and microdistribution of polyethylene glycol-modified humanized A33 antibody targeting colon cancer xenografts. *Int J Cancer* **87**, 382-90 (2000).
43. Deckert, P.M. et al. A33scFv-cytosine deaminase: a recombinant protein construct for antibody-directed enzyme-prodrug therapy. *Br J Cancer* **88**, 937-9 (2003).
44. Petrusch, U. et al. A33scFv-green fluorescent protein, a recombinant single-chain fusion protein for tumor targeting. *Protein Eng Des Sel* **20**, 583-90 (2007).
45. Antoniow, P. et al. Radioimmunotherapy of colorectal carcinoma xenografts in nude mice with yttrium-90 A33 IgG and Tri-Fab (TFM). *Br J Cancer* **74**, 513-24 (1996).
46. Deckert, P.M. et al. Specific tumour localisation of a huA33 antibody--carboxypeptidase A conjugate and activation of methotrexate-phenylalanine. *Int J Oncol* **24**, 1289-95 (2004).
47. Cortez, C. et al. Influence of size, surface, cell line, and kinetic properties on the specific binding of A33 antigen-targeted multilayered particles and capsules to colorectal cancer cells. *ACS Nano* **1**, 93-102 (2007).
48. Almqvist, Y. et al. Biodistribution of <sup>211</sup>At-labeled humanized monoclonal antibody A33. *Cancer Biother Radiopharm* **22**, 480-7 (2007).
49. Almqvist, Y., Steffen, A.C., Tolmachev, V., Divgi, C.R. & Sundin, A. In vitro and in vivo characterization of <sup>177</sup>Lu-huA33: a radioimmunoconjugate against colorectal cancer. *Nucl Med Biol* **33**, 991-8 (2006).
50. Barendswaard, E.C. et al. Relative therapeutic efficacy of (125)I- and (131)I-labeled monoclonal antibody A33 in a human colon cancer xenograft. *J Nucl Med* **42**, 1251-6 (2001).
51. Orlova, A. et al. Comparative biodistribution of the radiohalogenated (Br, I and At) antibody A33. Implications for in vivo dosimetry. *Cancer Biother Radiopharm* **17**, 385-96 (2002).
52. Ackerman, M.E. et al. A33 antigen displays persistent surface expression. *Cancer Immunol Immunother* **57**, 1017-27 (2008).
53. Graff, C.P. & Wittrup, K.D. Theoretical analysis of antibody targeting of tumor spheroids: importance of dosage for penetration, and affinity for retention. *Cancer Res* **63**, 1288-96 (2003).
54. Ackerman, M.E., Pawlowski, D. & Wittrup, K.D. Effect of antigen turnover rate and expression level on antibody penetration into tumor spheroids. *Mol Cancer Ther* **7**, 2233-40 (2008).
55. Ackerman, M. et al. Highly avid magnetic bead capture: an efficient selection method for de novo protein engineering utilizing yeast surface display. *Biotechnol Prog* **25**, 774-83 (2009).

## **Chapter 2: A33 antigen displays persistent surface expression**

### **2.1 Abstract**

A33 is a cell surface glycoprotein of colon epithelium with homology to tight junction-associated proteins of the immunoglobulin superfamily, including CAR and JAM. Its restricted tissue localization and high level of expression have led to its use as a target in colon cancer immunotherapy. Although the antigen is also present in normal colon, radiolabeled antibodies against A33 are selectively retained by tumors in the gut as well as in metastatic lesions for as long as 6 weeks<sup>1</sup>. Accordingly, we have studied the trafficking and kinetic properties of the antigen to determine its promise in two-step, pretargeted therapies. The localization, mobility, and persistence of the antigen were investigated, and this work has demonstrated that the antigen is both highly immobile and extremely persistent—retaining its surface localization for a turnover half-life of greater than 2 days. In order to explain these unusual properties, we explored the possibility that A33 is a component of the tight junction. The simple property of surface persistence, described here, may contribute to the prolonged retention of the clinically administered antibodies, and their uncommon ability to penetrate solid tumors.

---

Major portions of this chapter were previously published in:  
Ackerman ME, Chalouni C, Schmidt MM, Raman VV, Ritter G, Old LJ, Mellman I, Wittrup KD. “A33 antigen displays persistent surface expression” *Cancer Immunol Immunother.* 2008 Jul;57(7):1017-27.

## 2.2 Background

The recent success of several radioimmunotherapeutics has demonstrated proof of principle for this type of targeted cancer therapy<sup>2</sup>. Unfortunately, in many potential applications, bone marrow toxicity limits therapy. In order to circumvent this toxicity, a two-step strategy, known as pretargeted immunotherapy (PRIT) has been proposed, in which the targeting construct and radionuclide are separated into two distinct dosing steps. In this way, one preserves the specificity of antibody binding in tumor targeting, but eliminates the toxic effects of long-lived directly labeled antibodies. When compared to single step therapies using directly labeled antibodies, PRIT has generally lead to lower toxicity and better efficacy<sup>3-5</sup>. However, the addition of a separate step constrains the desirable kinetic attributes of the cellular target in comparison with direct RIT, immunotoxin therapy, or approaches relying on effector functions. In PRIT, the competing interests of target saturation, clearance of unbound construct from the circulation, availability of the construct to chelated radionuclide, sufficient proximity to the nucleus relative to decay pathlength, and the half-life of the radionuclide must all be taken into consideration. This study seeks to determine if the A33 antigen, a member of the immunoglobulin superfamily (IGSF) with homology to cell adhesion<sup>6</sup> and tight junction-associated (TJ) proteins, possesses the properties particularly suited for PRIT.

The A33 antigen is an abundant cell surface protein expressed in 95% of colon tumors, but not in other organs<sup>7</sup>. This restricted expression pattern led to interest in use of the A33 antigen in RIT, and directly <sup>125/131</sup>I radiolabeled A33 antibodies were administered to patients with colon cancer in a series of phase I and II clinical trials<sup>1,8-12</sup>. The results of these trials were mixed from a therapeutic perspective, as some patients

developed an anti-antibody response<sup>13</sup>, and there was dose-limiting bone marrow toxicity. Alternately, they were also quite promising in that they exhibited a startlingly localized persistence of radiolabel. A33 was constitutively expressed in the entire colon, and evenly throughout the entire crypt<sup>14</sup>. Provocatively, however, it was found that after an initial period of time in which the therapeutic conjugate bound the entire colon, after a period of a week, staining was present only in tumors<sup>8</sup> and whole body scans revealed labeling even 6 weeks after antibody administration<sup>1</sup>.

Distinguishing self from target cells poses a particular problem in cancer, in which the tumor cells are of self-origin and consequently share much antigenic similarity with the tissue of their origin. RIT rests on the premise that there are surface antigens with differential expression in tumors. Despite failing to fulfill this basic premise, and consequent dosing of the entire colon with radioactivity in A33 antigen RIT studies, dose-limiting toxicities were not gastrointestinal. However, the lack of gastrointestinal toxicity could be attributed to the relatively small dose of radiation to both tumor and normal colon in comparison to the dose absorbed by the blood, which was the limiting toxicity. Under conditions in which there was a therapeutic effect on tumor cells, it is likely that the expression on normal cells would present a toxicity problem. Accordingly, the presumptive ceiling imposed by normal tissue expression, and the tumor-specific staining observed after a week, provoke considerable interest in the study of A33 as a two-step immunotherapy target.

Several possible explanations have been advanced as to how tumor specificity occurs for A33 antibodies, including differential accessibility or endocytosis between normal and cancerous tissue. However, the simplest notion is that specificity results from

normal shedding of the colonic epithelium. As this process of migration and sloughing occurs over the course of several days, this theory is consistent with the clinical data.

Regardless of the mechanism by which tumor-specificity is gained, in order to be a useful target in PRIT, the antibody specifically localized to tumors after one week must be retained on the tumor cell surface—available to bind a radionuclide construct. Therefore, we undertook a study to determine the trafficking and persistence of the A33 antigen in cultured colon tumor cell lines, as well as some preliminary work to understand the etiology of this unique *in vivo* persistence.



## **2.3 Materials and Methods**

### **Cell Culture**

The A33-expressing cell lines LS174T, LIM1215, COLO205, and SW1222 cells were grown in advanced MEM supplemented with L-glutamine and 10% FBS (Gibco). Where appropriate, cells were fixed and permeabilized with BD cytofix and cytoperm (BD Biosciences) according to the manufacturer's instructions. Latrunculin B (Sigma) and nocodazole (Sigma) were dissolved in DMSO and added to culture for final concentrations of 100 nM and 50  $\mu$ M, respectively. EGTA was directly dissolved in culture media for a final concentration of 25 mM.

### **Fluorescent Labeling of Cells**

The mouse anti-A33 antibody m100.310 was conjugated to Alexa\*488 or fluorescein according to the manufacturer's instructions (Molecular Probes A-20181, F-6433), and goat anti-mouse PE was used as a secondary (Sigma). Anti-CEA shMFE was likewise conjugated to Alexa\*594 (Molecular Probes A30008). For colocalization experiments, LIM1215 cells were permeabilized-fixed with methanol, -20°C, for 5 min and then stained with either rabbit anti-human occludin (Zymed), or mouse anti-human ZO-1 (Zymed). They were detected by Cy3-conjugated donkey anti-rabbit and anti-mouse antibodies, respectively (Jackson immunoresearch Laboratories). Actin was labeled with Alexa\*546-conjugated phalloidin (Molecular Probes).

Vybrant DiI (Molecular Probes) was used to label bulk membrane for photobleaching experiments. For DiI labeling, the media above the monolayer was replaced with 300

mM sucrose in PBS, and then 2  $\mu$ l of the DiI label was slowly added to the sucrose solution above the monolayer.

### **Fluorescence Microscopy**

Cells were grown on coverslip-bottomed dishes (Mattek), labeled as previously described, and imaged on a Deltavision deconvolution microscope with 1.4 NA oil lens at 100x magnification and deconvolved and analyzed using the SoftWorx application.

Colocalization study images were acquired using a confocal LSM510 Zeiss microscope equipped with an oil immersion plan apochromatic 100x lens, NA 1.4.

### **Flow cytometric Internalization Assay<sup>15</sup>**

A suspension of  $4 \times 10^6$  cells/ml was labeled with m100.310 Alexa\*488 in media on ice for 1 hr at 100 ng/ml. CO<sub>2</sub>-independent media (Gibco) was then exchanged and cultures were diluted to  $4 \times 10^5$  cells/ml and set in a 37°C shaker for the course of the experiment. At each timepoint, 1 ml aliquots were taken, washed once with 0.5 ml PBS 0.1% BSA, and labeled with 100  $\mu$ l of 2:100 dilution of anti-mouse PE (Sigma) on ice for 15 min, before analysis on a Beckman Coulter XL-4 flow cytometer. The average fluorescence signals of primary and secondary antibodies were then plotted against time. Secondary-only and 4°C controls were maintained.

### **Transepithelial Electrical Resistance Measurements**

80,000 SW1222 cells were plated on a transwell insert (Corning 3470). One day after plating, 1µl of anti-FLAG antibody (Sigma) and huA33 antibody at 1mg/ml were added to both apical and basolateral chambers. Resistance measurements were taken daily with a millcell-ERS (Millipore) after equilibration of the plate for an hour at room temperature.

### **Fluorescence Recovery after Photobleaching**

LS174T cells were labeled with either fluoresceinated m100.310 or the membrane dye DiI as described previously. Bleaches were performed on a Zeiss LSM 510 confocal microscope with a 1.4 NA oil lens at 67x magnification on a heated stage. Sections of membrane were bleached with full laser power on all channels for 50 to 100 iterations, resulting in bleaches of between 20 and 80% of initial fluorescence. Fluorescence intensity in the bleach region was recorded and then adjusted to correct for background bleaching due to repetitive imaging over the course of the experiment. Appropriate controls were performed in order to ensure that bleaching was non-reversible. Data presented is the average of a minimum of 6 experiments. Relative diffusivities were then calculated<sup>16-18</sup>.

### **Biotinylation Turnover Assay<sup>19</sup>**

The biotinylation turnover assay was adapted from a protocol designed to measure endocytosis and recycling rates<sup>20</sup>. Briefly, cell surface proteins were pulse biotinylated by

incubation for 1 hour in 1 ml of ice cold PBS containing freshly dissolved NHS-SS-Biotin (Pierce 21217). Biotinylation media was replaced with 100 mM Tris to quench unreacted biotin for 5 min at 4°C, followed by replacement with culture media. At each timepoint, media was removed and cells were incubated in 1 ml lysis buffer for 10 minutes. They were washed off the plate and set on ice in a microfuge tube for another 10 minutes after vortexing briefly. Samples were then spun at 12,000 rpm for 15 min to clear the lysate. Supernatant was removed and then frozen. When the timecourse was complete, samples were rotated with 100 µl streptavidin resin beads (Pierce 53114) overnight at 4°C. Beads were then washed and biotinylated proteins were cleaved off the beads by incubation in 75 µl of 100 mM DTT in PBS at 37°C for 1 hour, mixing every 15 minutes. Samples were mixed with loading buffer and run on a 4-12% bis-tris gel (Invitrogen) and run and transferred onto nitrocellulose according the manufacturer's instructions. Nitrocellulose was blocked and blotted as previously described to detect denatured A33 antigen<sup>21</sup>.

## **2.4 Results**

### **2.4.1 Homeostatic and kinetic localization of A33 antigen**

A panel of A33-expressing colon tumor cell lines were fixed, permeabilized, and stained to detect A33 (Figure 2.4.1a). Surprisingly, and in contrast with earlier reports which used acid washes to demonstrate the internalization of 40% of the antigen<sup>22</sup>, there was very little evidence of intracellular staining in most of the lines tested, suggesting there may be little, if any endocytosis of the A33 antigen. LIM1215 cells were an exception and had clear intracellular accumulation. This cell line may be representative of a subclass of colonic crypt cells located at the extreme tip of the villus, which are about to be shed (C. Chalouni, unpublished). This surprising result was confirmed and quantified for a larger population of cells using a kinetic flow cytometry assay<sup>15</sup> capable of following the course of antigen internalization (Figure 2.4.1b). Suspended cells were A33-labeled on ice, washed, and incubated in media at 37°C. At various times, aliquots were removed and labeled with PE-conjugated anti-mouse secondary, such that primary signal corresponds to total antigen, and secondary signal to the fraction of antigen that remains surface accessible. Average fluorescence intensities were standardized to time zero and graphed over time. In most cell lines, the fractional decline in primary and secondary signals was roughly equal, indicating that the bulk of the primary-labeled antigen remained on the cell surface. In each experiment, primary signal was seen to decrease, which is likely due to dissociation of the primary antibody, as the antigen itself is not shed<sup>8</sup>. Thus, with the exception of LIM1215, there appeared to be little endocytosis in these cells (Figure 2.4.1b), consistent with the small amount of A33 residing in intracellular compartments (Figure 2.4.1a).

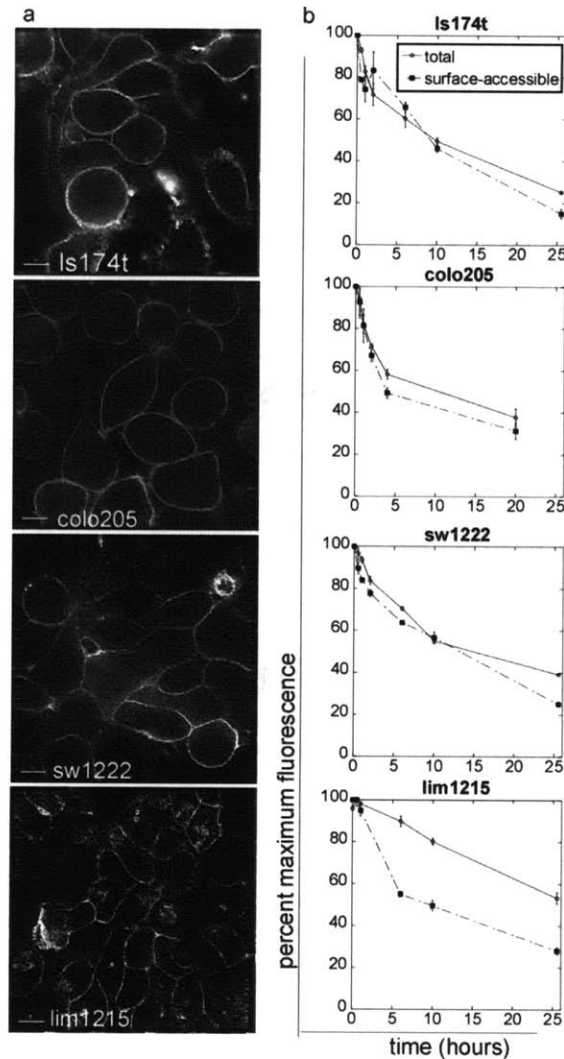


**Figure 2.4.1: Distribution of antibody-bound A33 antigen. (a) Cultured colon tumor epithelial cells contain little intracellular A33 antigen.** Each of 4 cell lines were grown on coverslips, fixed, permeabilized, and A33 antigen was labeled with the monoclonal antibody m100.310\*Alexa 488. Internal pools of antigen were seen only in LIM1215 cells. Bar represents 5  $\mu$ M. **(b) Antibody-bound A33 antigen shows persistent surface localization in a flow cytometric assay of dynamic internalization kinetics.** Suspended cells were A33-labeled at 0°C and then incubated at 37°C, allowing labeled antigen to be internalized. After shifting cultures to 37°C, aliquots were removed and labeled with anti-mouse PE and analyzed flow cytometry in order to determine the fraction of labeled A33 that remained surface accessible over time. The level of surface-accessible A33 did not fall significantly below the level of total A33, indicating little internalization of the A33 antigen in all cell lines tested except LIM1215. The decrease in total A33 signal is likely due to dissociation of the primary antibody, as the antigen is not shed.

### **2.4.2 Colocalization Profile**

The lack of significant internalization of the antigen in several tumor cell lines raised questions concerning the mechanism of this persistence at the surface. Given its homology to several tight junction-associated proteins and cell adhesion molecules (CAMs), a series of colocalization studies were performed (Figure 2.4.2). Despite differing substantially from the other lines tested, LIM1215 cells were used for this work, as they were potentially more discriminatory due to their internal reservoir of antigen. Indeed, in immunofluorescence images of LIM1215 cells, A33 was shown to partially colocalize with occludin (a), ZO-1 (b), and actin (c), not only at the plasma membrane, but also in a few intracellular vesicles.

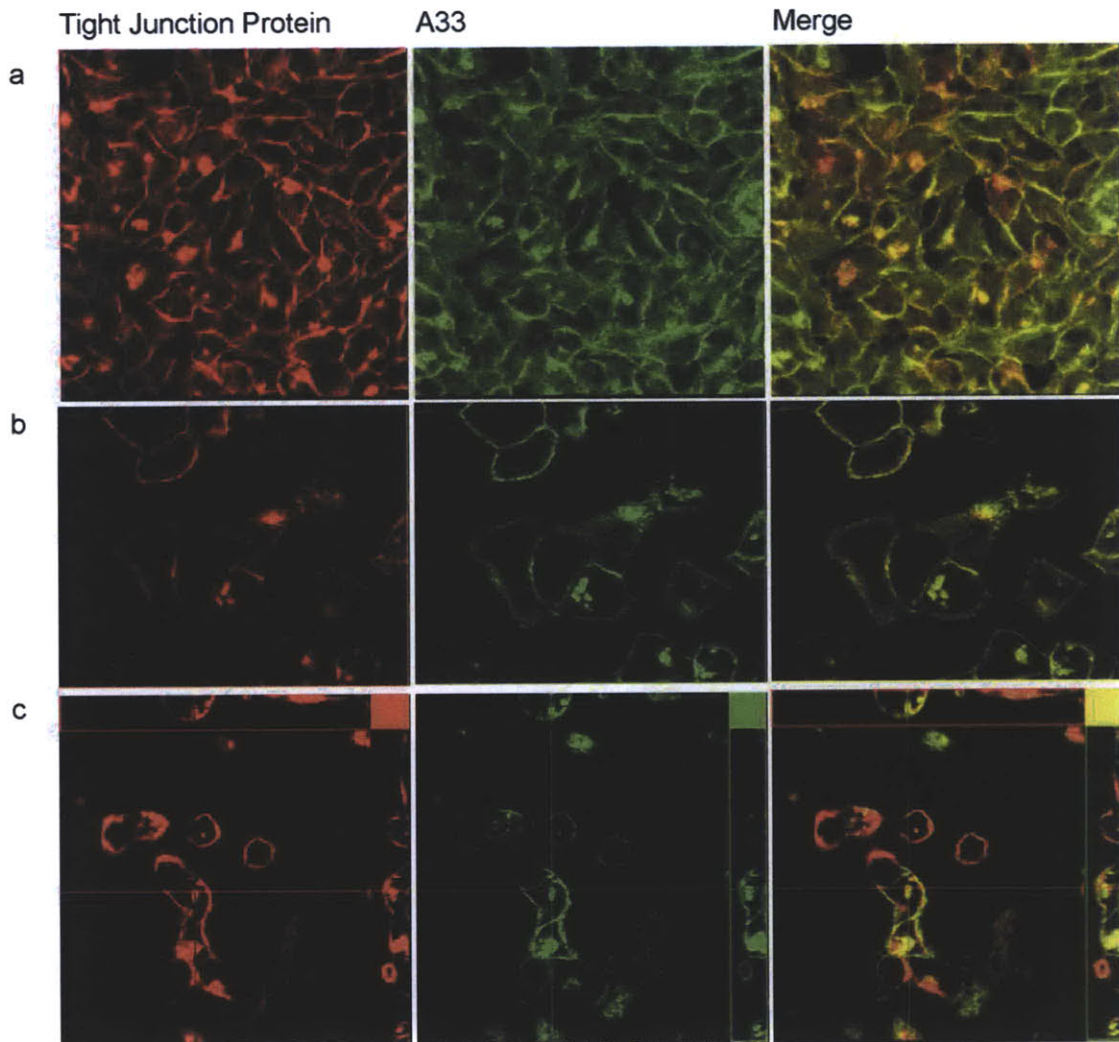


**Figure 2.4.2: Colocalization profile of A33 antigen.** Tight junction proteins are false-colored in red, and A33 antigen in green. **(a) A33 partially colocalizes with the tight junction protein occludin.** Immunofluorescence image of LIM1215 cells showing colocalization of A33 antigen and occludin. **(b) A33 partially colocalizes with the actin-binding, tight junction-associated protein, ZO-1.** Immunofluorescence image of LIM1215 cells showing colocalization of A33 antigen and ZO-1. **(c) A33 partially colocalizes with the cytoskeleton.** Immunofluorescence image of LIM1215 cells showing colocalization of A33 antigen and actin.



### 2.4.3 Investigation of A33 as a tight junction-associated protein

Next, based on its homology to and colocalization with various TJ proteins, we determined whether A33 is trafficked in a manner similar to other TJ proteins. A number of physiological changes and signaling molecules are capable of altering the composition or disrupting the localization of the TJ<sup>23-26</sup>. The best known of these disruption methods consists of a calcium switch from normal media concentrations to a low calcium environment, either by use of calcium-free media, or by chelation, resulting in endocytosis of the TJ.

Indeed, when A33-labeled LS174T cells were treated with 25 mM EGTA, a fraction of the surface A33 was endocytosed into intracellular compartments (Figure 2.4.3a) similar to those observed for TJ proteins such as JAM-1, occludin, and ZO-1, the adherens junction molecules  $\beta$ -catenin and E-cadherin<sup>27</sup>. As the various components of the TJ can be sorted into different compartments upon internalization, we also sought to determine the fate of endocytosed antigen. The internalization assay was modified such that LS174T cells were first A33-labeled and then internalization was triggered by a calcium switch. Low calcium media was then replaced with fresh, calcium-containing media (washout), and recycled antigen was detected by binding of a secondary antibody (Figure 2.4.3b closed squares). The clear increase in secondary signal indicates that internalized antigen was able to return to the surface. In order to distinguish the relative contributions of resurfacing and possible new synthesis following the calcium switch, samples were also re-labeled with primary (open circles) following the incubation with secondary antibody. Recycling accounted for the bulk of overall signal increase, as opposed to additional primary labeling, which includes both new synthesis as well as

replacement of primary label that may have dissociated during the course of the experiment.

Another behavior common to various IGSF proteins is a role in adhesion and subsequent establishment of barrier function—many A33 homologs participate in dimeric interactions involved in securing cell-cell contacts<sup>28-31</sup>. A number of viruses bind to IGSF proteins, even producing proteins that interfere with epithelial integrity by blocking these dimeric interactions<sup>32</sup>. We therefore investigated the ability of the clinical anti-A33 antibody to influence monolayer integrity. One day after plating on a transwell insert, SW1222 cells were treated with either huA33 antibody or mouse anti-FLAG antibody as a control. In the presence of A33 antibody, the monolayer did not fully tighten, as evidenced by a decrease in electrical resistance, indicating a greater degree of leakiness of the tight junctions (Figure 2.4.3c). This increased permeability not only connects A33 to other tight junction proteins and IGSF's, it implies a possible functional role in adhesion. Interestingly, when A33 antibodies were applied to fully formed monolayers, they were unable to increase permeability (data not shown), indicating that they lack the ability to actively pry open sealed junctions. This discrepant behavior may indicate that there is differential access to antigen between normal colon and tumors, which are known to possess disordered and leaky tight junctions<sup>33,34</sup>.

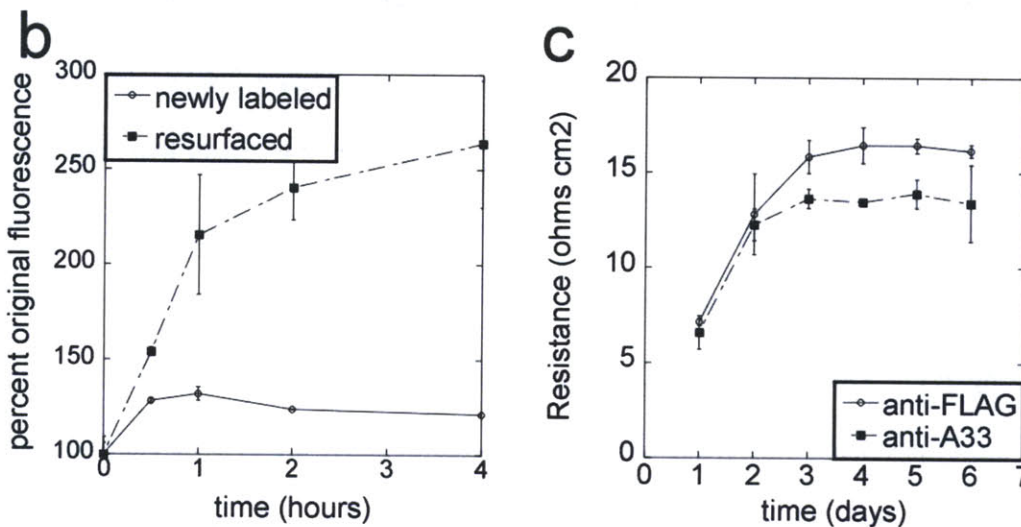
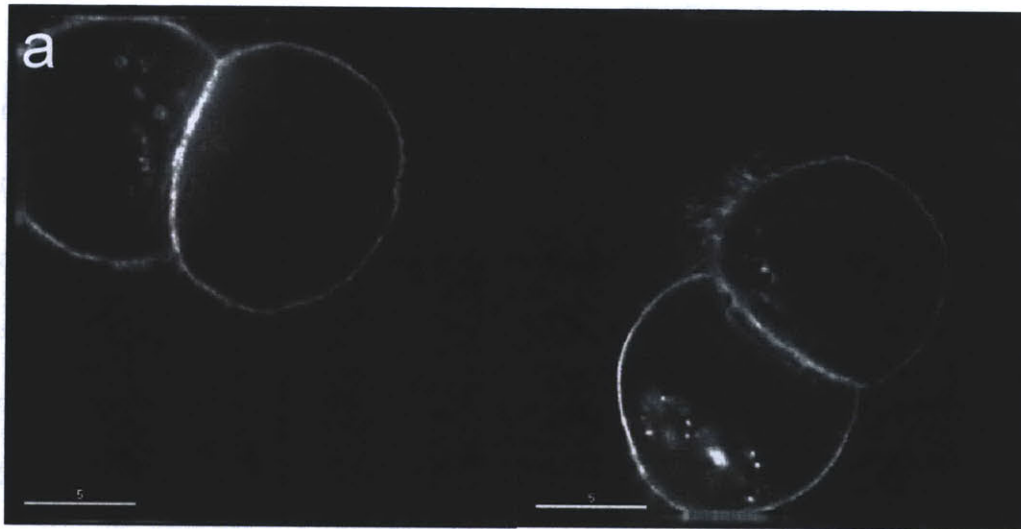


**Figure 2.4.3: Investigation of A33 as a tight junction-associated protein. (a) Calcium chelation triggers A33 internalization.** LS174T cells were labeled with m100.310\*Alexa 488, and culture media was treated with 25 mM EGTA to chelate calcium. At 2 hours, there were clear intracellular pools of antigen, a phenomenon common to junction-associated proteins. **(b) Replacement of calcium restores A33 surface localization.** When EGTA is washed out, previously labeled A33 returns to the surface. Cell aliquots were labeled with m100.310\*Alexa 488 and then treated with EGTA for 2 hours. Following media replacement, aliquots were removed and labeled with a secondary-PE conjugate, and then again with m100.310\*Alexa 488, and subjected to flow cytometry. **(c) Anti-A33 antibody decreases monolayer integrity.** SW1222 cells were grown on transwell inserts, treated with antibodies 1 day after plating, and transepithelial electrical resistance was measured across the monolayer.

#### **2.4.4 Determination of the role of cytoskeleton in A33 localization**

Thus far, we have demonstrated that A33 antigen is partially colocalized with various TJ components, is internalized upon calcium switch, and antibodies to A33 can influence monolayer resistance. These results suggest a role for A33 at the TJ—an interesting possibility given the disorder of the TJ in cancer<sup>33,35,36</sup> and some of the proposed mechanisms of how A33 antibodies may gain tumor specific localization despite expression throughout the colon. However, from a tumor-targeting perspective, these results are secondary to the unusual persistence of radiolabel in clinical patients, and the lack of internalization observed in cultured cells (Figure 2.4.1). In fact, the results of the internalization assay hint at surface persistence that is longer lived than bulk membrane and accompanying proteins. In order to avoid capture and degradation during normal membrane turnover, we next supposed that there might be a tether actively stabilizing A33. Due to its colocalization with actin, and the actin-TJ linking protein ZO-1, the cytoskeleton was clearly implicated. Additionally, the cytoskeleton has been shown to regulate junction assembly and remodeling<sup>37</sup>. Accordingly, actin and microtubules were disrupted by treatment with either latrunulin (Figure 2.4.4a) or nocodazole (Figure 2.4.4b). When A33-labeled cells were treated with these cytoskeleton-disrupting drugs, the antigen was internalized in a manner similar to the calcium switch—indicating that persistent surface localization requires intact cytoskeleton. Additionally, following a calcium switch, LS174T cells were washed into either normal media or media containing EGTA, nocodazole, or latrunulin, and at various timepoints aliquots were removed, A33 labeled, and analyzed by flow cytometry (Figure 2.4.4c). When EGTA was washed out and no drugs were washed in, the surface

localization of A33 was restored. However, restoration was prevented by disruption of the cytoskeleton.

Since many TJ proteins interact with the cytoskeleton and ZO-1 through a series of well-characterized binding domains, we looked for motifs within the A33 intracellular domain, which has been described as unusually acidic<sup>38</sup>. Upon closer inspection, a short region with high homology to occludin was found (Figure 2.4.4d). Initially, this region of occludin was found to be required for TJ/membrane localization<sup>39</sup>. When the crystal structure of occludin was solved, it was found that this region acts as a hinge between two positively charged, acidic domains that are required for binding to ZO-1<sup>40</sup>. Despite being otherwise non-homologous, the similarity between its intracellular domain and that of A33 are striking and point toward the possibility that they may have a common set of interactions with cytosolic proteins—most notably with the actin cytoskeleton, possibly through ZO-1.

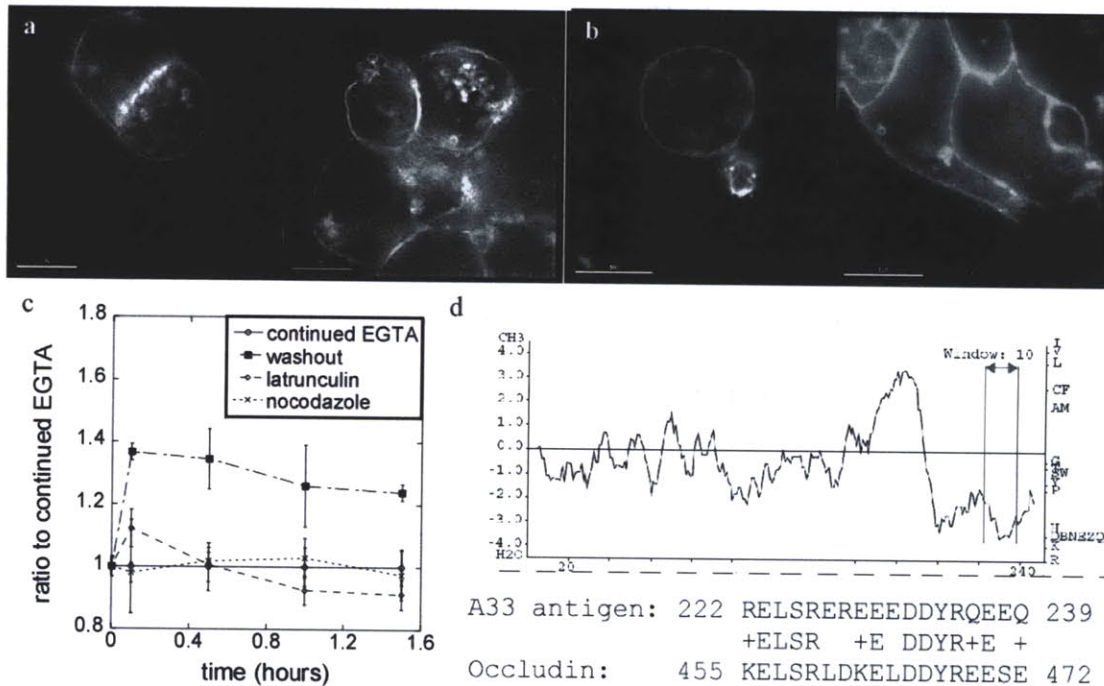


**Figure 2.4.4: Determination of the role of cytoskeleton in A33 localization. (a) Effect of disrupting actin on antigen distribution.** Immunofluorescence images of A33-labeled LS174T cells after treatment with 100 nM latrunculin B for 2 hours demonstrates internalization. **(b) Effect of disrupting microtubules on antigen distribution.** Immunofluorescence images of A33-labeled LS174T cells after treatment with 50  $\mu$ M nocodazole for 2 hours demonstrates internalization. **(c) Disruption of the cytoskeleton prevents recovery of surface-expressed A33.** LS174T cells were labeled and then incubated with EGTA. Following internalization, media was exchanged with either fresh media (washout), or fresh media containing latrunculin, nocodazole, or EGTA (continued EGTA). Surface localization was restored only in cells with intact cytoskeleton and normal calcium levels. **(d) Possible functional homology between A33 and occludin intracellular domains.** A33 and occludin share a highly acidic intracellular region and a negatively charged hinge found to be important for TJ localization. Hydrophobicity plot of A33 antigen, detailing the hinge region with high homology to occludin.

#### **2.4.5 Determination of the mobility and persistence of A33**

As another means of assessing whether the A33 antigen is tethered on the membrane or part of a large protein complex such as the TJ, a series of photobleaching experiments was performed, in which the cell membrane was bleached at cell-cell junctions, and the recovery of either fluorescein-conjugated A33 antibody or the membrane dye DiI was followed. The fluorescence of the membrane dye DiI had an almost complete recovery, while only 10% of A33 fluorescence was seen to recover over the course of one minute (Figure 2.4.5a). When observed over a longer period of time, A33 recovery was quite slow, and indicated that more than half of the antigen is immobile (Figure 2.4.5b). This dramatic surface immobility corresponds quite well to other tight junction proteins which have been studied in both cultured cells and live *drosophila* embryos<sup>41,42</sup>.

The bleach geometry used prevents reporting of an accurate diffusivity value, as diffusivity is highly dependent on the area of the bleach region, which could not be precisely determined. However, since bleach areas were similar for both A33 and DiI, relative diffusivities can be reported. Excluding the immobile fraction, the diffusivity of A33 was 2.5-3 orders of magnitude slower than that of DiI. As a second point of comparison, DiI recovery was compared to recovery of a CEACAM1-egfp fusion protein<sup>43</sup> in MCF-7 cells, which were a kind gift from Dr. John Shively (data not shown). CEACAM1-egfp is known to reside in lipid rafts and also associate with actin through its short cytoplasmic domain<sup>44,45</sup>. Using the same bleach methodology, the diffusivity of CEACAM1 was found to be on the same order of magnitude as DiI.

As there was no significant difference between the recovery of A33 at regions of cell-cell contact and at regions of the membrane not associated with other cells (data not shown), this stability must not depend on trans interactions between cells at the TJ, and points toward either the incorporation of A33 antigen into a larger protein complex which is highly stabilized, or a more direct interaction with static regions of the cytoskeleton. Regardless of mechanism, an interaction with the cytoskeleton is consistent with our colocalization observations, homology, and the data demonstrating that the cytoskeleton is necessary for localization.

Additionally, since the persistence of label in clinical patients is the key feature of this antigen, we next determined the turnover half-life of antigen in cultured LS174T monolayers (Figure 2.4.5c). Monolayers were pulse-biotinylated and at various timepoints total protein was extracted. Biotinylated proteins were pulled down by incubating the lysate with streptavidin resin, and then cleaved from the resin by reduction of a disulfide bond. The resulting samples were run on an SDS-PAGE gel, transferred to nitrocellulose, and blotted to detect A33. Band intensities were quantified and fitted to an exponential decay. In this manner, the half-life of A33 was found to be 56 hours. With a half-life of over 2 days, the A33 antigen is highly persistent relative to typical membrane proteins turnover times. This long half-life is certainly partially responsible for the sustained persistence of the therapeutic antibody to A33 in patients. Most significantly, this long half-life provides a strong motivation for further clinical study of the antigen as a target in PRIT.

Lastly, as there are a number of cell surface antigens with promise as targets in PRIT, we also directly compared A33 with what is perhaps the best studied of these



antigens. Carcinoembryonic antigen (CEA) is a cell surface antigen that is frequently expressed at high levels at the apical surface of epithelial cells, and in a nonpolarized surface pattern in colon tumors<sup>46</sup>. Numerous studies have been performed targeting this well-characterized protein. As accessibility to chelated radionuclide is a key requirement for successful PRIT, we sought to compare the accessibility of A33 with CEA. Accordingly, cells were labeled with both an anti-A33 antibody (m100.310 Alexa\*488) and an anti-CEA scFv (shMFE Alexa\*594), and incubated at 37°C for 2 hours prior to imaging. Intriguingly, after as short a period of 2 hours, there is significant internalization of CEA, while A33 remains stably located at the cell surface, available to bind the radionuclide construct (Figure 2.4.5d).

Taken together, these results demonstrate that the A33 antigen is a highly persistent, largely immobile, surface-localized protein. These findings help explain the unusual persistence of tumor associated anti-A33 antibodies in clinical trials, and indicate that the A33 antigen may have unique promise as a target in PRIT.

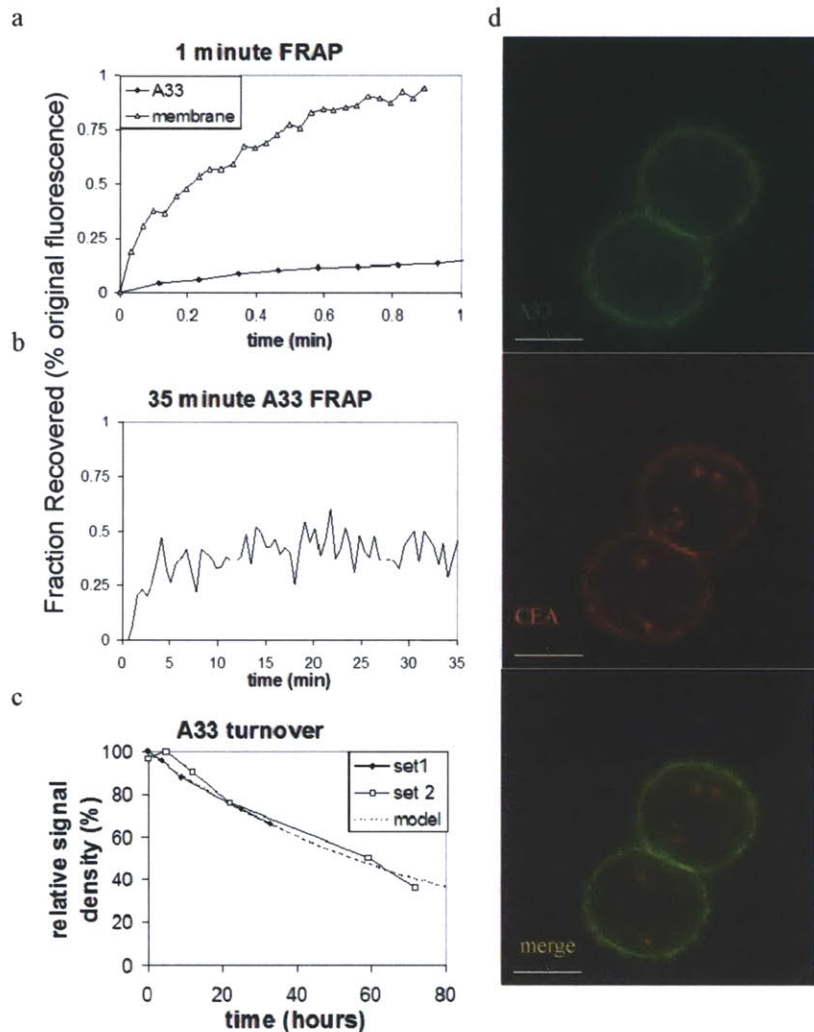


**Figure 2.4.5: Determination of the mobility and persistence of antibody-bound A33.** (a) Over the course of 1 minute, bleached plasma membrane has a near full recovery of fluorescence while very little A33 recovers. Fraction of fluorescence recovered over time for bleached m100.310 antibody bound to A33 and the plasma membrane marker DiI. (N=8, LS174T cells). (b) Even over much longer time scales, antibody-bound A33 fluorescence recovery is slow and incomplete. 35-minute time course of antibody bound to A33 after photobleaching. (N=6, LS174T cells). (c) The A33 antigen is persistent, having a surface expression halflife of 56 hours in cultured monolayers. Cell surface proteins of cultured LS174T cells were pulse-biotinylated, extracted, and pulled down with streptavidin beads. The precipitated proteins were reduced off the beads, subjected to gel electrophoresis and blotted to detect A33 antigen. Signal intensity of two data sets is plotted against time post-biotinylation, and fit to an exponential decay. (d) While other immunotherapy targets are internalized, A33 antigen remains on the surface. LS174T cells were labeled with both m100.310\*Alexa 488 and anti-CEA shMFE\*594 for 2 hours at 37°C before imaging on a deconvolution microscope.

## 2.5 Discussion

A33 is a highly persistent surface-localized antigen. While the antigen is not cancer-specific, antibodies against A33 gain tumor specificity over the course of a week, possibly as the normal colon epithelium is shed. Most tumor cell lines tested showed little to no internalization of the antigen, both by immunofluorescent imaging of permeabilized cells, and in a flow cytometric internalization assay which monitored accessibility to a secondary antibody. While initially surprising, as there had been reports that the antigen was largely internalized<sup>22</sup>, this result is consistent with immunofluorescence images of resected colon tissue, in which the steady-state distribution of antigen is entirely on the cellular surface, with the possible exception of cells at the very tip of the crypt which are about to be shed (C. Chalouni, unpublished). This phenotype may be reflected by the LIM1215 cell line, which unlike the rest of the lines tested, did internalize the antigen.

As a member of the immunoglobulin superfamily (IGSF) of proteins, which comprises a full 2% of the genome, A33 is a member of the largest class of mammalian proteins. Their basic extracellular structure consists of domains resembling the IgG fold, and they have notable diversity in their intracellular domains. Striking features of the A33 intracellular domain include a quadruple cysteine repeat followed by a highly acidic sequence. Its closest homologs include the coxsackie adenovirus receptor (CAR)<sup>47</sup>, cortical thymocyte receptor (CTX)<sup>47</sup>, endothelial cell adhesion molecule (ESAM), junction adhesion molecules 1-3 (JAM)<sup>48</sup>, and CEA-related cell adhesion molecules (CEACAMs)<sup>49</sup>. Many of these homologs have been implicated in cell-cell adhesion, and some are localized to regions of cell-cell contact or to the tight junction more specifically.

They typically participate in dimeric interactions, and many also serve as attachment points for various intestinal viruses.

Here, we have described experiments that reveal some of the molecular properties of the A33 antigen. Taken together, this work demonstrates the persistent, immobile, and stable surface expression of A33—properties which may result from a link to the cytoskeleton through a complex of tight junction components. Additionally, these properties may be the source of the A33 antigen's uniquely promising profile in clinical trials.

In the clinic, antibodies to A33 exhibit two distinctive properties. First, they remain tumor-localized for weeks. In some cases, persistent tumor localization is due to the residualizing properties of metal radionuclides. However, the A33 clinical trials have utilized radioactive iodine. Questions remain as to how these antibodies were able to persist—whether they were sequestered and stored along some trafficking route, or whether they simply remained bound to surface-localized antigen. Our studies here are consistent with the notion that the A33 antigen is surface-stabilized through a link to the cytoskeleton or as a part of a stable protein complex or membrane microdomain that allows the antigen to escape bulk membrane endocytosis and subsequent trafficking and endocytosis. The turnover half-life of greater than 2 days found here also likely underestimates the true turnover time *in vivo*. Over the course of the protocol used here, the cultures become overpopulated and some cells may respond by undergoing apoptosis, resulting in an artificially shorter half-life. Additionally, as mentioned previously, intracellular A33 staining is not seen in sections of human colon, except at the very tip of the villus, in cells that are proximal to being shed (C. Chalouni, unpublished). This data

indicates that the simple explanation of persistence due to a lack of antigen turnover may be correct.

Secondly, and more significantly, antibodies to A33 were found to penetrate solid tumors<sup>11</sup>. The ability to penetrate solid tumors has proven to be a significant obstacle in RIT. To date, few successful RIT therapeutics target solid tumors. This failure is due to what are generally the conflicting goals of avoiding bone marrow toxicity while at the same time penetrating and thoroughly dosing tumor tissue. As a means to evade this toxicity at the same time as increasing penetration, manipulations of targeting construct size have been studied extensively. While these alterations do have the desired effect on clearance parameters, thorough tumor penetration has still proven an elusive goal.

The difficulty in localizing therapeutics to the core of tumors may largely be due to a consumption-based barrier to diffusion<sup>15</sup>, in which antigen turnover reaches an equilibrium with diffusion and binding of the therapeutic at a given distance from the capillary—preventing penetration past that boundary. In the case of A33, perhaps this barrier is avoided as the antigen is not internalized and degraded on the time scale of diffusion<sup>50</sup>.

The simple asset of persistent surface localization, which we have described here, may account for both of A33's distinctive RIT properties. It may allow the clinical antibodies to gain tumor specificity as normal epithelium is shed, and to penetrate the core of a solid tumor as diffusion outpaces turnover. We likewise speculate that this surface persistence may allow antibodies to A33 to have high availability to a radionuclide construct in PRIT. Taken together, these results point to A33 as an excellent candidate for two-step therapies.

## 2.6 Works Cited

1. Welt, S. et al. Phase I/II study of iodine 125-labeled monoclonal antibody A33 in patients with advanced colon cancer. *J Clin Oncol* **14**, 1787-97 (1996).
2. DeNardo, G.L. Treatment of non-Hodgkin's lymphoma (NHL) with radiolabeled antibodies (mAbs). *Semin Nucl Med* **35**, 202-11 (2005).
3. Pagel, J.M. et al. Comparison of anti-CD20 and anti-CD45 antibodies for conventional and pretargeted radioimmunotherapy of B-cell lymphomas. *Blood* **101**, 2340-8 (2003).
4. Gruaz-Guyon, A., Raguin, O. & Barbet, J. Recent advances in pretargeted radioimmunotherapy. *Curr Med Chem* **12**, 319-38 (2005).
5. Boerman, O.C., van Schaijk, F.G., Oyen, W.J. & Corstens, F.H. Pretargeted radioimmunotherapy of cancer: progress step by step. *J Nucl Med* **44**, 400-11 (2003).
6. Johnstone, C.N. et al. Characterization of mouse A33 antigen, a definitive marker for basolateral surfaces of intestinal epithelial cells. *Am J Physiol Gastrointest Liver Physiol* **279**, G500-10 (2000).
7. Garin-Chesa, P., Junichi Sakamoto, Sydney Welk, Francisco X. Real, Wolfgang J. Rettig, Lloyd J. Old. Organ-specific expression of the colon cancer antigen A33, a cell surface target for antibody-based therapy. *International Journal of Oncology* **9**, 465-471 (1996).
8. Welt, S. et al. Quantitative analysis of antibody localization in human metastatic colon cancer: a phase I study of monoclonal antibody A33. *J Clin Oncol* **8**, 1894-906 (1990).
9. Welt, S. et al. Phase I/II study of iodine 131-labeled monoclonal antibody A33 in patients with advanced colon cancer. *J Clin Oncol* **12**, 1561-71 (1994).
10. Welt, S. et al. Phase I study of anticolon cancer humanized antibody A33. *Clin Cancer Res* **9**, 1338-46 (2003).
11. Scott, A.M. et al. A phase I trial of humanized monoclonal antibody A33 in patients with colorectal carcinoma: biodistribution, pharmacokinetics, and quantitative tumor uptake. *Clin Cancer Res* **11**, 4810-7 (2005).
12. Chong, G. et al. Phase I trial of 131I-huA33 in patients with advanced colorectal carcinoma. *Clin Cancer Res* **11**, 4818-26 (2005).
13. Ritter, G. et al. Serological analysis of human anti-human antibody responses in colon cancer patients treated with repeated doses of humanized monoclonal antibody A33. *Cancer Res* **61**, 6851-9 (2001).
14. Johnstone, C.N. et al. Analysis of the regulation of the A33 antigen gene reveals intestine-specific mechanisms of gene expression. *J Biol Chem* **277**, 34531-9 (2002).
15. Thurber, G.e.a. Manuscript in preparation.
16. Ellenberg, J. et al. Nuclear membrane dynamics and reassembly in living cells: targeting of an inner nuclear membrane protein in interphase and mitosis. *J Cell Biol* **138**, 1193-206 (1997).

17. Umenishi, F., Verbavatz, J.M. & Verkman, A.S. cAMP regulated membrane diffusion of a green fluorescent protein-aquaporin 2 chimera. *Biophys J* **78**, 1024-35 (2000).
18. Partikian, A., Olveczky, B., Swaminathan, R., Li, Y. & Verkman, A.S. Rapid diffusion of green fluorescent protein in the mitochondrial matrix. *J Cell Biol* **140**, 821-9 (1998).
19. Schmidt, M.e.a. Manuscript in preparation.
20. Le, T.L., Yap, A.S. & Stow, J.L. Recycling of E-Cadherin: A Potential Mechanism for Regulating Cadherin Dynamics. *The Journal of Cell Biology* **146**, 219-232 (1999).
21. Ji, H. et al. Electrophoretic analysis of the novel antigen for the gastrointestinal-specific monoclonal antibody, A33. *Electrophoresis* **18**, 614-21 (1997).
22. Daghighian, F. et al. Enhancement of radiation dose to the nucleus by vesicular internalization of iodine-125-labeled A33 monoclonal antibody. *J Nucl Med* **37**, 1052-7 (1996).
23. Bruewer, M. et al. Interferon-gamma induces internalization of epithelial tight junction proteins via a macropinocytosis-like process. *Faseb J* **19**, 923-33 (2005).
24. Kevil, C.G., Oshima, T., Alexander, B., Coe, L.L. & Alexander, J.S. H(2)O(2)-mediated permeability: role of MAPK and occludin. *Am J Physiol Cell Physiol* **279**, C21-30 (2000).
25. Harhaj, N.S. & Antonetti, D.A. Regulation of tight junctions and loss of barrier function in pathophysiology. *Int J Biochem Cell Biol* **36**, 1206-37 (2004).
26. Musch, M.W., Walsh-Reitz, M.M. & Chang, E.B. Roles of ZO-1, occludin, and actin in oxidant-induced barrier disruption. *Am J Physiol Gastrointest Liver Physiol* **290**, G222-31 (2006).
27. Ivanov, A.I., Nusrat, A. & Parkos, C.A. Endocytosis of Epithelial Apical Junctional Proteins by a Clathrin-mediated Pathway into a Unique Storage Compartment. *Molecular Biology of the Cell* **15**, 176-188 (2004).
28. Mandell, K.J. & Parkos, C.A. The JAM family of proteins. *Adv Drug Deliv Rev* **57**, 857-67 (2005).
29. Gray-Owen, S.D. & Blumberg, R.S. CEACAM1: contact-dependent control of immunity. *Nat Rev Immunol* **6**, 433-46 (2006).
30. Kostreva, D. et al. X-ray structure of junctional adhesion molecule: structural basis for homophilic adhesion via a novel dimerization motif. *Embo J* **20**, 4391-8 (2001).
31. Brummendorf, T. & Lemmon, V. Immunoglobulin superfamily receptors: cis-interactions, intracellular adapters and alternative splicing regulate adhesion. *Curr Opin Cell Biol* **13**, 611-8 (2001).
32. Walters, R.W. et al. Adenovirus fiber disrupts CAR-mediated intercellular adhesion allowing virus escape. *Cell* **110**, 789-99 (2002).
33. Mullin, J.M., Agostino, N., Rendon-Huerta, E. & Thornton, J.J. Keynote review: epithelial and endothelial barriers in human disease. *Drug Discov Today* **10**, 395-408 (2005).
34. Sawada, N. et al. Tight junctions and human diseases. *Med Electron Microsc* **36**, 147-56 (2003).

35. Mullin, J.M. Epithelial barriers, compartmentation, and cancer. *Sci STKE* **2004**, pe2 (2004).
36. Soler, A.P. et al. Increased tight junctional permeability is associated with the development of colon cancer. *Carcinogenesis* **20**, 1425-31 (1999).
37. Ivanov, A.I. et al. Microtubules regulate disassembly of epithelial apical junctions. *BMC Cell Biology* **7**(2006).
38. Heath, J.K. et al. The human A33 antigen is a transmembrane glycoprotein and a novel member of the immunoglobulin superfamily. *Proc Natl Acad Sci U S A* **94**, 469-74 (1997).
39. Furuse, M. et al. Direct Association of Occludin with ZO-1 and Its Possible Involvement in the Localization of Occludin at Tight Junctions. *The Journal of Cell Biology* **127**, 1617-1626 (1994).
40. Li, Y., Fanning, A.S., Anderson, J.M. & Lavie, A. Structure of the Conserved Cytoplasmic C-terminal Domain of Occludin: Identification of the ZO-1 Binding Surface. *J. Mol. Biol.* **352**, 151–164 (2005).
41. Cliffe, A., Mieszczanek, J. & Bienz, M. Intracellular shuttling of a Drosophila APC tumour suppressor homolog. *BMC Cell Biology* **5**(2004).
42. Thomas, T. et al. Mechanisms of Cx43 and Cx26 transport to the plasma membrane and gap junction regeneration. *Journal of Cell Science* **119**, 4451-4462 (2005).
43. Chen, C.J. & Shively, J.E. The cell-cell adhesion molecule carcinoembryonic antigen-related cellular adhesion molecule 1 inhibits IL-2 production and proliferation in human T cells by association with Src homology protein-1 and down-regulates IL-2 receptor. *J Immunol* **172**, 3544-52 (2004).
44. Kirshner, J., Schumann, D. & Shively, J.E. CEACAM1, a cell-cell adhesion molecule, directly associates with annexin II in a three-dimensional model of mammary morphogenesis. *J Biol Chem* **278**, 50338-45 (2003).
45. Schumann, D., Chen, C.J., Kaplan, B. & Shively, J.E. Carcinoembryonic antigen cell adhesion molecule 1 directly associates with cytoskeleton proteins actin and tropomyosin. *J Biol Chem* **276**, 47421-33 (2001).
46. Hammarstrom, S. The carcinoembryonic antigen (CEA) family: structures, suggested functions and expression in normal and malignant tissues. *Semin Cancer Biol* **9**, 67-81 (1999).
47. Chretien, I. et al. CTX, a Xenopus thymocyte receptor, defines a molecular family conserved throughout vertebrates. *Eur J Immunol* **28**, 4094-104 (1998).
48. Bazzoni, G. The JAM family of junctional adhesion molecules. *Curr Opin Cell Biol* **15**, 525-30 (2003).
49. Kuespert, K., Pils, S. & Hauck, C.R. CEACAMs: their role in physiology and pathophysiology. *Curr Opin Cell Biol* (2006).
50. Graff, C.P. & Wittrup, K.D. Theoretical analysis of antibody targeting of tumor spheroids: importance of dosage for penetration, and affinity for retention. *Cancer Res* **63**, 1288-96 (2003).



## **Chapter 3: Effect of Antigen Turnover Rate and Expression Level on Antibody Penetration into Tumor Spheroids**

### **3.1 Abstract**

Poor tissue penetration is a significant obstacle to the development of successful antibody drugs for immunotherapy of solid tumors, and diverse alterations to the properties of antibody drugs have been made to improve penetration and homogeneity of exposure. However, in addition to properties of the antibody drug, mathematical models of antibody transport<sup>1,2</sup> predict that the antigen expression level and turnover rate significantly influence penetration. As intrinsic antigen properties are likely to be difficult to modify, they may set inherent limits to penetration. Accordingly, in this study we assess their contribution by evaluating the distance to which antibodies penetrate spheroids when these antigen properties are systematically varied. Additionally, the penetration profiles of antibodies against CEA and A33, two targets of clinical interest, are compared. The results agree well with the quantitative predictions of the model, and demonstrate that dosing distal regions of tumors is best achieved by selecting slowly internalized targets that are not expressed above the level necessary for recruiting a toxic dose of therapeutic. Each antibody-bound antigen molecule that is turned over or present in excess incurs a real cost in terms of penetration depth—a limiting factor in the development of effective therapies for treating solid tumors.

---

Major portions of this chapter were previously published in:  
Ackerman ME, Pawlowski D, Wittrup KD, "Effect of antigen turnover rate and expression level on antibody penetration into tumor spheroids" *Mol Cancer Ther.* 2008 Jul;7(7):2233-40.

### 3.2 Background

Antibody therapeutics promise highly specific tumor targeting. However, their superior molecular recognition characteristics have not proved to be the magic bullet once hoped. This is partly due to difficulty in obtaining sufficiently uniform exposure, particularly in solid tumors. For example, radioimmunotherapy (RIT) has achieved relative success in treating blood cancers such as lymphoma, where it is emerging as a promising front-line treatment, but more limited success against solid tumors<sup>3</sup>. These discrepant results are reflective of the additional obstacles to delivering drugs to solid tissue, where efficient delivery depends on the interplay of several unfavorable transport rates<sup>4,5</sup>. Particularly significant rate processes include the rate of antibody escape from the vasculature and the ability of the therapeutic to penetrate tissue<sup>1</sup>.

Antibodies have very low rates of extravasation, making transport across the vasculature a considerable barrier. For directly conjugated antibody therapeutics, the resulting concentration profile, where the blood often contains a 100 to 1000-fold higher concentration of therapeutic than surrounding tissue<sup>1,2,6</sup>, obviously limits efficacy. When combined with a long circulatory half-life, the elevated blood concentration often results in bone marrow toxicity before therapeutic toxicity throughout a solid tumor is reached.

Once out of the vasculature, there are further obstructions to tumor permeation by antibody drugs. The specific architecture of solid tumors, such as limited convective flow, high interstitial pressure, and a dense extracellular matrix, acts to limit penetration<sup>5</sup>. The well-studied impediment of the “binding site barrier”<sup>7,8</sup> results from the intersection of the slow diffusion and fast association rates of high affinity antibodies. The combined effect of these rates is that binding sites closest to the vasculature are occupied before

further penetration occurs. This phenomenon results in a highly heterogeneous distribution of drug—with areas of saturation surrounding the blood supply, and a complete lack of antibody in more distal regions<sup>9</sup>.

In order to evade these barriers to penetration, numerous alterations have been made to the composition of the protein drug itself<sup>3</sup>. Decreased size increases both extravasation and diffusivity<sup>10,11</sup>, while albumin binding domains<sup>9,12</sup> and interactions with FcRn<sup>13,14</sup> have been engineered in order to lengthen plasma residence time and allow more therapeutic to extravasate before clearance. Low affinity binders have been shown to circumvent the binding site barrier and allow a more homogeneous distribution of therapeutic<sup>8</sup>, at the unacceptable cost however of significantly reducing the amount of antibody retained in the tumor.

Despite these efforts, solid tumor penetration remains an elusive goal. To account for the various processes affecting penetration, the simplified scaling model of Thurber, et al<sup>1</sup>, describes the relevant kinetic rates and processes determining penetration in spherical micrometastases and vascularized tumors. For the purposes of the present experiments with spheroids, the relationships for micrometastases will be tested. Rearrangement of the Thiele modulus, a dimensionless group describing the ratio of catabolism to transport, yields an expression predicting the distance (R) that a prevascular spheroidal metastasis will be penetrated by an antibody (Equation 1).

$$R = \sqrt{\frac{D[Ab]_{surface}}{k_e \left( \frac{[Ag]_{tumor}}{\epsilon} \right)}} \quad \text{equation 1}$$

While many of the parameters in this expression relate to the properties of the antibody, such as the dose ( $^{15}_{\text{surface}}$ ), void fraction ( $\varepsilon$ ), and diffusivity ( $D$ ), the remaining terms describe antigen properties which could set intrinsic limits to penetration. These terms include the antigen expression level ( $[\text{Ag}]_{\text{tumor}}$ ), and turnover rate ( $k_e$ ). Intuitively, it is clear how each of these parameters could limit the penetration of a high affinity therapeutic: the distance each antibody can penetrate before binding depends on the density of binding sites; and as bound antigen is turned over and replaced, new binding sites are exposed. In fact, if turnover occurs on a timescale comparable to vascular escape and diffusion, the result is a bottomless sink for therapeutic and a limit to further tissue penetration.

Accordingly, we experimentally varied antigen concentration and turnover rate in order to probe their importance in tissue penetration. Quantitative determinations of the radius of penetration were achieved by incubating tumor spheroids in fluorescent antibodies against carcinoembryonic antigen (CEA) and A33. These antigen-specific properties have been less well investigated than those of the therapeutic protein itself, despite the fact that under some conditions they may pose an intrinsic limit to tumor penetration. Identification of the antigen properties that significantly impact tumor penetration will aid in the selection of targets with favorable profiles and in optimizing this promising mode of cancer therapy.

### **3.3 Materials and Methods**

#### **Cell and Spheroid Culture**

LS174T and SW1222 cells were cultured as described previously<sup>16</sup>. Antigen expression levels were quantified using Quantum Simply Cellular Beads (Bangs Laboratories, Inc). Spheroids were grown by the hanging drop method<sup>17</sup>. Briefly, approximately 500 cells were suspended in 20 ul of media in each well of a 72 microwell plate (Nunc 448698) and incubated upside-down at 37°C and 5% CO<sub>2</sub> for 2-3 days. Spheroids were then transferred to glass coverslip-bottomed dishes (Lab-Tek 155411) and allowed to adhere for 2 days before imaging. Except where noted, antibodies were added to culture media after this transfer, and the spheroids at each condition were then imaged repeatedly over time. Care was taken to ensure that antibody binding did not result in depletion from the bulk.

#### **Fluorescent Antibodies**

The mouse anti-A33 antibody m100.310 was conjugated with Alexa\*488 according to the manufacturer's instructions (Molecular Probes A-20181) with an average of 2.76 fluorophores per antibody. Anti-CEA IgGs M85151a and M111147 were purchased from Fitzgerald and likewise conjugated with Alexa\*488 with resulting conjugation levels of 1.5 and 1.4 fluorophores per antibody, respectively for experiments comparing penetration distance with respect to internalization rate, and 2.1 fluorophores per molecule of antibody M85151a for all other CEA experiments presented.

## **Image Collection and Analysis**

A Zeiss LSM 510 confocal microscope with a 1.4 NA air lens at 10x magnification on a heated stage was used to collect spheroid images. Image collection conditions were optimized for each antibody used, and then maintained for all timepoints in each experiment. Care was taken to analyze images at an appropriate depth from the coverslip in order to avoid both artifacts based on incomplete adhesion to the coverslip and attenuation of signal due to the thickness of the sample. Images were transferred to ImageJ, in which they were despeckled and gated to eliminate background signal, yielding a binary image. A circular selection area was then drawn around each spheroid and the macro “spheroidspin” was run (see appendix for macro code). This protocol draws a line across the selection and gives a pixel by pixel readout of signal intensity on that line as the image is rotated in 18 projections, each varying by 20 degrees, and generates a results table listing the readout for each line, the sum of pixels with signal for each projection, and the average number of pixels with signal across projections. This average gives the diameter of the spheroid that has been penetrated by fluorescent antibody in pixels, which are then converted into microns. The penetration distances reported here are the averages of 3-10 spheroids under each condition, and therefore represent a total of 90-360 individual measurements of penetration radius. Error bars represent the standard deviation of the penetration distance between spheroids. However, at later time points and higher concentrations of antibody, the spheroids become completely saturated, and the standard deviation reflects variability in spheroid size.

## Macro for spheroid analysis

### Spheroid Spin Macro Code

```
var count;
var THRESHOLD;
var DEG_PER_ROTATION;
var TOTAL_ROTATION;

showMessage("Spheroid Spin Macro", "Macro is installed.");

macro "Spheroid Spin"
{
    THRESHOLD = 25; // threshold of what is considered an "on" pixel
    // if this value changes, update this line: run("Arbitrarily...", "angle=20 fill");
    DEG_PER_ROTATION = 20;
    TOTAL_ROTATION = 360;

    run("Colors...", "foreground=black background=black selection=yellow");
    run("Copy to System");
    run("System Clipboard");

    // make a line through the middle of image
    makeLine(0, getHeight, getWidth, 0);

    // make an array
    arr = newArray(TOTAL_ROTATION/DEG_PER_ROTATION);

    // loop through about the entire rotation, increasing by DEG_PER_ROTATION
    for(angle = 0; angle < TOTAL_ROTATION; angle += DEG_PER_ROTATION)
    { // sets an array of intensity values for the line
        profile = getProfile();
        count = 0;
        // loop through the array and update our output as well as tally up
        // all the "on" pixels
        for (j = 0; j < profile.length; j++)
        {
            setResult("p"+angle, j, profile[j]);
            if(profile[j] > THRESHOLD)
            {
                count++;
            }
        }
        // add the number of "on" pixels to our output and add that number to
        // our array
        setResult("p"+angle, 0, count);
    }
}
```

```
arr[angle/DEG_PER_ROTATION] = count;
updateResults();
// rotate by 20 degrees
run("Arbitrarily...", "angle=20 fill");
}

// now calculate the average number of "on" pixels over all rotations
count = 0;
for(i = 0; i < arr.length; i++)
{
    count += arr[i];
}
count = count / arr.length;
// and then add to our results
setResult("avg", 0, count);
updateResults();
}
```



## 3.4 Results

### 3.4.1 Processing of spheroid images

Spheroids - spherical clusters of growing, self-adhered tumor cells - were used extensively in this study as a model system intermediate between monolayer tissue culture and xenografts, to capture the effects of simultaneous diffusion, binding, and endocytic uptake. Spheroids present a 3-dimensional environment in which cells grow without any solid or artificial support. At large sizes, spheroids also recapitulate phenomena of tumors such as hypoxic and necrotic cores<sup>18</sup>. Lacking any blood or lymph-driven convective flow they provide a reasonable model for transport within the center of a bulk vascularized tumor<sup>19</sup>. After an initial period of growth, they may be analyzed by either 2-photon or confocal microscopy, or fixed and handled as a histological specimen.

In this study, spheroids were grown in a hanging drop<sup>17</sup>, allowed to adhere to coverslips, incubated in the presence of various fluorescently labeled antibodies, and imaged by confocal microscopy. Raw images (Figure 3.4.1a) were analyzed in order to determine the average distance that antibody penetrated into the spheroid at a given time. After acquisition, images were gated to generate a binary version (Figure 3.4.1b), such that background signal was excluded. A circular region of interest was drawn around each spheroid, and pixel-by-pixel intensity was taken along a bisecting diagonal line as the region of interest was rotated in 18 projections around 360° (Figure 3.4.1c). The number of pixels above the selected intensity threshold was summed and then averaged over all projections, giving the diameter of the spheroid that had been penetrated by label.

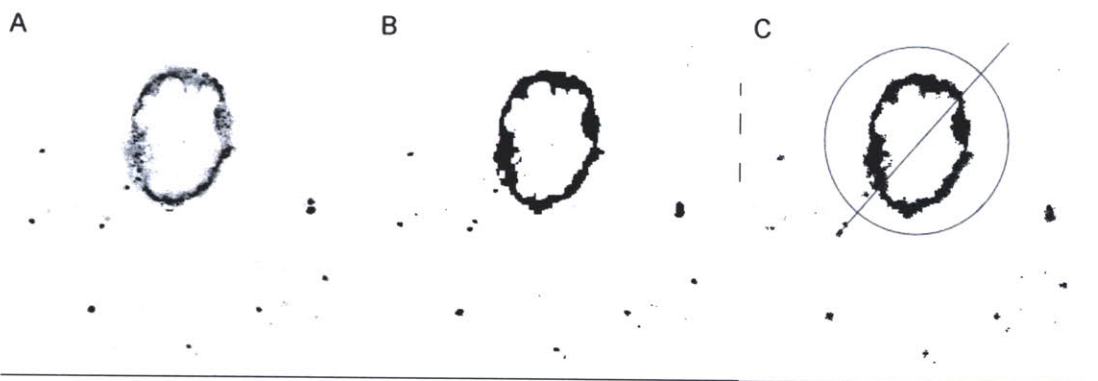


**Figure 3.4.1: Processing of spheroid images.** (a) Original confocal images were transferred into ImageJ. (b) They were then processed to eliminate background signal and generate binary data. (c) A circular region of interest was drawn around each spheroid, and a readout of pixel intensity along a bisecting diagonal line was taken as the image was rotated in 18 projections around 360 degrees. The number of pixels with signal from each projection was then averaged, yielding the diameter of the spheroid that had been penetrated by label.

### 3.4.2 Antigen density affects spheroid penetration

Equation 1 predicts that penetration distance,  $R$ , will increase proportionally to  $\sqrt{[Ab]_{surface}}$  and inversely proportional to  $\sqrt{[Ag]_{tumor}}$ . Accordingly, a ten-fold decrease in antigen density is expected to yield a  $\sqrt{10}$ -fold increase in penetration distance. Similarly, the model also predicts that a tenfold decrease in antigen density will negate the effect of a tenfold decrease in antibody dose.

In order to experimentally test these predictions, spheroids were incubated in either a given concentration of fluorescent anti-A33 antibody, or a mixture of fluorescent antibody and non-fluorescent competitor. The non-fluorescent competitor functions to occupy a fraction of binding sites as both antibodies diffuse through the spheroid, blocking the fluorescent antibody from binding and allowing it to diffuse further into the spheroid before encountering an available binding site. Accordingly, the non-fluorescent competitor acts as a means to effectively tune the density of available antigen binding sites.

When spheroids were incubated in either a given concentration of fluorescent anti-A33 antibody, or a mixture of one-tenth that concentration of fluorescent and nine-tenths non-fluorescent competitor antibody, penetration was indeed equivalent (Figure 3.4.2a)—as would be expected given that the total antibody dose is equivalent in both cases. The decrease in fluorescent antibody dose worsens the signal to noise ratio, however the equivalence of total dose leads to equivalent penetration distance, as can be seen in representative images at 24 hours (Figure 3.4.2b and c).

For a given dose of fluorescent antibody, penetration distance is predicted to vary proportionally to  $\sqrt{[Ag]_{tumor}}$ . Therefore, when available  $[Ag]_{tumor}$  is decreased 10-fold due

to the presence of unlabeled competitor, the model predicts that the penetration distance will increase by a factor of  $\sqrt{10}$ —close to the value observed at a concentration of 0.15 nM at 24 hours (Figure 3.4.2d, black bars). At higher concentrations (gray bars) and later time points, this ratio decreases to 1, as the spheroids become completely saturated to their centers under both conditions (error bars represent the variation in spheroid size). As predicted theoretically<sup>1,2</sup> and shown experimentally previously<sup>20</sup>, increasing antibody dose is one route to overcoming the binding site barrier.

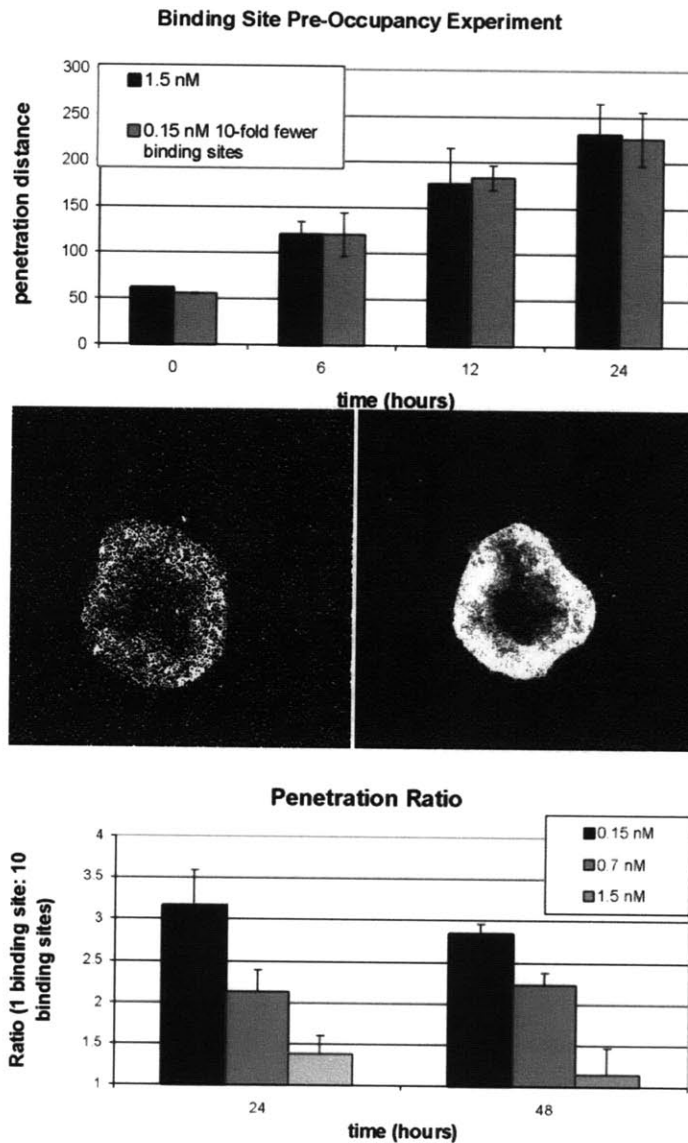


**Figure 3.4.2: Antigen density affects spheroid penetration.** (a) LS174T spheroids were labeled with 1.5 nM fluorescent A33 antibody (black), or 0.15 nM fluorescent and 1.35 nM non-fluorescent competitor (gray). The penetration distance of the fluorescent antibody into spheroids under each condition was highly correlated over time. (b-c) Representative image of an LS174T spheroid at 24 hours labeled with 0.15 nM fluorescent and 1.35 nM non-fluorescent competitor (b), or 1.5 nM fluorescent antibody (c). (d) Ratio of penetration for spheroids with differing numbers of available binding sites (1:10) at 0.15, 0.7, and 1.5 nM doses of fluorescent antibody at 24 and 48 hours. The penetration ratio is a maximum of 3.2 at the lowest concentration, very close to the predicted value of  $\sqrt{10}$  (horizontal line). Over time and at greater concentrations, this ratio approaches a value of 1 as the spheroids become saturated, setting an upper limit on the penetration distance.

### **3.4.3 Penetration studies utilizing different cell lines**

In order to explore the dependence on antigen density by an independent method, spheroids were grown from cell lines expressing different levels of antigen. SW1222 cells express one-fifth as much A33 antigen as LS174T cells (data not shown). This five-fold decrease in antigen density is predicted to lead to a  $\sqrt{5}$  increase in penetration distance. As can be seen at 12 hours, 1.5 nM antibody almost completely penetrates the SW1222 spheroid, while advancing only a few cell layers in an LS174T spheroid (Figure 3.4.3a vs. b). The relative distance that the antibody front penetrates in each spheroid cell type was quantified and is given over a range of concentrations at 12 hours (Figure 3.4.3c). When these penetration distances are taken as a ratio, they agree well with the model prediction (Figure 3.4.3d).

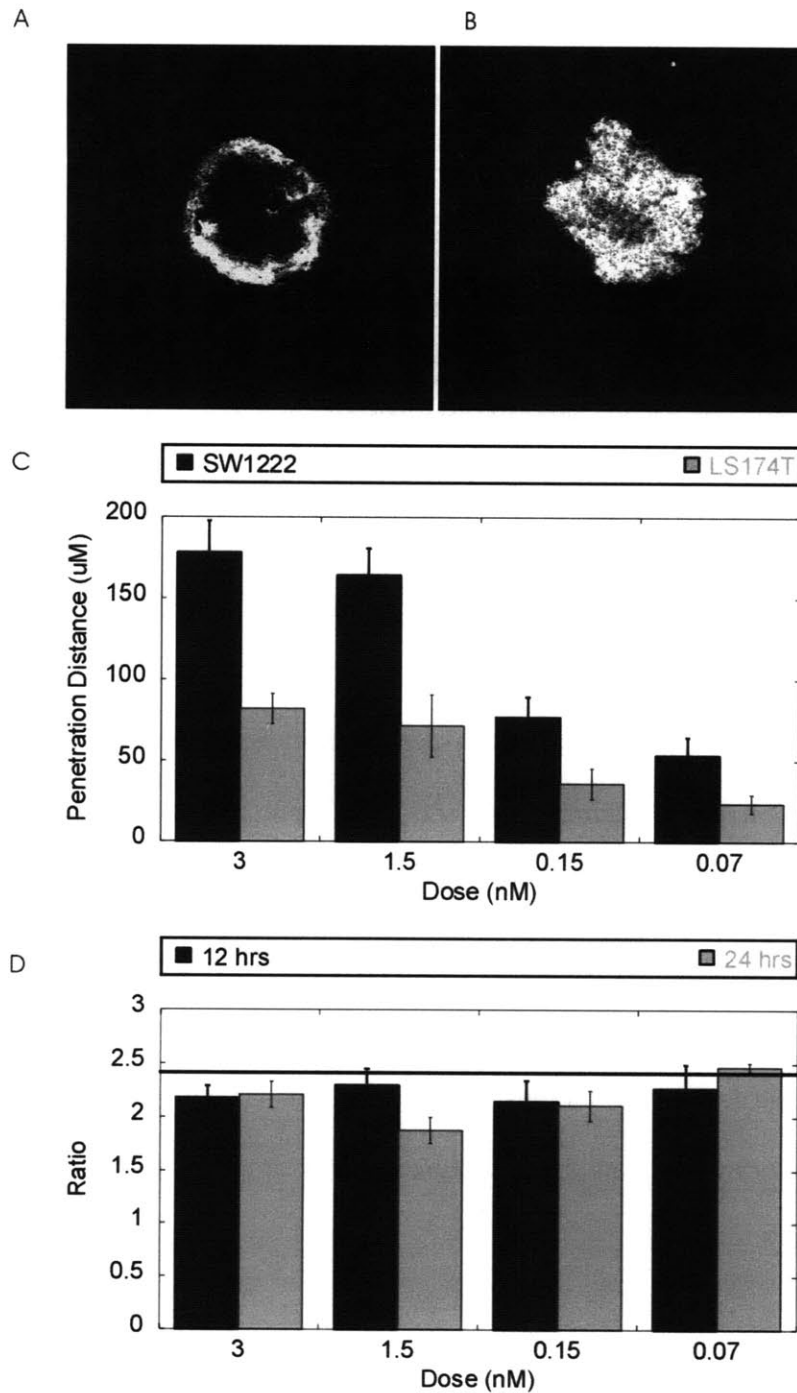


**Figure 3.4.3: Antigen density affects spheroid penetration.** (a-b) Representative images of an LS174T (a) and SW1222 (b) spheroids labeled with 1 nM A33 antibody at 12 hours. (c) Penetration distance into SW1222 (black) and LS174T (gray) spheroids at 12 hours. (d) Ratio of penetration (SW1222:LS174T) at 12 (black) and 24 (gray) hours, and the predicted value of 2.45 (horizontal line).

#### **3.4.4 Antigen internalization and turnover affects penetration**

In order to study the effect of internalization rate on penetration, we utilized antibodies against CEA that exhibit differing internalization rates. Despite binding to the same cellular target, M85151a and M111147 display an approximately 3-fold difference in internalization rate<sup>21</sup>. This difference is likely related to antibody M85151a's recognition of two epitopes per CEA molecule, allowing crosslinking of the antigen. When the increased internalization rate of M85151a and a 2-fold increase in binding sites are incorporated into the model, M111147 is predicted to penetrate into spheroids 2.3-fold further than M85151a. Indeed, when LS174T spheroids were incubated with each of these antibodies, there were clear differences in penetration. The more quickly internalizing M85151a ( $t_{1/2}$  5 hours) clearly penetrates the spheroid to a lesser extent than M111147 ( $t_{1/2}$  13 hours). Figures 3.4.4a and b are representative sections of spheroids labeled with M85151a and MS111147, respectively. To quantitatively compare the difference in penetration, the ratio of the penetration distances of slow to fast internalizing antibodies was taken at various concentrations (Figure 3.4.4c). Here again, at early times and low concentrations, before spheroids become saturated and the ratio approaches unity, the data was found to agree well with the model prediction of a 2.3-fold difference.



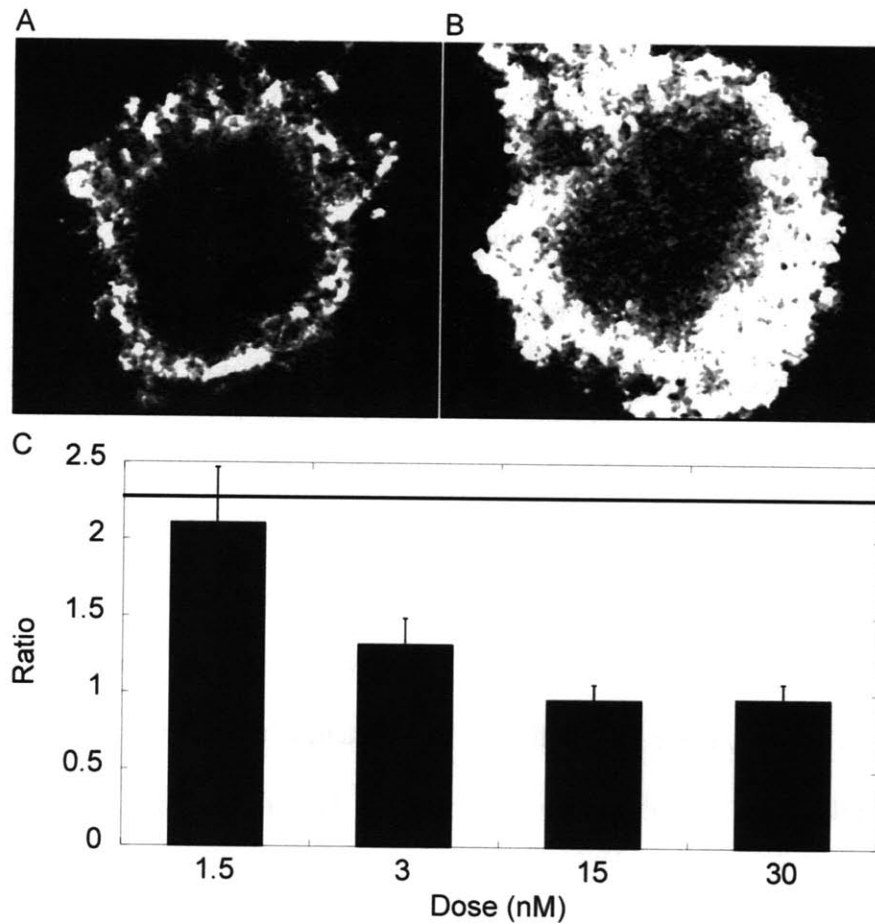


**Figure 3.4.4: Antigen internalization and turnover affects penetration. (a-b)** Representative images of LS174T spheroids labeled with 1.5 nM CEA antibody M85151a (a) or M111147 (b). **(c)** Ratio of penetration depth (slow-M111147: fast-M85151a) over a range of concentrations at 48 hours, as compared to the predicted value of 2.3. At greater concentrations this ratio damps out to a value of 1 as the spheroids become saturated, setting an upper limit on the penetration distance.

### 3.4.5 Antigen internalization reaches a steady state with diffusion

Thus, both antigen turnover and antigen density have significant effects on tumor penetration and should be considered in the selection of targets. While a high antigen density is beneficial for increasing the exposure of each cell to the therapeutic, excessively high density inhibits penetration and increases heterogeneity. Likewise, antigen turnover results in continual replenishment of available binding sites, and can thereby act as a bottomless sink for therapeutic and block further tissue penetration. Figure 3.4.5 compares two alternative antigens. Both A33 and CEA are present at similar expression levels in LS174T cells and each has a long history of study as a target in radioimmunotherapy of colon cancer<sup>22-26</sup>. However, CEA has a metabolic turnover half-life of 15 hours<sup>21</sup>, while the half-life of A33 stretches out to almost 60 hours<sup>16</sup>. Even the seemingly slow internalization rate of CEA has a significant effect on tumor penetration. Figures 3.4.5a and b present the distance penetrated by various antibody doses over time. A 150 nM concentration of anti-CEA antibody has saturated the spheroid by the first timepoint, at 6 hours. Therefore, at this concentration, the increase in the penetration distance beyond that at 6 hours is due to growth of the spheroid, and this line represents the maximum penetration distance achievable. At low concentrations, penetration arrests when antibody diffusion comes to steady state with antigen turnover (Figure 3.4.5a). This arrest is evident as a stalled fluorescence front, which can be observed in 24 and 48 hour images of cells exposed to 1.5 nM anti-CEA antibody (Figure 3.4.5c top panel). As a result, at this concentration of therapeutic, cells at the center of the spheroid will never be exposed.

In contrast, the slower internalization rate of A33 not only allows 1.5 nM antibody (Figure 3.4.5c center panel) to continue to progress towards the center, but even 0.07 nM doses (bottom panel) continue to progress and reach the spheroid center eventually. Significantly, antibodies to A33 have been shown to accomplish penetration to the core of tumors in vivo in clinical trials<sup>22,23</sup>—an unusual result for an IgG. We hypothesize that the slow rate of antigen turnover contributes significantly to this highly desirable attribute.

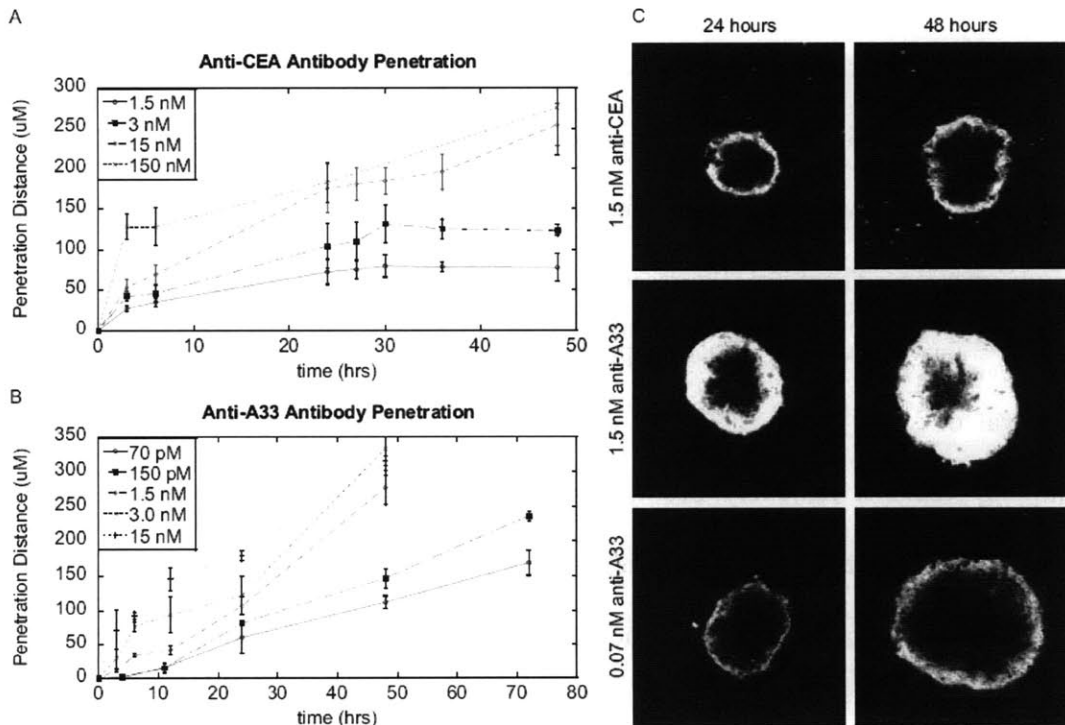


**Figure 3.4.5: Antigen internalization reaches a steady state with diffusion and can limit penetration.** Penetration of anti-CEA (a) and anti-A33 (b) antibodies into LS174T spheroids. At low concentrations, anti-CEA antibody penetration plateaus at a given radius, while antibodies to A33 accomplish penetration at much lower concentrations. (c) Representative images of spheroids at 24 (left) and 48 (right) hours with 1.5 nM anti-CEA Ab (top), 1.5 nM anti-A33 Ab (middle), and 0.07 nM anti-A33 Ab. After 24 hours, antibody to CEA does not penetrate further into the spheroid mass, despite elapsed time.

### **3.4.6 Differential turnover and accessibility of A33 and CEA**

Therapeutic strategies such as pre-targeted radioimmunotherapy (pRIT), antibody-directed enzyme prodrug therapy (ADEPT), and antibody-dependent cellular cytotoxicity (ADCC) rely on sustained accessibility of the tumor-bound therapeutic to a second agent, and are therefore negatively impacted by internalization. As a means to study the effect of internalization and turnover on the surface accessibility of antibody over time, spheroids were grown in antibody, washed, incubated in fresh media, and imaged daily in order to follow the fate of bound antibody. Over the period of observation, fluorescent signal may decrease due to antibody internalization and degradation, or unbinding and diffusion out of the spheroid, or, in the case of CEA, when antigen is shed. As in previous experiments, spheroids continue to grow over the period of observation. Therefore, fluorescence is also diluted via the division of labeled cells. Figure 3.4.6a shows the observed patterns of staining over the course of 4 days after removal of label. A33 and CEA show dramatically different staining patterns: A33 antibody remains relatively evenly distributed throughout the spheroid, while CEA exhibits a punctuate localization pattern.

In order to visualize the amount of antibody that remained surface localized 4 days after removal of the antibody from culture media, spheroids were incubated with a secondary antibody (anti-mouse PE conjugate), washed, and imaged (Figure 3.4.6b). Strikingly, much of the anti-A33 antibody remains surface-localized and accessible to secondary, while with the exception of a few punctuate regions, accessible anti-CEA antibody is largely absent. Considering the secondary labeling antibody as a proxy for

the second agent in any multistep targeting strategy such as PRIT or ADEPT, Figure 3.4.6b illustrates a marked preference for A33 as a target.

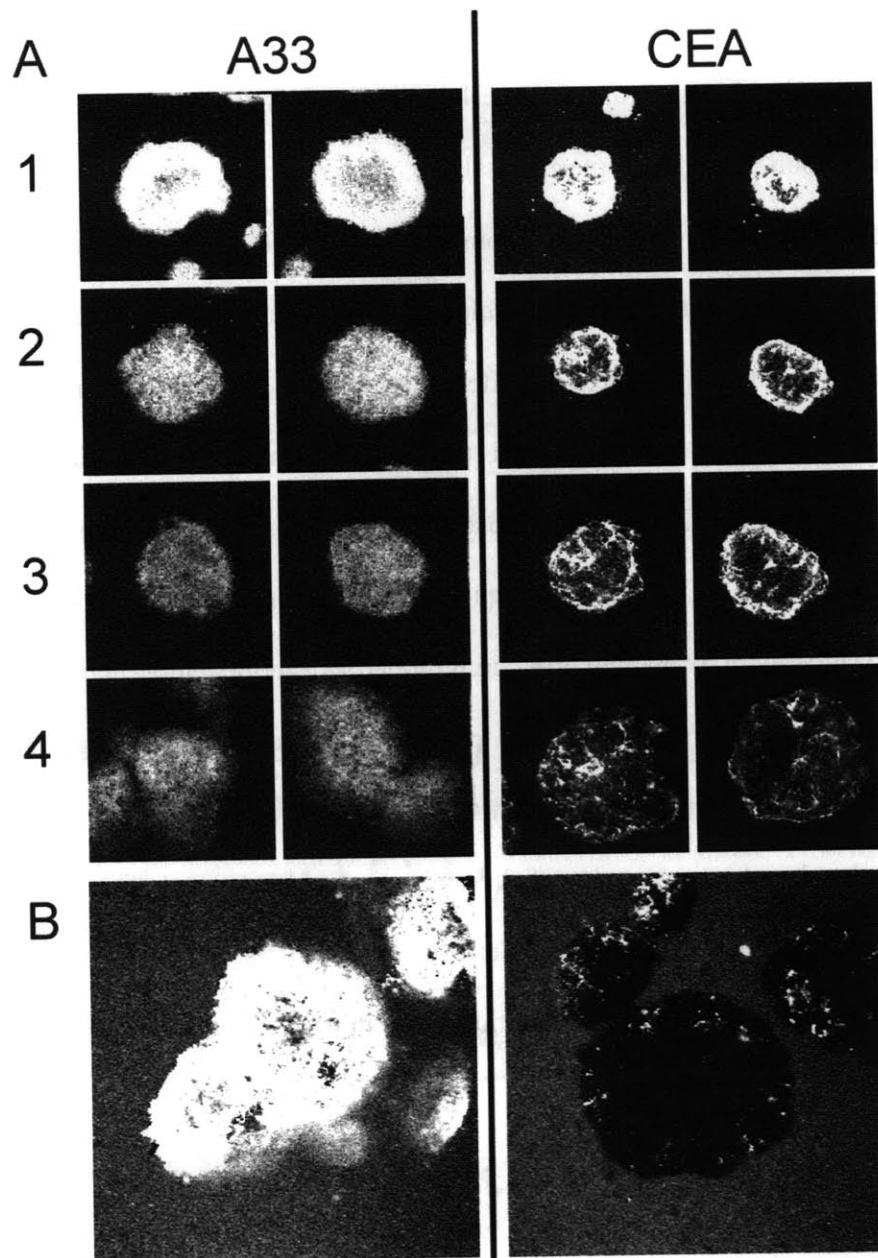


**Figure 3.4.6: Differential in-spheroid turnover and accessibility of A33 and CEA antibody over time.** (a) Images of LS174T spheroids grown in A33 (left) or CEA (right) antibody. Antibody was then removed from the bulk, and spheroids were imaged 1-4 days post removal to follow the localization and persistence of fluorescent antibody. (b) 4 days after label was washed out, spheroids were labeled with an anti-mouse antibody conjugated with PE, allowing identification of the surface accessible primary antibody.

### 3.5 Discussion

The limited tissue penetration of antibody drugs is an obstacle to successful solid tumor immunotherapy and has led to diverse efforts to increase tumor exposure<sup>3</sup>. A variety of drug-level optimizations have been pursued, including increasing diffusivity and extravasation, extending plasma half-life, and lowering affinity—each aimed to increase penetration and improve the homogeneity of solid tumor exposure. Similarly, tumor microenvironment has been manipulated in order to favor better penetration. Various investigators have studied the effect of altering the extracellular matrix, vascular transport, and interstitial pressure and transport parameters, often via combination therapy<sup>15,27-31</sup>. Clearly, there is widespread recognition that a good penetration profile is critical to therapeutic success and consequently much effort has been put into optimizing tumor exposure—both by manipulating drug properties and the tumor microenvironment.

However, less attention has been paid to the properties of the target antigen that might pose intrinsic limits to penetration. Previous theory predicts that both the expression level and turnover rate of the antigen can affect penetration<sup>1,2</sup>. This study provides experimental evidence that under some circumstances antigen properties can be the determining factor in tumor penetration, and supports the selection of antigens with slower turnover and lower expression.

As this report demonstrates, antigen density can have a dramatic effect on tumor penetration. Of course, the greater penetration observed with lower antigen density is in direct opposition to the practice of selecting highly expressed tumor antigens in order to increase the amount of drug to which each cell is exposed. And, somewhat ironically, to the extent that expression level has been manipulated in targeting, it has been to

upregulate expression via interferon gamma treatment<sup>28</sup>, which, as shown here, would be predicted to decrease overall penetration depths.

In practice, once an antigen is expressed at levels sufficient to recruit a lethal dose of therapeutic, additional antigen counterproductively leads to poorer tumor penetration, and a more heterogeneous dosing of the tumor. Since the level of expression sufficient to induce cytotoxicity may vary widely depending on the mode of therapy used, bounds for optimal antigen expression levels will be case-specific. Highly potent toxic modalities such as alpha emitters or some protein toxins may be best suited for low antigen expression, while other less potent therapeutics may require high expression to be effective. Nonetheless, regardless of the expression level required for cytotoxic effect, incremental expression above that level incurs a cost in terms of reduced penetration.

We have also demonstrated that turnover can set an inherent limit to penetration: if the target is replaced at a rate similar to the diffusion of the therapeutic through tissue, complete penetration may be impossible. Here too, however, the preferred antigen turnover rate will depend on the mechanism of cell killing, since internalization is critical to immunotoxin and antibody-drug conjugate therapies, for example. Slow turnover remains desirable for penetration, but internalization is necessary for efficacy in such cases—leaving the goals of reaching distal cells and high drug activity in direct opposition. In contrast, two step therapies, such as ADEPT, pRIT, or effector function rely on persistent surface localization and antibody/antigen turnover acts to directly decrease cell killing. Because altering a single parameter can have multiple and even competing effects, it is instructive to look to quantitative, predictive models to assess such tradeoffs when designing therapies. The complexity of relationships between

transport, binding, and other kinetic processes can lead to non-intuitive outcomes which are captured by a properly formulated model.

Differences between A33 and CEA, the two targets used in this study, likewise highlight the importance of target-tailored therapy design. The more rapid turnover of CEA has multiple implications. First, a greater dose of therapeutic is required to achieve equivalent penetration. Secondly, as time passes, progressively less targeting drug remains surface localized and able to bind a second agent in a two-step therapy. Conversely, more molecules of immunotoxin are internalized during a given period of time, likely making CEA the preferred target for immunotoxin therapy, relative to A33.

In contrast, the relative stability of A33 is especially promising for two-step therapies. Observations made here as to the ability of antibodies to A33 to penetrate spheroids at even extremely low doses are paralleled by experience in the clinic, where even the necrotic centers of tumors are labeled<sup>22,23</sup>, and where antibody is detectable a month and a half after administration. This stable profile would allow for both improved dosing of distal cells, as well as the recruitment of the toxic effector at a level similar to antigen expression. The fact that clinically observed differences between the penetration of antibodies against A33 relative to other targets are reproduced here suggests both that the spheroids used here are a reasonably representative model of *in vivo* tumors, and that antigen properties are indeed relevant to clinical biodistribution results.

While antibody therapeutics have well-demonstrated difficulty in penetrating tissue, this difficulty is generally ascribed to their large size. However, there is a significant body of literature describing the inability of even small molecule drugs to penetrate tissue. Clearly, if even orders of magnitude changes in size, extravasation, and



diffusivity cannot lead to thorough tumor penetration, there are other parameters that must have a considerable impact on distribution and penetration. Minchinton and Tannock provide an excellent review of the distribution of small molecules in tumors as a factor in therapeutic outcome<sup>4</sup>. Many of the factors cited to influence antibody penetration also figure prominently for small molecules, and it is likely that the target properties explored here can play a similar role in determining the distribution and efficacy of small molecules.

Overall, the data presented here quantitatively validates the model of Thurber et al.<sup>1</sup> and demonstrates the importance of antigen-specific parameters in tumor penetration. As tissue penetration is a significant hurdle in the success of therapeutics, care must be taken not only to optimize the properties of the drug itself in order to maximize penetration, but also in the selection of target antigen. Dosing of distal regions of tumors is best achieved by selecting highly stable targets that are not expressed above the level necessary for recruitment of a toxic dose of therapeutic. While a high antigen density is beneficial for increasing the exposure of each cell to the therapeutic, excessively high density inhibits penetration and increases heterogeneity. Likewise, antigen turnover results in continual replenishment of available binding sites, and can thereby act to block further tissue penetration. Each molecule of antigen that is either turned over or present in excess incurs a real cost in terms of penetration—a significant obstacle to the development of effective therapies for solid tumors.

### 3.6 Works Cited

1. Thurber, G.M., Zajic, S.C. & Wittrup, K.D. Theoretic criteria for antibody penetration into solid tumors and micrometastases. *J Nucl Med* **48**, 995-9 (2007).
2. Graff, C.P. & Wittrup, K.D. Theoretical analysis of antibody targeting of tumor spheroids: importance of dosage for penetration, and affinity for retention. *Cancer Res* **63**, 1288-96 (2003).
3. Beckman, R.A., Weiner, L.M. & Davis, H.M. Antibody constructs in cancer therapy: protein engineering strategies to improve exposure in solid tumors. *Cancer* **109**, 170-9 (2007).
4. Minchinton, A.I. & Tannock, I.F. Drug penetration in solid tumours. *Nat Rev Cancer* **6**, 583-92 (2006).
5. Jain, R.K. Transport of molecules, particles, and cells in solid tumors. *Annu Rev Biomed Eng* **1**, 241-63 (1999).
6. Thurber, G.M., Schmidt, M.M. & Wittrup, K.D. Antibody tumor penetration: Transport opposed by systemic and antigen-mediated clearance. *Advanced Drug Delivery Reviews* **in press**(2007).
7. van Osdol, W., Fujimori, K. & Weinstein, J.N. An analysis of monoclonal antibody distribution in microscopic tumor nodules: consequences of a "binding site barrier". *Cancer Res* **51**, 4776-84 (1991).
8. Adams, G.P. et al. High affinity restricts the localization and tumor penetration of single-chain fv antibody molecules. *Cancer Res* **61**, 4750-5 (2001).
9. Dennis, M.S. et al. Imaging tumors with an albumin-binding Fab, a novel tumor-targeting agent. *Cancer Res* **67**, 254-61 (2007).
10. Covell, D.G. et al. Pharmacokinetics of monoclonal immunoglobulin G1, F(ab')<sub>2</sub>, and Fab' in mice. *Cancer Res* **46**, 3969-78 (1986).
11. Colcher, D. et al. Pharmacokinetics and biodistribution of genetically-engineered antibodies. *Q J Nucl Med* **42**, 225-41 (1998).
12. Dennis, M.S. et al. Albumin binding as a general strategy for improving the pharmacokinetics of proteins. *J Biol Chem* **277**, 35035-43 (2002).
13. Kenanova, V. et al. Tailoring the pharmacokinetics and positron emission tomography imaging properties of anti-carcinoembryonic antigen single-chain Fv-Fc antibody fragments. *Cancer Res* **65**, 622-31 (2005).
14. Ghetie, V. et al. Increasing the serum persistence of an IgG fragment by random mutagenesis. *Nat Biotechnol* **15**, 637-40 (1997).
15. Netti, P.A. et al. Enhancement of fluid filtration across tumor vessels: implication for delivery of macromolecules. *Proc Natl Acad Sci U S A* **96**, 3137-42 (1999).
16. Ackerman, M.E. et al. A33 Antigen Displays Persistent Surface Expression *Cancer Immunol Immunother* **in press**(2008).
17. Kelm, J.M., Timmins, N.E., Brown, C.J., Fussenegger, M. & Nielsen, L.K. Method for generation of homogeneous multicellular tumor spheroids applicable to a wide variety of cell types. *Biotechnol Bioeng* **83**, 173-80 (2003).
18. Sutherland, R.M. & Durand, R.E. Radiation response of multicell spheroids--an in vitro tumour model. *Curr Top Radiat Res Q* **11**, 87-139 (1976).

19. Pluen, A. et al. Role of tumor-host interactions in interstitial diffusion of macromolecules: cranial vs. subcutaneous tumors. *Proc Natl Acad Sci U S A* **98**, 4628-33 (2001).
20. Saga, T. et al. Targeting cancer micrometastases with monoclonal antibodies: a binding-site barrier. *Proc Natl Acad Sci U S A* **92**, 8999-9003 (1995).
21. Schmidt, M.M., Thurber, G.M. & Wittrup, K.D. Kinetics of anti-CEA antibody internalization: negligible effects of affinity, bivalency, or stability. **manuscript in preparation**(2008).
22. Welt, S. et al. Quantitative analysis of antibody localization in human metastatic colon cancer: a phase I study of monoclonal antibody A33. *J Clin Oncol* **8**, 1894-906 (1990).
23. Scott, A.M. et al. A phase I trial of humanized monoclonal antibody A33 in patients with colorectal carcinoma: biodistribution, pharmacokinetics, and quantitative tumor uptake. *Clin Cancer Res* **11**, 4810-7 (2005).
24. Liersch, T. et al. Update of carcinoembryonic antigen radioimmunotherapy with (131)i-labetuzumab after salvage resection of colorectal liver metastases: comparison of outcome to a contemporaneous control group. *Ann Surg Oncol* **14**, 2577-90 (2007).
25. Goldenberg, D.M., Gaffar, S.A., Bennett, S.J. & Beach, J.L. Experimental radioimmunotherapy of a xenografted human colonic tumor (GW-39) producing carcinoembryonic antigen. *Cancer Res* **41**, 4354-60 (1981).
26. Begent, R.H. et al. Clinical evidence of efficient tumor targeting based on single-chain Fv antibody selected from a combinatorial library. *Nat Med* **2**, 979-84 (1996).
27. Jang, S.H., Wientjes, M.G. & Au, J.L. Enhancement of paclitaxel delivery to solid tumors by apoptosis-inducing pretreatment: effect of treatment schedule. *J Pharmacol Exp Ther* **296**, 1035-42 (2001).
28. Brouwers, A.H. et al. Interferons can upregulate the expression of the tumor associated antigen G250-MN/CA IX, a potential target for (radio)immunotherapy of renal cell carcinoma. *Cancer Biother Radiopharm* **18**, 539-47 (2003).
29. Jain, R.K. Antiangiogenic therapy for cancer: current and emerging concepts. *Oncology (Williston Park)* **19**, 7-16 (2005).
30. Mok, W., Boucher, Y. & Jain, R.K. Matrix metalloproteinases-1 and -8 improve the distribution and efficacy of an oncolytic virus. *Cancer Res* **67**, 10664-8 (2007).
31. McKee, T.D. et al. Degradation of fibrillar collagen in a human melanoma xenograft improves the efficacy of an oncolytic herpes simplex virus vector. *Cancer Res* **66**, 2509-13 (2006).

## Chapter 4: Multi-step tumor targeting with a bispecific A33 antibody

### 4.1 Abstract

Here we describe the *in vitro* characteristics and *in vivo* biodistribution of a multi-step tumor targeting therapy utilizing a novel bispecific antibody which recognizes both the A33 antigen and a small molecule radiometal chelate. This bispecific antibody consists of a typical IgG molecule with an additional scFv domain fused to the C-terminus of the IgG light chain, generating a tetravalent molecule capable of recognizing 2 copies of the A33 tumor antigen, and 2 small molecule radiometal chelates. Following *in vitro* testing, the A33 bispecific was administered to mice bearing SW1222 xenograft tumors and its biodistribution was determined. Subsequent preliminary experiments have characterized the effect of a clearing step utilized to block and eliminate the remaining blood pool fraction of bispecific prior to administration of a radioactive DOTA chelate and determinations of its biodistribution and tumor uptake. These studies strongly support further investigation of the A33 antigen as a target in multi-step immunotherapy.

---

Major portions of this chapter are the result of collaborations with Kelly Davis, MIT and Peter Smith-Jones, Memorial Sloan Kettering Cancer Center

## 4.2 Background

The recent success of several radioimmunotherapeutics has demonstrated proof of principle for this type of targeted cancer therapy<sup>1</sup>. Unfortunately, in many potential applications, bone marrow toxicity limits therapy. In order to circumvent this toxicity, a two-step strategy, known as pretargeted immunotherapy (PRIT) has been proposed, in which the targeting construct and radionuclide are separated into two distinct dosing steps. In this way, one preserves the specificity of antibody binding in tumor targeting, but eliminates the toxic effects of long-lived directly labeled antibodies. When compared to single step therapies using directly labeled antibodies, PRIT has generally lead to lower toxicity and better efficacy<sup>2-4</sup>. However, the addition of a separate step constrains the desirable kinetic attributes of the cellular target in comparison with direct RIT, immunotoxin therapy, or approaches relying on effector functions. In PRIT, the competing interests of target saturation, clearance of unbound construct from the circulation, availability of the construct to chelated radionuclide, sufficient proximity to the nucleus relative to decay pathlength, and the halflife of the radionuclide must all be taken into consideration. This study seeks to determine if the A33 antigen, a member of the immunoglobulin superfamily (IGSF) with homology to cell adhesion<sup>5</sup> and tight junction-associated (TJ) proteins, possesses the properties particularly suited for PRIT.

The A33 antigen has been a target for immunotherapy of colon cancer in numerous clinical studies<sup>6-13</sup>. However, the clinical success of the directly radiolabeled antibodies used has been limited by both the high level of expression in normal colon, and high blood and bone marrow toxicity caused by the long plasma halflife of the antibody. In order to circumvent these toxicities, we have aimed to target the A33

antigen in a multi-step therapeutic strategy, in which a bifunctional antibody-based drug which possesses recognition domains to both the A33 antigen and small molecule radionuclide chelate is administered, allowed to clear from blood and normal colon, and then a small molecule radionuclide, with rapid clearance pharmacokinetics is administered and allowed to bind to the bifunctional antibody localized to the tumor. This multistep strategy separates targeting from toxic functionalities and thereby allows the slow blood clearance to work in favor of better tumor uptake and distribution rather than against therapeutic success as a cause of dose-limiting toxicity. The subsequent administration of a small molecule radiometal chelate that is cleared rapidly from circulation unless bound to the bispecific provides highly specific tumor dosing.

We utilize a novel and simple bispecific antibody format in which an scFv is fused to the C-terminus of the light chain of an IgG to create an IgG-like bifunctional antibody. This topology, which has been developed and characterized by Kelly Orcutt in the Wittrup lab, functions as a general platform to combine two binding specificities, and retains parental affinity of the binding domains, and IgG-like stability and *in vivo* pharmacokinetics. Similarly, simple production and purification after mammalian cell expression is performed by protein A chromatography. This format, schematized in Figure 4.2, is a simple standardized platform for the construction of functional bispecific antibodies.

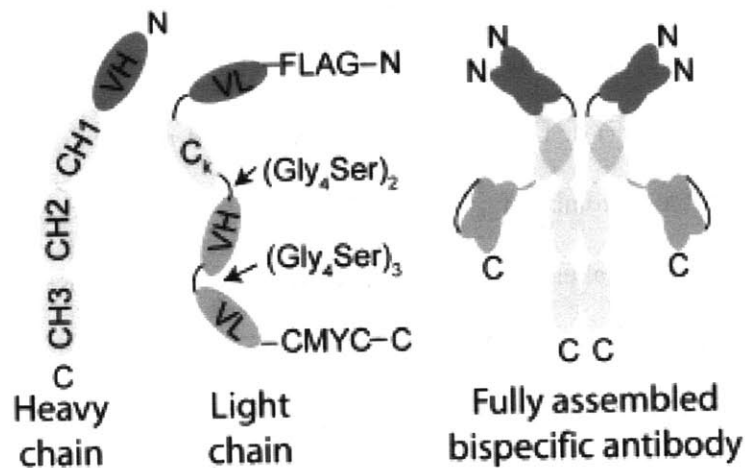


**Figure 4.2: Schematic of bispecific antibody topology.** Design of IgG light chain with C-Terminal scFv Fusion. Pictorial representation of heavy chain, light chain, and fully assembled bispecific antibody with indicated N- and C- termini. The light chain is modified with an scFv fusion to the C-terminus, while a completely native heavy chain is preserved.

While monoclonal antibodies have shown success in the clinic for a variety of diseases<sup>14</sup>, multi-specific antibodies, with an ability to bind to more than one target, may further improve clinical efficacy via novel mechanisms. Multi-specific antibodies have been engineered for a variety of applications including enhanced antibody-dependent cell mediated cytotoxicity (ADCC)<sup>15,16</sup>, surface-receptor blocking and downregulation<sup>17</sup>, simultaneous binding to two soluble effector molecules, and pretargeting tumor cells for the subsequent capture of radionuclides<sup>4</sup>, drugs<sup>18</sup>, and prodrugs<sup>19</sup>.

The simple bispecific format utilized here contrasts sharply with alternatives including chemical conjugation<sup>20</sup>, co-expression of two antibodies with different specificities through the hybrid hybridoma technique<sup>21</sup>, complex alterations to heavy chain domains<sup>22</sup>, recombinant methods to produce scFv fusions, diabodies, scFv Fc fusions, and single variable domain IgGs, among others which frequently require construct-specific optimization<sup>23-27</sup>.

Two versions of A33 targeting bispecific were constructed, each incorporating a different A33-binding variable domain<sup>10,28</sup>, and an scFv domain capable of recognizing either fluorescein<sup>29</sup> (ALF) or DOTA<sup>30</sup> (ALDO), and tested *in vitro*. Based on improved *in vivo* stability after radiolabeling, studies of ALDO in xenografted SW1222 tumors in nude mice were undertaken at Memorial Sloan Kettering Cancer Center by our collaborators, Steve Larson and Peter Smith-Jones. While preliminary, these studies demonstrate the superior tumor targeting profile of a multi-step strategy, and encourage the development of clinical protocols utilizing this target as well as the multistep and clearing agents strategies.



### 4.3 Materials and Methods

#### Constructs and protein production

The bispecific format was designed as an scFv fusion to the C-terminus of the light chain of an IgG. The heavy chain is the same as that of an IgG1 and was subcloned into the mammalian expression vector gwiz (Aldevron cat. #5008) as follows: leader-VH-CH1-CH2-CH3, where VH is the variable heavy domain and CH1, CH2, and CH3 are the heavy chain constant domains of IgG1.

The light chain is constructed as leader- VL-VK-(G4S)<sub>2</sub>-scFv-cmyc, where VL is the variable light domain and VK is the kappa light chain constant domain. The heavy chain and light chain were cloned into two separate gwiz plasmids between the pst1 and sal1 restriction sites. The heavy chain and light chain plasmids were transiently co-expressed in HEK293 cells (Invitrogen cat. #11625-019). HEK293 cells were grown in flasks on an orbital shaker platform rotating at 140 rpm at 37°C, 5% CO<sub>2</sub> and were subcultured following the manufacturer's protocols.

Co-transfection of heavy and light chain plasmids was performed with polyethyleneimine (PEI) as the transfection reagent. Briefly, HEK293 cells were subcultured to a cell density of  $0.5 - 0.7 \times 10^6$  cells/mL 24 h before transfection. Immediately before transfection, cells were adjusted to a cell density of  $1 \times 10^6$  cells/mL. 500 µg of each purified plasmid (1 mg/mL) was added to 19 mL Optipro (Invitrogen cat. #12309-019). 2 mL of 1 mg/mL polyethyleneimine pH 7.0 (PEI, MW 25,000, Polysciences cat. # 23966) dissolved in water was added to 18 mL Optipro. Both Optipro solutions were incubated at room temperature for 5 min. The DNA/optipro solution was

added to the PEI/optipro solution and incubated for an additional 10 min at room temperature and then added drop wise to 1 L HEK293 culture. Supernatant was collected 6-8 days after transfection. Antibodies were purified by protein A chromatography (Pierce cat. #22811) following the manufacturer's instructions.

ALF (A33 Light chain bispecific to Fluorescein) and ALDO (A33 Light chain bispecific to DOTA) constructs were made by overlap extension PCR and Quickchange mutagenesis. The ALF bispecific antibody was cloned and produced as described above as an A33 IgG with a 4m5.3 scFv<sup>31</sup> light chain fusion using the VH and VL domains from the A33 binding scFv generated from a rabbit antibody<sup>28</sup>. The ALDO bispecific antibody was based on the clinical A33 antibody<sup>10</sup> with an affinity matured DOTA-binding scFv designated C825 (Orcutt et al., manuscript submitted) based on the wild type 2D12.5 antibody<sup>32</sup>. Both scFvs were disulfide-stabilized by introducing two cysteine residues<sup>33</sup>.

A33 IgG plasmid was produced by introducing two stop codons in the light chain immediately following the CK sequence via Quickchange PCR.

### ***In vitro testing***

#### **Simultaneous Binding Assay**

10<sup>5</sup> trypsinized LS174T cells were washed with 500  $\mu$ L PBS with 0.1% bovine serum albumin (PBSA) and incubated with 50 nM bsAb or IgG for 1 h at room temperature. Cells were then washed once with PBSA and incubated with 100 nM fluorescein (Fl, Invitrogen A-10466), 100 nM DOTA-biotin chelated with yttrium (DOTA-Y-biotin), 50 nM bsAb, or 100  $\mu$ L PBSA. Cells were then washed once with

PBSA and incubated with 20 nM DOTAY-647 or FITC-647. Cells were washed once before analysis by flow cytometry.

Specificity was verified by preincubation of bispecific or IgG with soluble A33 antigen. Antigen extracellular domain was produced in HEK cells as described as a fusion to a short glycine-based linker, a sortase A reaction site, and a his tag.

Recombinantly produced A33 antigen was also chemically biotinylated (Pierce) and used to coat streptavidin beads (Invitrogen 11407) as an alternative to the use of live cells in analysis of the function of bispecific and IgG.

#### Synthesis of haptens

DOTA-biotin was synthesized by dissolving Amine-PEG<sub>3</sub>-Biotin (Pierce 21347) and p-SCN-Bn-DOTA (S-2-(4-Isothiocyanatobenzyl)-1,4,7,10-tetraazacyclododecane-tetraacetic acid; Macrocyclics B-205) in dimethyl sulfoxide (DMSO) with a 10 fold molar excess of triethylamine (TEA, VWR #EM-TX1200-5). The reaction mixture was vortexed at room temperature for 3 h, and then purified by high performance liquid chromatography (HPLC). Briefly, HPLC purification was performed on a C-18 reverse-phase column (Agilent Model 1100 HPLC, 1 x 25 cm, buffer A = 0.05% trifluoroacetic acid (TFA), buffer B = 0.0425% TFA in 80% acetonitrile, 2 – 100% B gradient for 98 min). Flow through was monitored by absorbance detection at 280 nm. Fractions containing DOTA-biotin were confirmed using matrix assisted laser desorption / ionization - time of flight (MALDI-TOF) mass spectrometry (Applied Biosystems Model Voyager DE-STR).

DOTA-647 was synthesized by reacting 1 mM p-SCN-Bn-DOTA with 1 mM Alexa Fluor 647 cadaverine (Invitrogen A-30679) in DMSO with 40 mM TEA overnight at room temperature with rotation. DOTA-647 was purified by HPLC as described above.

Yttrium complexes of DOTA conjugates were prepared by incubating a molar excess of yttrium nitrate hexahydrate (Sigma 237957) with the DOTA conjugates in 0.4 M sodium acetate pH 5.2 buffer overnight at room temperature. The pH was adjusted to 7.0 with 10 M sodium hydroxide and the solution was diluted with PBSA.

Fluorescein-647 (Fl-647) was synthesized by reacting 1 mM (Invitrogen F6130) with 1 mM Alexa Fluor 647 cadaverine in DMSO with 40 mM TEA and rotating overnight at room temperature and used without further purification

#### Affinity Measurements

A33 binding affinities for ALF, ALDO, and A33 IgG were measured using trypsinized LS174T cells that were washed with PBSA and then labeled with varying concentrations of bispecific or IgG for a minimum of 3 hours at 37°C. Cells were then washed once with PBSA and incubated with a 1:200 dilution of protein A Alexa Fluor 647 (Invitrogen P21462) before being washed once again and analyzed by flow cytometry.

#### Clearing Agent

Clearing agent consisted of fluorescein or DOTA-dextran conjugates, and was synthesized by Kelly Orcutt, and its ability to block binding to block the binding of either

fluorescein or DOTA was assessed by incubating bispecific-labeled cells with the dextran-based clearing agent prior to labeling with hapten using flow cytometry.

### ***In vivo testing***

*In vivo* testing was carried out by Peter Smith-Jones at Memorial Sloan Kettering Cancer Center according to standard protocols. Briefly, nude mice were inoculated with human colonic SW1222 cells which were then allowed to grow until tumors reached an appropriate size<sup>34</sup>. Bispecific was labeled using the iodogen method<sup>35</sup>, and the quality and purity of radiolabeled material was assessed by lindmo assay<sup>36,37</sup> and thin layer chromatography. Mice were then injected with <sup>131</sup>I-labeled bispecific, and at varying timepoints, biodistribution was determined. In pre-targeting experiments, 24 hours after 0.2 mg <sup>131</sup>I-nALDO bispecific was administered, 31 pmoles[Y-DOTA]-dextran clearing agent was injected, followed by <sup>111</sup>In-containing DOTA was 4 hours later, and animals were sacrificed one hour later.

## 4.4 Results

### 4.4.1 Bifunctionality tests

In order to test the function of the ALF and ALDO bispecifics, both magnetic beads coated with recombinantly-produced A33 antigen extracellular domain (Figure 4.4.1a), and a suspension of LS174T human colonic cells (Figure 4.4.1b) were incubated with a 50 nM concentration of either ALF or ALDO, and then incubated with either Fluorescein-647 (FL-647), or DOTA-647 hapten, as appropriate. Positive 647 signal in both cases indicates concurrent binding of both arms of the bispecific—both the A33 variable domain to A33 antigen, as well as the scFv to hapten.

Figure 4.4.1c demonstrates the specificity of these interactions on LS174T cells using a series of negative controls, in which preincubation with soluble IgG blocks subsequent labeling with bispecific (wide dash), and preincubation with fluorescein blocks subsequent labeling with FL-647 (thin line), while IgG, which possesses no anti-fluorescein scFv domain, is likewise unlabeled by FL-647 (narrow dash). Similarly, Figure 4.4.1d demonstrates that preincubation with soluble A33 antigen blocks the binding of the bispecific.

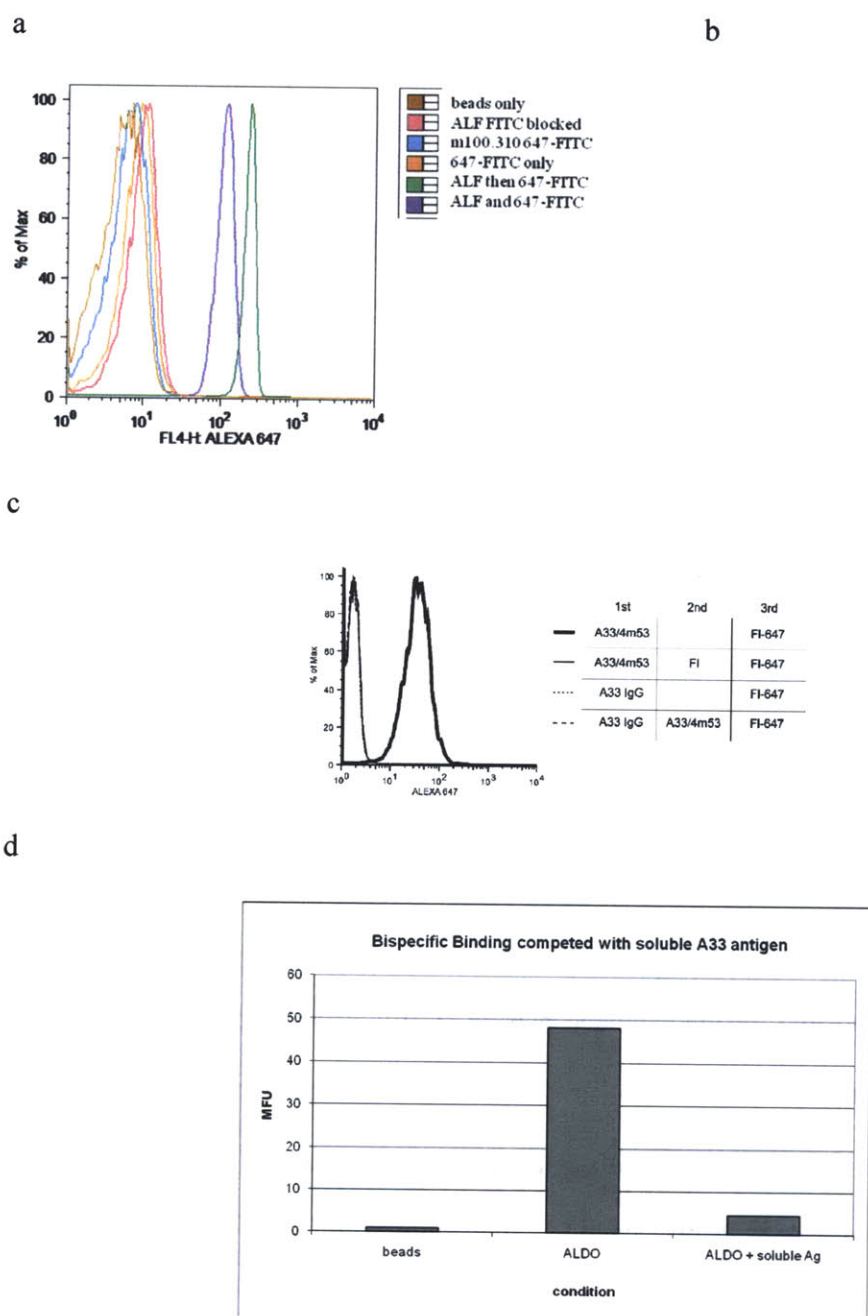


**Figure 4.4.1 Bifunctionality tests:** (a) Histogram of ALF bispecific binding to A33 antigen coated beads and detected by Fl-647. (b) Histogram of ALDO bispecific binding to LS174T cells and detected by DOTA-647 (c) Specificity tests of ALF bispecific indicating that both A33 and fluorescein binding capabilities are competed by soluble ligand and therefore specific. (d) Competition with soluble A33 antigen.

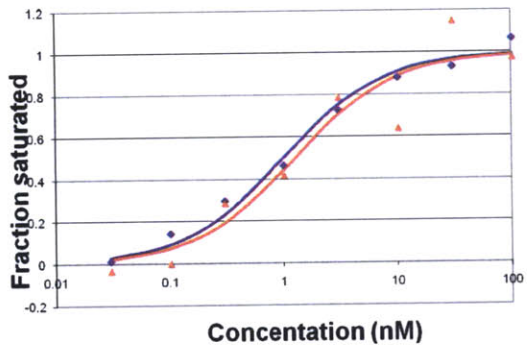
#### 4.4.2 Kd assessments and FcRn binding

The affinity of A33 binding domains were assessed by performing a series of Kd measurements in which LS174T cells were incubated with excess bispecific at varying concentrations for a minimum of 3 hours at 37°C, prior to labeling with a Protein A-647 conjugate. Figure 4.4.2 presents Kd (a) and dissociation (b) curves for both the ALF bispecific and its corresponding IgG derivative. The midpoints, or Kd values for both IgG and bispecific show excellent agreement. Similarly, ALF and ALDO were incubated with human colonic cell lines, and measurements of their Kd values were made. Figure 4.4.2c indicates that both retain the same affinity to antigen as their construct of origin (~1 nM). Additionally, the ability to bind to Protein A indicates that the Fc portion of the bispecific and antibody constructs are folded properly, indicating that they will likely have maintained clearance and pharmacologic properties as derived from interactions with neonatal and Fcγ receptors and complement.

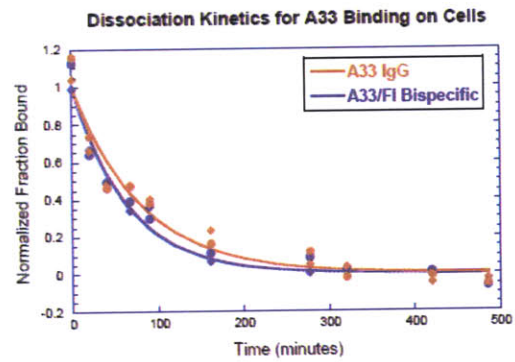
As a means to more directly test binding to FcRn, T84 cells, which express the FcRn receptor responsible for the extended plasma half-life of antibodies were incubated with a panel of antibodies and bispecific. Because the interaction with FcRn is pH dependent, proteins were incubated with cells at both pH 6.0 and 8.0, and detected via labeling with Protein A-488. A pH-dependent interaction is apparent for both the control rabbit IgG as well as ALF bispecific (Figure 4.4.2d).



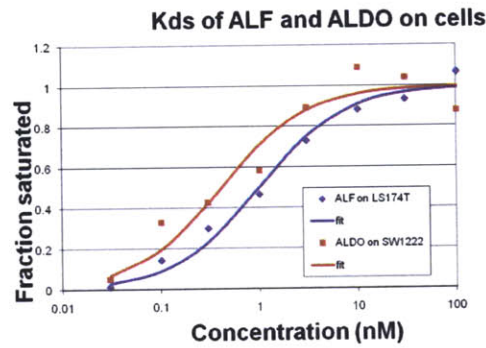
a



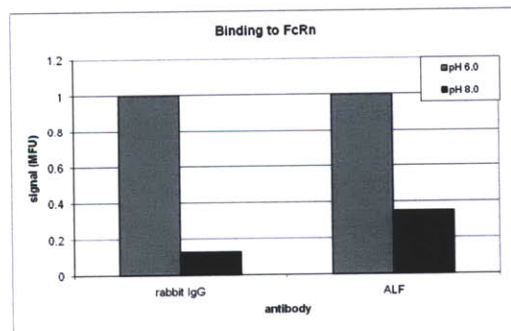
b



c



d



**4.4.2 Kd assessments and binding to FcRn:** (a) Kd curves for ALF (red) and IgG (blue). (b) Dissociation curve of ALF and IgG. (c) Kd curves of ALF and ALDO on human colonic cells. The use of different variable domains and cell lines results in differing Kd values. (d) FACS analysis of the interaction and pH dependence of rabbit IgG and ALF bispecific binding to FcRn expressing T84 cells.

#### 4.4.3 Clearing agent characterization

While the long plasma half-life of antibodies is an excellent feature for increasing the tumor penetration of these molecules, it can be undesirable in terms of blood toxicity, even in with a pre-targeted strategy. Because the tumor localized bispecific will be internalized and degraded at some rate, there are competing interests in terms of having the maximum amount of bispecific accessible in the tumor, and the minimum amount of blood exposure. Even with a stable target antigen such as A33, timepoints prior to complete blood clearance are likely to lead to optimum tumor uptake. Therefore, it is desirable to have a means to decrease blood exposure without waiting for natural IgG clearance mechanisms. We theorized that a blood pool blocking or clearing agent could reduce blood exposure to the radiometal chelate by either blocking the hapten binding sites on the bispecific remaining in circulation, or by triggering rapid clearance of the bispecific. In order to have an effect on only the blood pool of bispecific and not bispecific localized to the tumor, our blocking agent must have a limited ability to extravasate from the blood stream. Accordingly, we have synthesized a high molecular weight dextran conjugated with 10-100s of either DOTA or fluorescein molecules. Bispecific in the blood stream will bind to the hapten conjugated to the dextran, which results in a functional clearing of the blood pool even if the dextran does not trigger rapid clearance of these large complexes. Therefore, we undertook *in vitro* tests to observe whether the hapten binding sites on the bispecific molecule could be blocked by our dextran conjugates by preincubating bispecific with the blocking/clearing agent, and then incubating with antigen coated beads or cells, and detection by Protein A-647, FL-647 or DOTA-647 (Figure 4.4.3, dextran-DOTA results shown only).

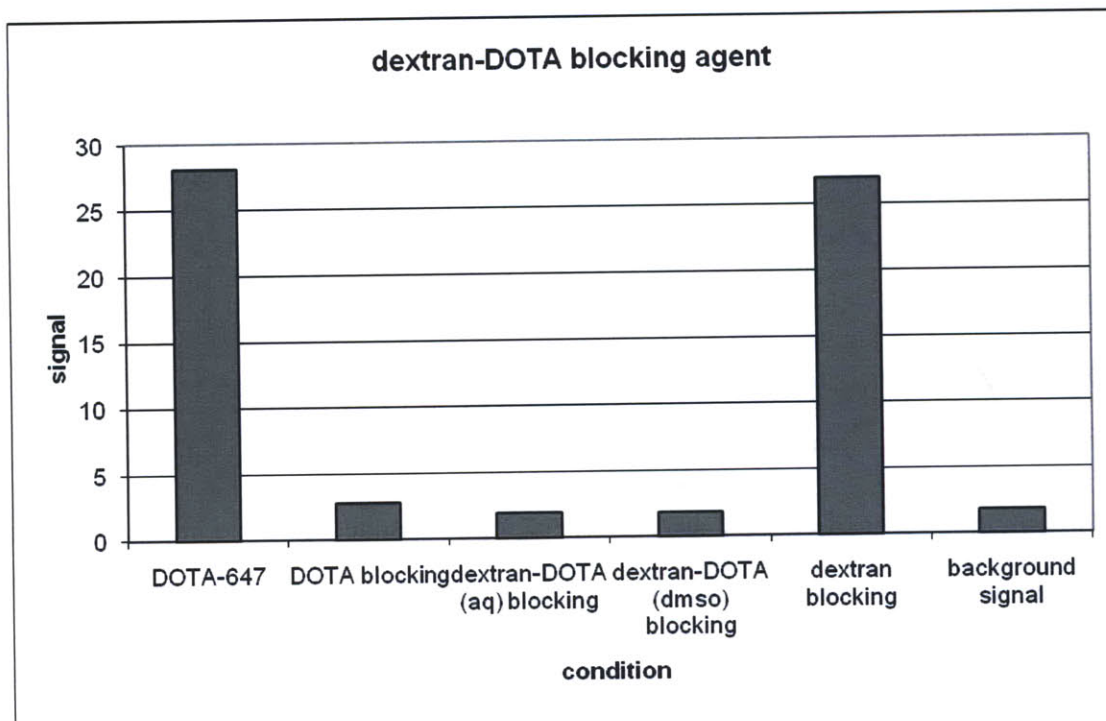


**Figure 4.4.3: Functional tests of blood pool blocking/clearing agent.** FACS analysis of cells incubated with bispecific with and without preincubation with dextran-DOTA synthesized in either water (aq) or dms, and negative controls include blocking by dextran alone.

#### 4.4.4 *In vivo* biodistribution of ALDO

Nude mice bearing SW1222 tumors were injected with  $^{131}\text{I}$  labeled ALDO bispecific at 20  $\mu\text{g}$  per mouse, and biodistribution of bispecific was determined at 4 and 24 hours post injection. Despite having a native Fc domain, ALDO shows a more rapid blood clearance profile than expected. Interestingly, when bispecific is labeled with a DTPA-based method rather than the iodogen method used here, the blood clearance kinetics correspond with IgG (Kelly Orcutt, data not shown), indicating that perhaps the iodogen labeling method used here is damaging. Despite the more rapid clearance profile, ALDO bispecific is seen to accumulate in the tumor.

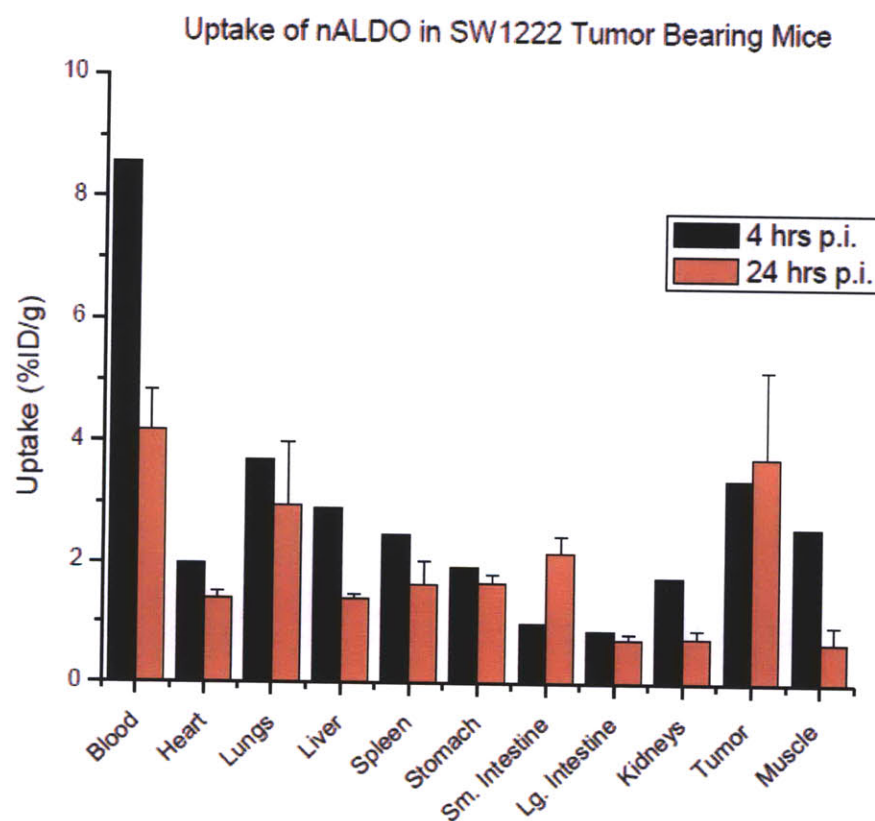


**Figure 4.4.4 *In vivo* biodistribution of ALDO:** The biodistribution of 20  $\mu\text{g}$  of  $^{131}\text{I}$ -ALDO bispecific was determined at 4 and 24 hours post-injection. Uptake is reported as percent injected dose per gram. Clearance from blood is more rapid than expected (8% at 4 hours as opposed to >30%), but tumor uptake is good.

#### 4.4.5 Impact of clearing step

In order to assess the utility of the clearing step, mice were injected with either 0.02 mg of bispecific and imaged at 24 hours or 0.2 mg, followed by clearing agent at 24 hours and imaging at 28 hours. The results of these tests are depicted in Figure 4.4.5. Notably, the clearing agent seems to act not only as a blood pool blocking agent, but actually does trigger rapid clearance of the bispecific from the blood. Consistent with this interpretation of the decreased blood values, uptake is seen to increase in the stomach, which is commonly observed when  $^{131}\text{I}$  metabolites are liberated.

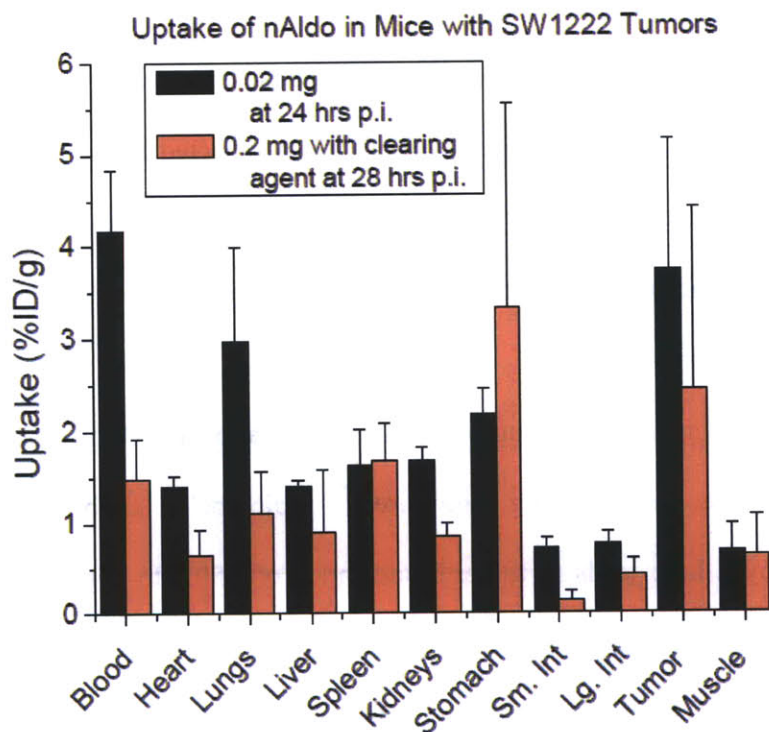


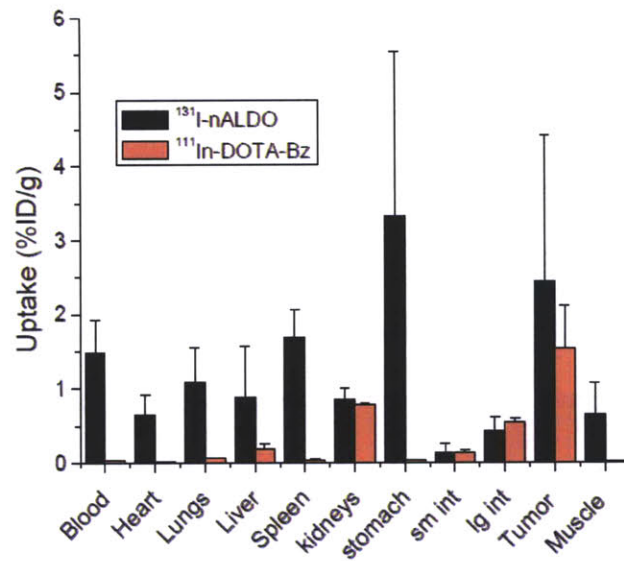
**Figure 4.4.5 Impact of clearing step.** Biodistribution of ALDO with and without subsequent injection of dextran-DOTA clearing agent. The concomitant decrease in blood levels and increase in stomach uptake are consistent with rapid clearance from the blood, and degradation to yield  $^{131}\text{I}$  metabolites demonstrated by the increase in stomach uptake.

#### 4.4.6 *In vivo* biodistribution of DOTA

Finally, in mice treated with 0.2 mg of  $^{131}\text{I}$ -ALDO, followed by dextran-DOTA clearing agent at 24 hours,  $^{111}\text{In}$ -DOTA-Benzene was injected, and its biodistribution was determined. Figure 4.4.6a presents the uptake of ALDO and DOTA in these mice. Notably, though there are significant levels of bispecific in the blood, very little DOTA is located in that compartment. This result indicates that our dextran-DOTA clearing agent functions by both accelerating clearance of the bispecific from the blood, but also by simply blocking the DOTA-binding sites and making them unavailable to bind the  $^{111}\text{In}$ -DOTA-Benzene administered subsequently. Also, in agreement with the release of metabolites, the high stomach level of  $^{131}\text{I}$  does not cause accumulation of DOTA in the stomach. In contrast, there is a high level of DOTA detected in the kidneys, as DOTA undergoes almost exclusive renal clearance. Nonetheless, the tissue with the greatest DOTA uptake is the tumor, resulting in excellent tumor:normal tissue ratios for many compartments (Figure 4.4.6b).

In fact, for most organs, tumor:normal tissue ratios are 10 or more. Notably, as blood toxicity was dose limiting with directly radiolabeled antibody, the multi-step method employed here leads to tumor:blood ratios of  $>50$ . In contrast, this ratio was typically around 2 in single-step therapy protocols. Similarly, the ratios are much improved for a number of other tissues as well. Therefore, pre-targeting has achieved its objective of decreasing the dose-limiting blood toxicity. Unfortunately, the tumor:kidney ratio is only about 2, and this is likely to be the dose limiting organ, as has been true for numerous other pre-targeting systems.

Uptake of nAldo and DOTA-Bz in mice with SW1222 Tumors



MST with nAldo and DOTA-Bz in Mice with SW1222 Tumors

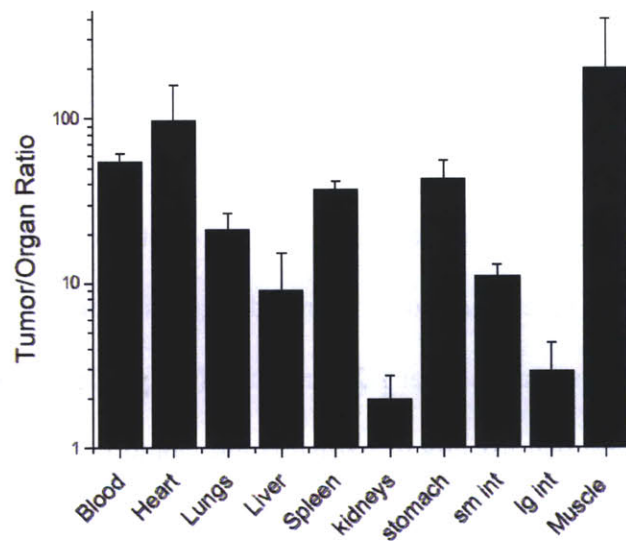


**Figure 4.4.6** *In vivo* biodistribution of DOTA: (a) Biodistribution of <sup>131</sup>I-ALDO (black) and <sup>111</sup>In-DOTA-Benzene (red). (b) Tumor:organ uptake ratios of <sup>111</sup>In-DOTA-Benzene presented on a log scale.

## 4.5 Discussion

Though the results presented here are preliminary, they are encouraging and demonstrate promising outcomes utilizing both this novel bispecific antibody format as well as use of the A33 antigen as a tumor target in multi-step therapy. We have validated a treatment system consisting of administration of a bispecific antibody, a dextran-based clearing agent, followed by a small molecule radionuclide chelate. Other pre-targeting strategies exist, and have shown promise in both animal and clinical studies<sup>38-41</sup>. Compared to multi-step targeting systems utilizing larger haptens, which can lead to uptake in other organs due to altered clearance pharmacology, or utilize streptavidin:biotin, which has high kidney uptake and issues involving endogenous biotin and immunogenicity<sup>42-44</sup>, our system uses simple, well-validated components. DOTA has a long clinical history as an MRI contrast agent, and antibodies and scFvs have been studied extensively.

The A33 antigen is a particularly appropriate choice for pre-targeted radioimmunotherapy on several accounts. First, due to its expression in normal colon, and resulting clinical observations that A33 antibodies only gain tumor specificity after elapsed time, it is likely that toxicity to normal colon would be a likely result of single step treatments. Second, *in vitro* studies have indicated that A33 is a particularly stable target, and that antibodies to A33 have improved penetration profiles and tumor surface persistence compared to other common tumor targets such as CEA<sup>45-47</sup>. By adopting a multi-step strategy, we have improved the tumor:blood radiation ratio from about 2 in the case of directly radiolabeled antibodies to >50.



Furthermore, use of the dextran based clearing or blocking agent has the possibility to improve pre-targeting in numerous systems, and afford particular gains in cases in which less stable antigens are targeted. For a more rapidly turned over tumor target, waiting for bispecific to clear from the blood stream leads to significant turnover of tumor antigen and resulting degradation of tumor-localized bispecific. In these cases, it is highly desirable to dose radioactive hapten shortly after injecting bispecific, and in all cases, *the use of an effect clearing or blocking agent allows investigators to inject hapten when tumor uptake is maximal, rather than when tumor:blood ratio is maximal.*

Unfortunately, our system currently suffers from a flaw common to other pre-targeting strategies: because DOTA undergoes renal clearance, kidney uptake will likely be dose-limiting<sup>41</sup>. Interestingly, as DOTA has been considered an excellent choice for pretargeting due to its rapid clearance, it may be that a slower clearance profile would decrease kidney exposure, as a longer plasma residence time would allow lower doses to achieve improved tumor uptake—resulting in much improved tumor:kidney ratios.

Overall, we have demonstrated that the bispecific construct used in these studies is a robust format, able to maintain the properties of the parental variable domains, is stable *in vivo*, accumulates specifically in tumors and is furthermore able to localize hapten to tumor sites. We have accomplished our end of improving the blood toxicity in A33 immunotherapy. It remains to be seen whether this improvement leads to improved therapeutic outcomes, or whether we have simply substituted dose limiting kidney toxicity for dose limiting blood toxicity. To that end, as mentioned, there are numerous means by which optimization of reagents and protocols might reduce the high kidney uptake observed in these preliminary studies.

#### 4.6 Works Cited

1. DeNardo, G.L. Treatment of non-Hodgkin's lymphoma (NHL) with radiolabeled antibodies (mAbs). *Semin Nucl Med* **35**, 202-11 (2005).
2. Pagel, J.M. et al. Comparison of anti-CD20 and anti-CD45 antibodies for conventional and pretargeted radioimmunotherapy of B-cell lymphomas. *Blood* **101**, 2340-8 (2003).
3. Gruaz-Guyon, A., Raguin, O. & Barbet, J. Recent advances in pretargeted radioimmunotherapy. *Curr Med Chem* **12**, 319-38 (2005).
4. Boerman, O.C., van Schaijk, F.G., Oyen, W.J. & Corstens, F.H. Pretargeted radioimmunotherapy of cancer: progress step by step. *J Nucl Med* **44**, 400-11 (2003).
5. Johnstone, C.N. et al. Characterization of mouse A33 antigen, a definitive marker for basolateral surfaces of intestinal epithelial cells. *Am J Physiol Gastrointest Liver Physiol* **279**, G500-10 (2000).
6. Chong, G. et al. Phase I trial of <sup>131</sup>I-huA33 in patients with advanced colorectal carcinoma. *Clin Cancer Res* **11**, 4818-26 (2005).
7. Sakamoto, J. et al. A phase I radioimmunolocalization trial of humanized monoclonal antibody huA33 in patients with gastric carcinoma. *Cancer Sci* **97**, 1248-54 (2006).
8. Scott, A.M. et al. A phase I trial of humanized monoclonal antibody A33 in patients with colorectal carcinoma: biodistribution, pharmacokinetics, and quantitative tumor uptake. *Clin Cancer Res* **11**, 4810-7 (2005).
9. Welt, S. et al. Phase I/II study of iodine <sup>131</sup>-labeled monoclonal antibody A33 in patients with advanced colon cancer. *J Clin Oncol* **12**, 1561-71 (1994).
10. Welt, S. et al. Quantitative analysis of antibody localization in human metastatic colon cancer: a phase I study of monoclonal antibody A33. *J Clin Oncol* **8**, 1894-906 (1990).
11. Welt, S. et al. Phase I study of anticolon cancer humanized antibody A33. *Clin Cancer Res* **9**, 1338-46 (2003).
12. Welt, S. et al. Preliminary report of a phase I study of combination chemotherapy and humanized A33 antibody immunotherapy in patients with advanced colorectal cancer. *Clin Cancer Res* **9**, 1347-53 (2003).
13. Welt, S. et al. Phase I/II study of iodine <sup>125</sup>-labeled monoclonal antibody A33 in patients with advanced colon cancer. *J Clin Oncol* **14**, 1787-97 (1996).
14. Hudson, P.J. & Souriau, C. Engineered antibodies. *Nat Med* **9**, 129-34 (2003).
15. de Palazzo, I.G., Kitson, J., Gercel-Taylor, C., Adams, S. & Weiner, L.M. Bispecific monoclonal antibody regulation of Fc gamma RIII-directed tumor cytotoxicity by large granular lymphocytes. *Cell Immunol* **142**, 338-47 (1992).
16. McCall, A.M. et al. Increasing the affinity for tumor antigen enhances bispecific antibody cytotoxicity. *J Immunol* **166**, 6112-7 (2001).
17. Lu, D. et al. A fully human recombinant IgG-like bispecific antibody to both the epidermal growth factor receptor and the insulin-like growth factor receptor for enhanced antitumor activity. *J Biol Chem* **280**, 19665-72 (2005).
18. Ford, C.H., Osborne, P.A., Rego, B.G. & Mathew, A. Bispecific antibody targeting of doxorubicin to carcinoembryonic antigen-expressing colon cancer cell lines in vitro and in vivo. *Int J Cancer* **92**, 851-5 (2001).

19. Bagshawe, K.D. Antibody-directed enzyme prodrug therapy (ADEPT) for cancer. *Expert Rev Anticancer Ther* **6**, 1421-31 (2006).
20. Graziano, R.F. & Guptill, P. Chemical production of bispecific antibodies. *Methods Mol Biol* **283**, 71-85 (2004).
21. Menard, S., Canevari, S. & Colnaghi, M.I. Hybrid antibodies in cancer diagnosis and therapy. *Int J Biol Markers* **4**, 131-4 (1989).
22. Ridgway, J.B., Presta, L.G. & Carter, P. 'Knobs-into-holes' engineering of antibody CH3 domains for heavy chain heterodimerization. *Protein Eng* **9**, 617-21 (1996).
23. Kontermann, R.E. Recombinant bispecific antibodies for cancer therapy. *Acta Pharmacol Sin* **26**, 1-9 (2005).
24. Marvin, J.S. & Zhu, Z. Recombinant approaches to IgG-like bispecific antibodies. *Acta Pharmacol Sin* **26**, 649-58 (2005).
25. Shen, J. et al. Single variable domain antibody as a versatile building block for the construction of IgG-like bispecific antibodies. *J Immunol Methods* **318**, 65-74 (2007).
26. Wu, C. et al. Simultaneous targeting of multiple disease mediators by a dual-variable-domain immunoglobulin. *Nat Biotechnol* **25**, 1290-7 (2007).
27. Goldenberg, D.M., Rossi, E.A., Sharkey, R.M., McBride, W.J. & Chang, C.H. Multifunctional antibodies by the Dock-and-Lock method for improved cancer imaging and therapy by pretargeting. *J Nucl Med* **49**, 158-63 (2008).
28. Rader, C. et al. The rabbit antibody repertoire as a novel source for the generation of therapeutic human antibodies. *J Biol Chem* **275**, 13668-76 (2000).
29. Midelfort, K.S. et al. Substantial energetic improvement with minimal structural perturbation in a high affinity mutant antibody. *J Mol Biol* **343**, 685-701 (2004).
30. Corneillie, T.M., Whetstone, P.A., Fisher, A.J. & Meares, C.F. A rare earth-DOTA-binding antibody: probe properties and binding affinity across the lanthanide series. *J Am Chem Soc* **125**, 3436-7 (2003).
31. Boder, E.T., Midelfort, K.S. & Wittrup, K.D. Directed evolution of antibody fragments with monovalent femtomolar antigen-binding affinity. *Proc Natl Acad Sci USA* **97**, 10701-5 (2000).
32. Corneillie, T.M., Fisher, A.J. & Meares, C.F. Crystal structures of two complexes of the rare-earth-DOTA-binding antibody 2D12.5: ligand generality from a chiral system. *J Am Chem Soc* **125**, 15039-48 (2003).
33. Reiter, Y. & Pastan, I. Antibody engineering of recombinant Fv immunotoxins for improved targeting of cancer: disulfide-stabilized Fv immunotoxins. *Clin Cancer Res* **2**, 245-52 (1996).
34. Lee, F.T. et al. Immuno-PET of human colon xenograft-bearing BALB/c nude mice using 124I-CDR-grafted humanized A33 monoclonal antibody. *J Nucl Med* **42**, 764-9 (2001).
35. Salacinski, P.R., McLean, C., Sykes, J.E., Clement-Jones, V.V. & Lowry, P.J. Iodination of proteins, glycoproteins, and peptides using a solid-phase oxidizing agent, 1,3,4,6-tetrachloro-3 alpha,6 alpha-diphenyl glycoluril (Iodogen). *Anal Biochem* **117**, 136-46 (1981).
36. Lindmo, T., Boven, E., Cuttitta, F., Fedorko, J. & Bunn, P.A., Jr. Determination of the immunoreactive fraction of radiolabeled monoclonal antibodies by linear

- extrapolation to binding at infinite antigen excess. *J Immunol Methods* **72**, 77-89 (1984).
37. Lindmo, T. & Bunn, P.A., Jr. Determination of the true immunoreactive fraction of monoclonal antibodies after radiolabeling. *Methods Enzymol* **121**, 678-91 (1986).
  38. Schultz, J. et al. A tetravalent single-chain antibody-streptavidin fusion protein for pretargeted lymphoma therapy. *Cancer Res* **60**, 6663-9 (2000).
  39. Weiden, P.L. et al. Pretargeted radioimmunotherapy (PRIT) for treatment of non-Hodgkin's lymphoma (NHL): initial phase I/II study results. *Cancer Biother Radiopharm* **15**, 15-29 (2000).
  40. Axworthy, D.B. et al. Cure of human carcinoma xenografts by a single dose of pretargeted yttrium-90 with negligible toxicity. *Proc Natl Acad Sci U S A* **97**, 1802-7 (2000).
  41. Knox, S.J. et al. Phase II trial of yttrium-90-DOTA-biotin pretargeted by NR-LU-10 antibody/streptavidin in patients with metastatic colon cancer. *Clin Cancer Res* **6**, 406-14 (2000).
  42. Wilbur, D.S., Hamlin, D.K., Sanderson, J. & Lin, Y. Streptavidin in antibody pretargeting. 4. Site-directed mutation provides evidence that both arginine and lysine residues are involved in kidney localization. *Bioconjug Chem* **15**, 1454-63 (2004).
  43. Wilbur, D.S. et al. Biotin reagents in antibody pretargeting. 6. Synthesis and in vivo evaluation of astatinated and radioiodinated aryl- and nido-carboranyl-biotin derivatives. *Bioconjug Chem* **15**, 601-16 (2004).
  44. Hamblett, K.J. et al. A streptavidin-biotin binding system that minimizes blocking by endogenous biotin. *Bioconjug Chem* **13**, 588-98 (2002).
  45. Ackerman, M.E. et al. A33 antigen displays persistent surface expression. *Cancer Immunol Immunother* **57**, 1017-27 (2008).
  46. Ackerman, M.E., Pawlowski, D. & Wittrup, K.D. Effect of antigen turnover rate and expression level on antibody penetration into tumor spheroids. *Mol Cancer Ther* **7**, 2233-40 (2008).
  47. Schmidt, M.M., Thurber, G.M. & Wittrup, K.D. Kinetics of anti-carcinoembryonic antigen antibody internalization: effects of affinity, bivalency, and stability. *Cancer Immunol Immunother* **57**, 1879-90 (2008).

## **Chapter 5: Highly avid magnetic bead capture: an efficient selection method for *de novo* protein engineering utilizing yeast surface display**

### **5.1 Abstract**

Protein engineering relies on the selective capture of members of a protein library with desired properties. Yeast surface display technology routinely enables as much as million-fold improvements in binding affinity by alternating rounds of diversification and flow cytometry-based selection. However, flow cytometry is not well-suited for isolating *de novo* binding clones from naïve libraries due to limitations in the size of the population that can be analyzed, the minimum binding affinity of clones that can be reliably captured, the amount of target antigen required, and the likelihood of capturing artifactual binders to the reagents. Here we demonstrate a method for capturing rare clones that maintains the advantages of yeast as the expression host, while avoiding the disadvantages of FACS in isolating *de novo* binders from naïve libraries. The multivalency of yeast surface display is intentionally coupled with multivalent target presentation on magnetic beads—allowing isolation of extremely weak binders from billions of non-binding clones, and requiring far less target antigen for each selection, while minimizing the likelihood of isolating undesirable alternative solutions to the selective pressure. Multivalent surface selection allows 30,000-fold enrichment and almost quantitative capture of micromolar binders in a single pass using less than one microgram of target antigen.

---

Major portions of this chapter were previously published in:  
Ackerman ME, Levary D, Tobon G, Hackel B, Orcutt KD, Wittrup KD. “Highly avid magnetic bead capture; an efficient selection method for *de novo* protein engineering utilizing yeast surface display. *Biotechnol Prog*. 2009 May-Jun;25(3):774-83.

## 5.2 Background

The growing applications of yeast surface display (YSD) reflect several advantages over alternative technologies<sup>1</sup>. YSD mimics the protein processing machinery of higher eukaryotes, thereby minimizing expression biases against the complex protein structures that require foldases and chaperones for efficient assembly, and allowing presentation of sequence variants and structural architectures less accessible to prokaryotic hosts<sup>2</sup>. In a recent study in which the same cDNA library was transformed into both phage and yeast display systems, YSD identified three times as many binding clones, and when cloned back into phage, these additional sequence variants could not be expressed as functional protein<sup>3</sup>. Additionally, YSD is amenable to engineering increased expression, stability, pH sensitivity, and enzymatic properties such as enantioselectivity<sup>4-6</sup>. Thus, yeast serve as an excellent host organism for presentation of proteins for diverse engineering goals.

Flow cytometry (FACS) is the method of choice for quantitative selection. FACS permits facile comparison between display level and antigen binding, allowing for selection without expression level bias, and discrimination between clones with very fine differences in affinity<sup>7</sup>. FACS also allows the stringency of the selection to be set in live time based on actual sample data rather than being rigidly pre-defined. Unfortunately, while well-suited for affinity maturation, FACS is problematic for the isolation of *de novo* binding interactions. Flow cytometry simply cannot directly query a library for the ability to recognize a target antigen, but instead relies on the acquisition of fluorescence as a proxy for antigen binding. Most commonly this is attempted by tagging the antigen and using a fluorescent secondary reagent to identify the clones that have bound the

target antigen. However, the naïve libraries used in *de novo* selections are not biased toward any particular epitope or target molecule, and any binding interaction resulting in acquired fluorescence will be selected. Accordingly, direct interactions between the yeast-displayed construct and fluorescent reagents satisfy the selection criteria. In fact, such an interaction regrettably represents the fittest solution to the selective pressure. Additionally, an interaction with the reagent may also be the most accessible result as the fluorophore itself may present the most electronically distinct epitope, and may be present at multiple sites, granting it an avidity advantage relative to the desired interaction with the target molecule. These factors promote binding to the secondary reagent above and beyond any target quality issues such as the heterogeneity, glycosylation, questionable purity, or improper folding that may trouble antigens produced for the purpose of such selections.

In order to avoid such undesirable outcomes, steps are generally taken to minimize the chances of isolating secondary binders and to bias the selection to favor an interaction with the desired target. For instance, incubation with secondaries can be performed for a minimum amount of time and at a minimum concentration, the target itself can be directly conjugated with the fluorescent tag using a site-specific modification<sup>8</sup>, and positive selections against target and secondary can be alternated with negative selections against the secondary alone. However, even these modifications may not prove sufficient to steer the system toward isolating the desired interaction.

The efficiency of FACS selections compounds these difficulties and poses a serious impediment to the isolation of *de novo* interactions. FACS machines analyze and sort on the order of  $10^8$  cells per hour. To ensure that almost all clones are analyzed at

least once, a ten-fold excess of the library diversity should be analyzed, requiring a day of sort time for a library of  $10^8$  cells, and setting this size as a reasonable upper limit for the diversity that can be easily analyzed with this degree of diligence.

Unfortunately, by one estimate, a library of  $10^{10}$  cells may be necessary to obtain binders with affinities in the nanomolar range<sup>9</sup>. As a recent example, a library of  $2.3 \times 10^7$  clones was FACS selected to identify binders to lysozyme, and the initial hit from this search had micromolar affinity—so low that it could not accurately be measured using FACS<sup>10</sup>. The likely absence of nanomolar binders against any given *de novo* target is a considerable obstacle for two reasons. First, weaker binding interactions require that more antigen be present in the incubation steps in order to be captured, as by definition only half of the antigen binding sites will be occupied when a micromolar binder is incubated in a micromolar concentration of antigen. For a weak interaction, this can translate into a significant quantity of antigen. For example, FACS selections of naïve libraries typically require on the order of 10 nmole (hundreds of micrograms) of target antigen.

Additionally, weak interactions have very fast dissociation rates. The half-life of a micromolar interaction is generally on the order of 5 seconds, and nanomolar binders only a few minutes. Such a rapid dissociation rate is extremely unfavorable for a detection scheme requiring a separate incubation in fluorescent secondary followed by a lengthy selection on a flow cytometer. While pre-incubating the secondary with the antigen before labeling the yeast or using a directly conjugated antigen can help to offset such a rapid dissociation rate, it increases the probability of isolating binders to either the secondary or the conjugated fluorophore as described previously.



A new selection methodology surpassing these barriers to isolating *de novo* binders from naïve libraries is needed. Given the confounding factors described here, the ideal yeast selection platform would first use no tags, secondary reagents, or proxy read-outs of antigen binding—preventing alternative solutions to the selective pressure. Secondly, it would allow rapid screening of upwards of  $10^{10}$  cells, so that the size of the library that can be thoroughly searched is limited by library construction rather than by the selection method. Third, it would have the ability to capture even the very weak binders likely to be present in a naïve library. Finally, it would do so in a rapid, inexpensive, and straightforward manner without requiring the production of large quantities of the target antigen.

Accordingly, we have considered alternatives to FACS with the goal of defining a technique for isolation of even very weak binders from large populations using a minimum amount of antigen and secondary reagents. In order to capture weak interactions, we have coupled the multivalency of YSD with antigen multivalency—allowing avidity effects to drive the selection. Simple mathematic and geometric treatments of bivalent binding interactions demonstrate the dramatic effects of avidity<sup>11</sup>. In a simplified system involving 2 binding sites separated by a flexible linker, bivalency boosted the effective affinity of the interactions by 4 orders of magnitude<sup>12</sup>. As yeast typically display approximately 50,000 copies of the molecule to be engineered, there is likely the opportunity to reach interactions that are highly multivalent, and thus have overall dissociation rates of days as opposed to their monovalent dissociation rates of seconds.

A concomitant benefit of multivalent antigen display is that it greatly increases the effective concentration of the antigen. In fact, the high effective concentration drives the apparent increase in affinity. Once a yeast cell associates with surface bound antigen, it encounters a very high local concentration of antigen, favoring the formation of additional interactions. This fortuitously allows a much smaller amount of antigen to be used in the selection. As long as the multivalent antigen and yeast are well mixed—affording each yeast cell the opportunity to contact and associate with the antigen during the selection, high local concentrations can substitute for the high systemic concentrations used in a FACS selection, dramatically decreasing the amount of antigen required.

As a means to present multivalent antigen and capture weak interactions we have investigated the use of solid surfaces. Successful in phage selections for years, *e. coli* selections more recently<sup>13</sup>, and having precedence in yeast selection in the form of mammalian cell-based selections employing density gradient centrifugation<sup>14,15</sup> or monolayer panning<sup>16</sup>, the use of synthetic multivalent surfaces represents a logical extension of past methodology. Here we test a variety of surfaces and demonstrate that extremely low affinity binders can be captured with high efficiency from large populations using multivalency and we validate multivalent antigen presentation as a selection method by successfully isolating confirmed *de novo* binders from naïve libraries.

### 5.3 Materials and Methods

#### Yeast Strains and Plasmids

All plasmids were transformed into EBY100 yeast using the EZ Yeast Transformation II kit (Zymo Research D2004) according to the manufacturer's instructions. Surface displayed constructs were all expressed as *aga2p* fusions on the galactose-inducible, tryptophan selectable plasmids pCT-CON or pCTCON2 and grown and induced as described previously<sup>17</sup>. Table 5.3.1 lists the plasmids used in this study.

**Table 5.3.1:**

clone	scaffold	target	target type	citation	affinity
L0.7.1	fibronectin	lysozyme	protein	<sup>10</sup>	> 1 $\mu$ M
L1.5.1	fibronectin	lysozyme	protein	<sup>10</sup>	~1 $\mu$ M
L3.3.1	fibronectin	lysozyme	protein	<sup>10</sup>	8 nM
L7.5.1	fibronectin	lysozyme	protein	<sup>10</sup>	3 pM
2D12.5	scFv	DOTA	small molecule	<sup>18,19</sup>	10 nM
4m5.3	scFv	fluorescein	small molecule	<sup>20</sup>	48 fM
his6 tag	scFv	chelated cobalt	small molecule	<sup>21</sup>	~1 $\mu$ M
		anti-his antibody	protein	n.a.	n.a.

#### Surfaces

Nickel and streptavidin-coated wells (Qiagen), immunotubes (Nunc), tissue culture plastic (BD Biosciences), glass slides and nitrocellulose membrane (VWR International), agarose talon resin (Clontech), and magnetic beads (Invitrogen 101-01D, 110-47, and 162-03) were used as multivalent surfaces.

#### Flow Cytometry

Cells were labeled for FACS analysis as necessary<sup>17</sup>. Lysozyme-binding clones were identified via labeling with biotinylated hen egg lysozyme (Sigma) followed by

streptavidin-PE (Invitrogen), or via their c-myc tag by means of a chicken anti-c-myc antibody (Invitrogen) followed by goat anti-chicken 488 secondary (Invitrogen). His tagged clones were labeled with biotinylated mouse anti-his6 antibody (Qiagen) followed by streptavidin-PE. Samples were analyzed on a Coulter Epics XL, or sorted on FACSAria cytometers after labeling.

### **Pilot Selections**

Briefly, populations of binding and non-binding yeast, usually a ratio of 1:100 or 1:1000, were mixed and incubated with the materials, allowed to bind, and then washed. Growth media was added to the material and bound yeast were allowed to divide off for a period of time before enrichment and yield were measured by either FACS or plating, as described previously<sup>22</sup>.

*Agarose Talon Resin:* Binding and non-binding yeast were mixed and incubated with 2 ml of washed and equilibrated resin in a 15 ml conical for 1 hour. The yeast slurry mixture was then poured into a column and washed and eluted per the manufacturer's instructions. Fractions were diluted into growth media, induced, and FACS was performed in order to determine the prevalence of binders after the selection.

*Plastic, glass, nitrocellulose, and immunotubes:* These materials were incubated in a concentrated solution of lysozyme (>2 mg/ml) in PBS for at least 2 hours at room temperature, or 4°C overnight on a rocker platform, allowing coating to occur by passive adherence. A western blot was performed on the nitrocellulose sample in to confirm the

lysozyme coating. The surfaces were washed with PBS-BSA (0.1%) three times for five minutes to remove unbound lysozyme. Binding and non-binding yeast were incubated with the materials for at least 1 hour at room temperature on a rocker platform. Washes were performed to remove unbound yeast, and growth media was added allowing bound yeast to divide off the surfaces before an aliquot was removed for subsequent analysis by either FACS or plating.

*Nickel and streptavidin coated wells:* These functionalized plastics were handled similarly except nickel wells were left bare, and streptavidin wells were incubated with biotinylated lysozyme for the selection.

*Biotin Binder magnetic beads:* Except where otherwise noted,  $2.5 \times 10^6$  streptavidin coated beads (Invitrogen 110-47) were washed twice in PBS-BSA (0.1%) and then incubated in 100  $\mu$ l of 350 nM biotinylated lysozyme overnight at 4°C in a microfuge tube on a rotator. Beads were washed twice and then mixtures of binding and non-binding yeast were added to the beads and allowed to bind for 1-3 hours at 4°C on a rotator. The beads were then washed and diluted and plated to quantitatively determine enrichment and yield.

*M-270 Amine magnetic beads:*  $6 \times 10^8$  amine functionalized beads (Invitrogen 162-03) in DMSO were incubated with a 100-fold excess of solid, dry fluorescein-PEG-NHS (Nektar), or p-SCN-Bn-DOTA (Macrocyclics) and a 1000-fold excess of TEA and incubated at room temperature overnight on a rotator, then washed twice with DMSO.

Bound DOTA was loaded with either gallium or yttrium by adding a 100-fold excess of metal and incubating in a 37°C shaker for 5 hours in 0.4 M ammonium acetate. Conjugated beads were then washed with PBS-BSA (0.1%) and used in selections as described above.

*Talon magnetic beads*: 25 µl of talon beads (Invitrogen 101-01D) were washed twice in PBS-BSA(0.1%) and then mixed with populations of yeast and handled as described above.

### ***de novo* Library Selection**

Two fibronectin libraries, with variation in both loop length and sequence were used to isolate *de novo* lysozyme binders.  $1-2.5 \times 10^9$  yeast from each library were first incubated with  $1 \times 10^7$  bare biotin binder beads for 1 hour as a negative selection. Unbound yeast were then removed and incubated with  $4 \times 10^7$  lysozyme-coated biotin binder beads for at least 1 hour as a positive selection for lysozyme binders. Unbound yeast were removed and discarded. Beads and bound yeast were then resuspended in 5-50 ml of growth media and yeast allowed to grow off the beads overnight. For successive rounds of selection, the procedure was repeated as described with the exception of decreasing the number of lysozyme-coated biotin binder beads to  $1 \times 10^7$ . In addition, the number of cells used in each round was modified to reduce the number of cells processed yet maintain at least tenfold sampling of library diversity. After two selections, a flow cytometric sort for c-myc positive cells was performed to prevent the accumulation of truncation clones. The library was then diversified as described<sup>10</sup>. Two

further bead selections and a c-myc flow cytometric selection were subsequently performed. Plasmids were isolated from the yeast cells, transformed into bacteria, individual clones were sequenced and their binding properties analyzed and confirmed by FACS.

Similarly, selections against biotin-streptavidin were performed essentially as described above, except that multiple negative selections against streptavidin were performed each round.

## **5.4 Results**

### **5.4.1 Profile of Multivalent Selection Methods**

The multivalency of yeast display was coupled with multivalent target presentation utilizing a variety of solid surfaces, as diagrammed in Figure 5.4.1a, in order to identify a selection method capable of isolating rare, weak interactions among large non-binding populations. Each surface was coated with a target molecule and then incubated with a mixture of yeast, a small fraction of which expressed a protein capable of binding to the target. Unbound yeast were removed by washing the surface and the captured yeast were analyzed in order to determine the ability of the surface to enrich binding clones from the initial mixture.

#### Profile of Materials Tested

Figure 5.4.1b presents the ability of each surface tested to enrich binding yeast. Non-functionalized surfaces were coated by passive adherence of the target protein, lysozyme, to the surface, and the lysozyme-binding fibronectin clone L3.3.1 (nanomolar affinity) was used as the binding population. Cobalt, or Talon® conjugated surfaces were simply washed and then used to select yeast with a surface displayed his6 tag. Streptavidin coated surfaces were incubated with biotinylated lysozyme and used to enrich L3.3.1-expressing yeast. The surfaces tested included nitrocellulose, several plastics, glass, agarose, and magnetic beads. Binding yeast were mixed with a 10 to 1000-fold excess of non-binding yeast, such as EBY100 yeast lacking any display construct plasmid, or yeast expressing a non-binding construct. Surfaces were incubated with the mixed yeast population, washed to remove unbound yeast, and the selected yeast



populations were then either plated or analyzed by FACS to determine the final prevalence of binding clones. The ability of each surface to select binding yeast was determined by evaluating the enrichment of the binding clone population (final prevalence/initial prevalence), which could then be compared the theoretical maximum enrichment to purity. For all materials, a number of wash and incubation conditions were tested, and several materials, including each of the functionalized surfaces, had some ability to enrich binding yeast.

Interestingly, none of the passively coated materials were able to enrich the lysozyme binding clone L3.3.1. This inability may be due to our use of a relatively small protein target and a binder with a conformationally sensitive epitope. Passive adherence may have partially or completely denatured the lysozyme and destroyed the epitope recognized by L3.3.1. While larger proteins may avoid complete denaturation when passively attached, partial unfolding is still likely to both abolish native and generate novel epitopes—a highly undesirable presentation of the target antigen in a *de novo* selection method. So, while a tag-free means to perform selections is desirable, the use of tag is preferable to altering the conformation of the target antigen—especially as a tag may be necessary for purification of the antigen even if unnecessary for the selection. Additionally, if the tag is present at only a single site and is used to immobilize the target on the selection material, much of its surface may be buried or occluded.

The two surfaces with the best selective profiles identified from these initial tests were agarose and magnetic beads, and these materials were characterized more extensively. First, a mixture of yeast expressing either a his6 tagged scFv or a c-myc tagged fibronectin domain at a 1:4 ratio were incubated with Talon agarose in order to

test enrichment of the his6-expressing population. The yeast:bead slurry was poured into a column and washed and eluted. Fractions were then labeled for FACS analysis to determine the relative prevalence of each population in the various fractions. Figure 5.4.1c presents the percentage of each yeast population present in each column fraction and clearly shows the ability of agarose beads in a column format to be used in selections.

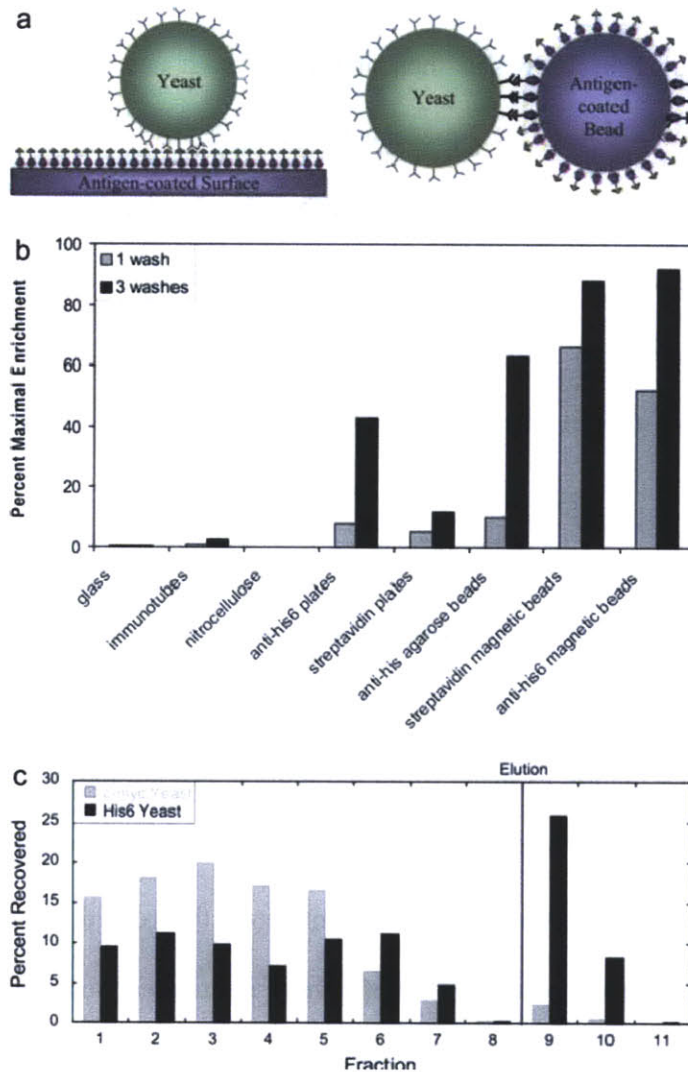


**Figure 5.4.1: Profile of Multivalent Selection Methods.** (a) Diagram of multivalent interaction between yeast and surface. (b) Yeast can be selected by multivalent surfaces: The ability of each multivalent surface to select and capture binding yeast from a larger population of non-binding yeast was determined. In each case, the enrichment ratio was determined and is presented as a fraction of the maximum theoretical enrichment (enrichment from 1 in 100 or 1 in 1000 to purity). Non-functionalized materials had no ability to enrich binders, perhaps due to denaturation of the target protein to the surface. Functionalized surfaces, including agarose and magnetic beads showed a strong ability to select binders and were characterized further. (c) Selection on agarose resin in column format: Talon agarose resin was used to select yeast expressing a His6 tag from a larger population of c-myc positive yeast. The percent of each clonal population recovered from wash (fractions 1-8) and elution (fractions 9-11) is given and demonstrates the ability to isolate binders specifically.

#### **5.4.2 FACS profile of selected populations**

As a direct means of comparison, his6-tagged yeast were mixed with non-binding yeast at a ratio of 1 in 1000 and then applied to both agarose and magnetic Talon-functionalized beads. Figure 5.4.2 presents the profile of the initial population as well as that of the yeast eluted from each type of bead. Despite being present below the threshold of detection in the initial population (red trace), binding yeast have been enriched to approximately 1 in 4 yeast by agarose beads (blue trace), and to near purity by magnetic beads (green trace), indicating the excellent ability of these materials to isolate binders.

However, since one of the criteria for the selection methodology is use of a minimum amount of antigen, agarose beads, which by design have a high binding capacity due to extensive porosity, while ideal for protein purification, are non-ideal for target antigen presentation as many of these binding sites are likely to be inaccessible to the yeast. A less porous surface with fewer contours, such as magnetic beads is better suited for efficient presentation of the target antigen in this regard.

Having demonstrated the ability of several multivalent surfaces to isolate binding yeast, we next determined whether magnetic beads, the most promising of these surfaces, met the other criteria for naïve library selections.

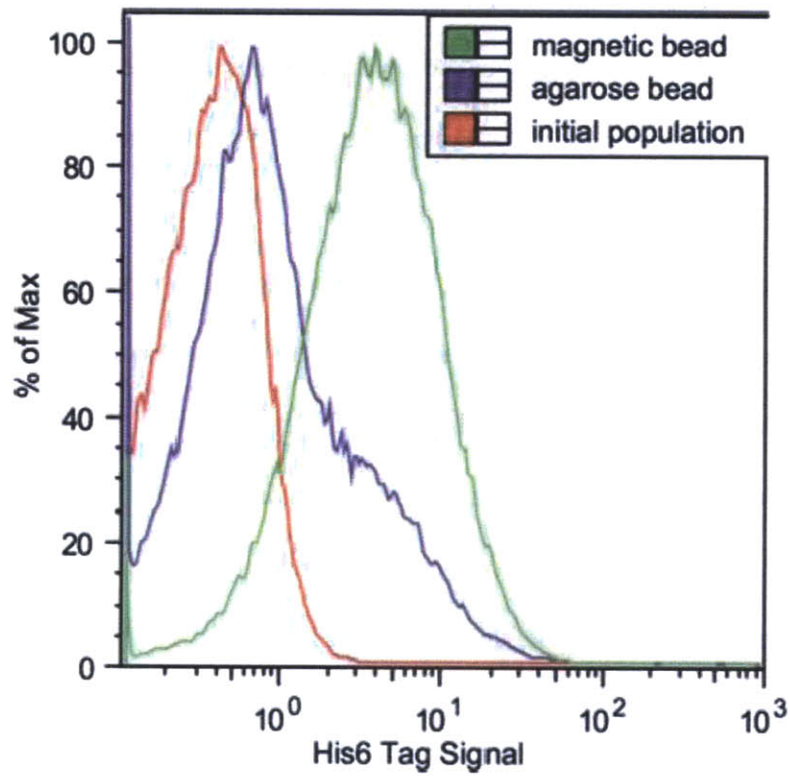


**Figure 5.4.2: FACS profile of selected populations** FACS data presenting the prevalence of His6 yeast before (red) and after selection on Talon agarose resin (blue) and magnetic beads (green) demonstrating the excellent enrichment profiles of these multivalent surfaces.

### 5.4.3 Efficiency of magnetic bead sorting

First, we desired a method capable of isolating extremely weak binders, so magnetic beads were coated with lysozyme and used to select a series of lysozyme-binding fibronectin domains with affinities spanning a million-fold range from  $\mu\text{M}$  to  $\text{pM}$ . The weakest clone, L0.7.1, was identified by FACS selections of solubly multivalent lysozyme<sup>10</sup>, and has such a low affinity that it could not accurately be measured by FACS, while the tightest binder, L7.5.1 interacts with 3  $\text{pM}$  affinity. Figure 5.3.3a presents the enrichment of lysozyme binding clones from non-binding clones at a starting ratio of 1:1000 (gray bars). The million-fold decrease in affinity has no effect on the ability of the beads to select the binding clone.

In contrast, when yeast are first incubated with soluble lysozyme and then quickly washed and allowed to bind to beads as was done previously in the protocol of Yeung and Wittrup<sup>22</sup>, enrichment is highly dependent on affinity (black bars). In fact, this seemingly minor protocol alteration drastically reduces the ability to enrich the clone with the weakest binding, which is likely most representative of the binders present in naïve libraries. In each case, selection depends on the ability to generate and maintain an interaction between yeast and bead, and the ability of each yeast to interact multivalently with a bead is dependent on the surface density of the interacting molecules. In utilizing a soluble target incubation, multivalency is limited by affinity as only some subset of surface displayed molecules will be bound to the target antigen, and capable of interacting with the beads. Alternatively, the degree of multivalency that can be achieved between target-coated beads is set by either the display level of the yeast, or the coating

density of the target, and is therefore an inherent property of system, and these parameters can be set to maximize possible valency.

As a means to estimate the lower affinity limit for capture with a target-coated surface, a rough calculation of the effective concentration of the target can be made by quantifying the amount of antigen on each bead and dividing that value by the bead volume, giving an approximate local concentration. The magnetic beads used in this study present the target antigen at an effective local concentration in the millimolar range, and therefore may be able to isolate extremely weak interactions.

Having established the ability to isolate very weak interactions, we investigated the effect of rarity on enrichment. Binding and non-binding yeast were mixed at ratios varying from 1:10 to 1:100,000 and were bead selected, resulting in the enrichment values presented in Figure 5.3.3b. For both interactions between a his6 tag and chelated cobalt, and the L0.7.1 fibronectin clone and lysozyme, enrichment scaled well with the theoretical maximal enrichment for each initial prevalence (lines), with a maximal increase in prevalence from 1 in 100,000 cells to 1 in 3 (30,000-fold enrichment). Thus, magnetic bead selection easily captures rare clones.

One of the limits of FACS selections is that it limits the size of a population that can be sorted; thus, the number of yeast that can be screened effectively by magnetic beads was investigated. Lysozyme-binding (L0.7.1) and non-binding yeast were mixed at a ratio of 1:1000 at total population sizes varying from  $5 \times 10^7$  to  $4 \times 10^9$ , and enrichment values after 1 and 3 washes were determined for each population (Figure 5.4.3c). Consistent enrichment values were found across all population sizes, and demonstrate that 4 billion yeast can be straightforwardly surveyed in a single microcentrifuge tube in

1 hour. Whereas scaling up FACS selections requires either multiple sorters or significantly more time, magnetic bead selections can be scaled up by simply using a larger vessel or running several microcentrifuge tube-sized selections in parallel—allowing even the largest yeast libraries to be screened to high coverage multiplicity with ease.

In order to evaluate the flexibility of magnetic bead selections, the ability to enrich clones displaying several different scaffolds capable of interacting with various targets was investigated. Figure 5.4.3d shows the enrichment values of clones expressing either fibronectin or scFv domains that recognize both small molecule and protein targets. Proteins were immobilized on streptavidin-coated beads via a biotin tag, while small molecules were chemically conjugated to amine-functionalized beads. Binding yeast were efficiently isolated from a larger population of non-binding yeast, independently of their displayed scaffold, size of the target antigen, and whether the targets were chemically conjugated or immobilized via a tag.



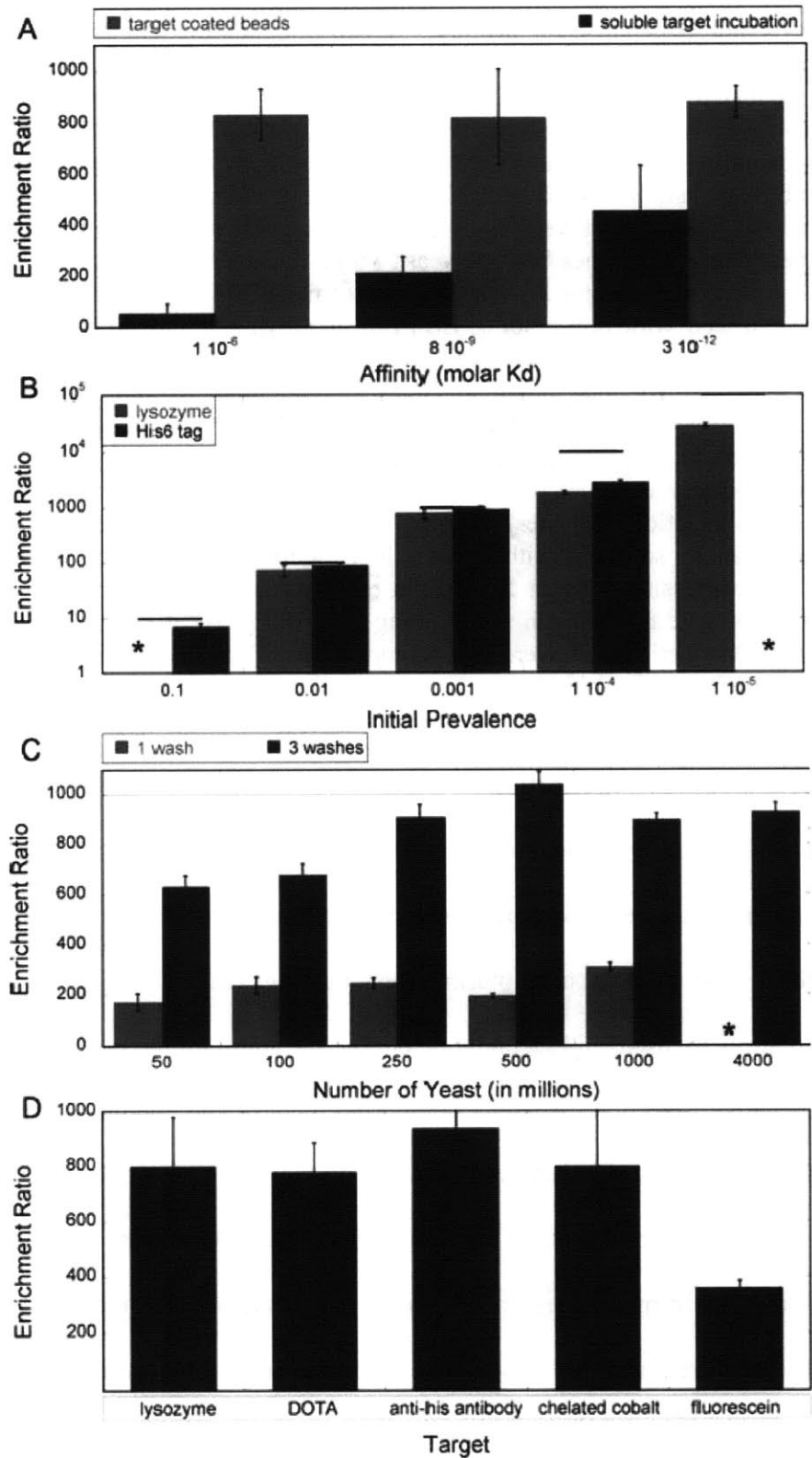


**Figure 5.4.3: Efficiency of Magnetic Bead Sorting** (a) **Affinity:** Magnetic bead enrichment is not dependent on affinity. Lysozyme binding clones with affinities spanning 6 orders of magnitude were mixed with non-binding EBY100 at a ratio of 1 in 1000 and incubated with either soluble lysozyme for 1 hour followed by a wash and 2 minute incubation with streptavidin coated beads (black bars), or were incubated with lysozyme-coated beads for 1 hour (gray bars). The ability of each clone to be selected via the soluble incubation method is highly dependent on affinity, while lysozyme-coated beads enrich all clones at a very high efficiency regardless of affinity. (b) **Rarity:** Magnetic bead sorting enriches binding yeast with an efficiency close to the theoretical maximum. Yeast expressing a low affinity (micromolar) lysozyme-binding fibronectin domain were mixed with non-binding EBY100 at varying initial prevalences ranging from 1 in 100 to 1 in 100,000, and bead selected with resulting enrichment ratios that scaled well with the theoretical maximum (line), yielding up to 30,000-fold enrichment in a single selection. \*Data not available. (c) **Population size:** Magnetic bead sorting easily and quickly processes large populations of yeast. Varying numbers of yeast at a ratio of 1 low affinity lysozyme binder per 1000 non-binders were bead selected. Enrichment ratios at each population size are presented after 1 and 3 washes, demonstrating that  $4 \times 10^9$  yeast can be screened with no loss in enrichment. \*Data not available. (d) **Target:** Yeast expressing scFv or fibronectin recognizing a range of protein and small molecule targets were mixed with non-binding EBY100 yeast at a ratio of 1:1000 and bead selected. Magnetic beads were able to enrich for all scaffolds, targets, and binding interactions tested.

#### 5.4.4 Yield of magnetic bead sorting

Finally, we tested the yield of bead selections in order to determine the probability that each binding yeast cell would be captured. Yield is a critical selection parameter in two respects. The chances of capturing each binding yeast will first influence the coverage multiplicity used, and secondly determine the ability of the method to act as an effective negative selection, wherein yeast with undesirable binding properties are removed from the library population. Figure 5.4.4a shows the percent of binders present that were recovered from selections of binding yeast (L0.7.1) present at a ratio of 1 in 1000 non-binders. In most cases, more than three-quarters of the binders present were successfully recovered, and this fraction declined significantly only when the number of binders present was comparable to the binding capacity of the beads (several million

binders) decreasing the likelihood that binding yeast would encounter available binding sites.

Similarly, Figure 5.4.4b shows the number of yeast isolated from repeated rounds of selection against streptavidin. After each selection, yeast in the supernatant were reapplied to fresh streptavidin beads. The number of binders isolated from each round is approximately equal to 80% of the total number present. Thus, after 4 rounds of selection, approximately 99.8% of streptavidin-binding clones have been captured, leaving only 0.16% in the population. The ability to thoroughly deplete the population of streptavidin binders via such negative selection serves as a highly efficient means to constrain the undesirable selection of reagent binders and steer the selective pressure of each positive selection toward the intended target. This restraint of alternative solutions to the selective pressure represents a significant advantage over negative selections by FACS, particularly as extremely weak interactions can be captured and because the yeast do not require subsequent regrowth and induction before positive selection. Therefore, negative selections using magnetic beads coated with reagents would be useful when paired with any method of positive selection in order to improve the chances of isolating the desired binding interaction.

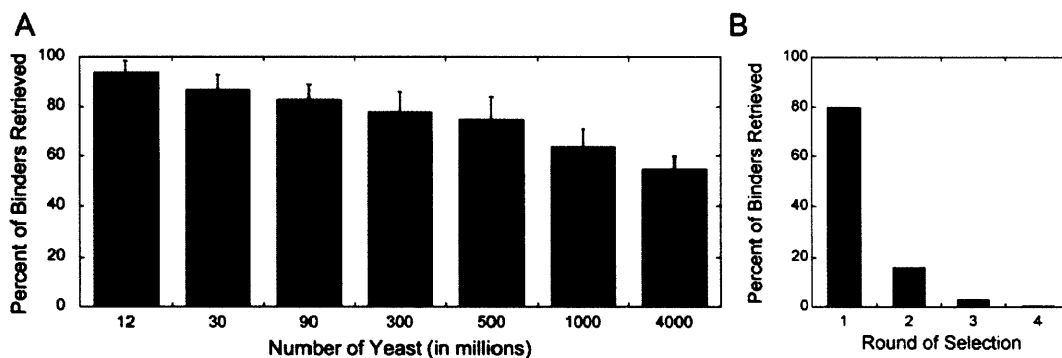


**Figure 5.4.4: Yield of Magnetic Bead Sorting (a) Yield:** Magnetic bead sorting retrieves binding yeast in high quantitative yield. Low affinity lysozyme-binding yeast were mixed with non-binding EBY100 at a ratio of 1:1000, and the size of the total population sorted was varied between  $1.2 \times 10^7$  and  $4 \times 10^9$ . Bead selections were performed and the total number binding yeast retrieved after each selection was compared to the number initially present. Under all conditions, bead selection captured the majority of binding yeast present, and was not highly dependent on the total number of yeast present in the selection. **(b) Yield of negative selections:** Magnetic bead sorting retrieves binding yeast in high quantitative yield. A fibronectin library was repeatedly incubated with streptavidin-coated beads as a means to deplete clones capable of binding to the beads independent of the target ligand. Each negative selection captured 75-80% of the streptavidin-binding population present. After the 4<sup>th</sup> negative selection, only about 0.16% of bead binders remain and yeast can be incubated with target-coated beads with a dramatically reduced chance of isolating reagent-binders.

#### 5.4.5 Dependencies of magnetic bead sorting

Thus far, we have demonstrated that magnetic beads can be used to isolate highly rare and very weak binders to both protein and small molecule targets with high quantitative yield from very large populations. In order to further profile the factors affecting these selective abilities, we carried out a series of experiments in which parameters such as the time of incubation and surface density of interacting molecules were varied. Figure 5.4.5a presents the enrichment of lysozyme binding clones (L0.7.1) from non-binding yeast after 1 wash when incubated at a starting ratio of 1:1000 for

varying periods of time. The magnetic beads rapidly isolate the binding population, showing near maximal enrichment after 1 hour.

Additionally, since the binding affinities that can be captured using this method are so low, and because in most tests the non-binding population consisted of yeast that did not express a surface-displayed construct, we undertook extensive testing of negative controls in order to ensure that only specific interactions were selected. Beads coated with a given target were used in tests against yeast expressing constructs capable of interactions with other targets. Four such mismatched pairs were tested, and all prevalences after selection were comparable to the initial prevalence of 1 in 1000 (Figure 5.4.5b), demonstrating that the enrichment of binding yeast represents a specific interaction and is not an artifact of a biased comparison, nor the effect of a promiscuous system.

Lastly, as described previously, this method depends on the number of molecular interactions or degree of multivalency that can be achieved, and is therefore predicted to be impacted by both the density of the target ligand coating the beads, and the density of the construct displayed on the surface of the yeast. Accordingly, Figures 5.4.5c and d show the effect of construct display level and target presentation level on enrichment. As expected, the higher the surface density of interacting molecules—whether limited by the bead or the yeast, the more likely a multivalent interaction can be achieved resulting in higher enrichment values. Because the yeast expression level is a significant factor in determining enrichment, care should be taken to ensure use of cultures that have been induced to express as highly as possible.

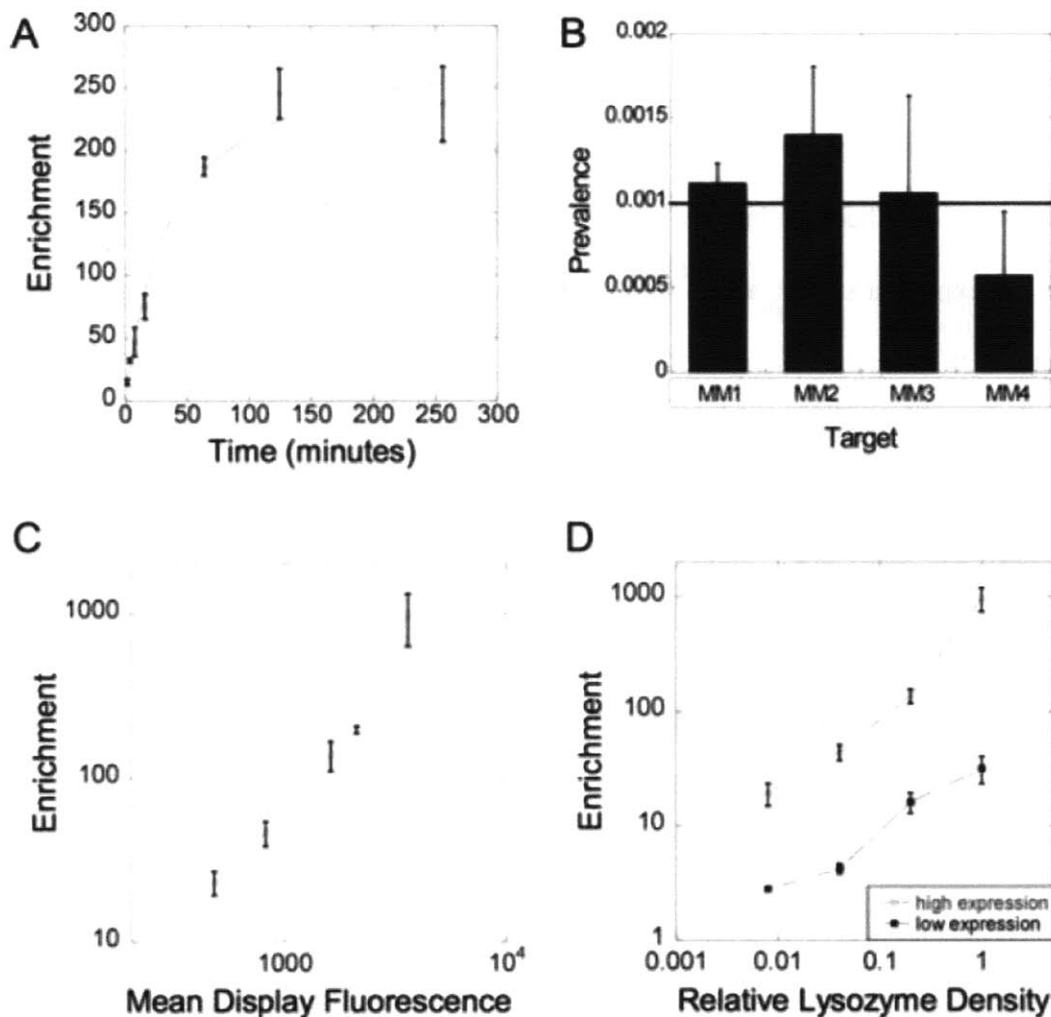


**Figure 5.4.5: Dependencies of Magnetic Bead Sorting** (a) **Time:** Magnetic bead sorting selects binding yeast rapidly. A population of  $10^7$  yeast at a ratio of 1 low affinity lysozyme binder in 1000 non-binding EBY100 were bead selected for various times and washed once, yielding a halflife of association under 30 minutes. (b) **Specificity of interaction:** Despite the very low affinity requirements, selection of yeast is highly specific. Mismatched pairings of yeast expressing scFvs and target-coated beads were selected in order to determine the specificity of interaction necessary for enrichment. The line represents the presort prevalence. (c) **Yeast valency:** Enrichment is dependent on yeast valency. Low affinity lysozyme binding yeast were induced for varying periods of time resulting different densities of surface expression, and the bead selected. A clear dependence on the yeast expression level can be observed. (d) **Bead Valency:** Enrichment is dependent on target valency. Beads were coated with varying densities of lysozyme and used to select a low affinity lysozyme-binding clone. A clear dependence on the density of ligand on the beads is observed regardless of yeast expression level.

#### 5.4.6 Demonstrations of Method Utility in *de novo* Isolation

In order to fully test the ability of the method, we also sought to select *de novo* binders from two naïve libraries, including the same fibronectin library utilized to generate the clones presented in Hackel et al, was selected using lysozyme-coated beads as opposed to the FACS methodology applied previously, allowing direct comparison of the two methods. In the bead selections carried out here, each library was first depleted of streptavidin or bead binders by an initial incubation with beads as a means to avoid enriching reagent-binding clones. Non-binding yeast were removed from the supernatant and applied to beads coated with lysozyme. These beads and the yeast bound to them were then directly transferred into growth media and subsequently induced for the next round of the process. After 2 such selections, a FACS sort to isolate c-myc positive clones was performed to remove truncated clones from the population. The clones were diversified as described<sup>10</sup>, and the resulting population was bead selected twice followed by a c-myc positive FACS sort. Several clones were isolated, sequenced, and characterized.

Interestingly, L0.7.1, the initial binder isolated by FACS selections was also identified in these bead sorts. However, this clone was not the dominant member (present once in eight sequenced clones) of the selected population, and therefore it appears as though the bead selections were able to identify additional binders that were not isolated by FACS. As we cannot determine accurate affinity values by FACS for such weak binders, it is unclear whether these additional clones represent stronger binders that happened to be missed by FACS, or weaker ones that FACS could not

isolate. In either case, the inclusion of additional diversity in subsequent rounds of evolution is likely to be beneficial, especially given the use of a loop shuffling protocol.

A second fibronectin library was bead sorted in parallel, and clones with nM binding affinities were isolated following the same protocol—allowing isolation of validated lysozyme-binding clones from two different libraries in 1 week using only about 100 pmol (10 micrograms) of target antigen.

Additionally, as a means to demonstrate the excellent ability of the method to function in negative selections, bead selections were used to isolate clones capable of discriminating between streptavidin and biotin-streptavidin. Multiple negative selections against streptavidin with its biotin-binding site unoccupied were performed prior to each positive selection against biotin-streptavidin. After 6 selections and 2 rounds of mutagenesis, clones with nanomolar binding affinity to biotin-streptavidin, but undetectable affinity to streptavidin were isolated (data not shown). This result shows the robust nature of beads in both positive and negative selections, and the ability to isolate interactions of interest with a high degree of specificity.

The excellent capabilities of this multivalent selection method establish it as the method of choice for *de novo* selections. Bead-based selections followed by mutagenesis can be iterated, and the success of each round can be assessed by comparing binding to reagent-coated beads to antigen-coated beads. Once a population displays increased binding to the target antigen, it can be mutagenized and selection stringency can be increased in the following rounds. Stringency may be tuned by altering the duration and frequency of wash steps, decreasing expression of the surface-displayed construct or decreasing antigen density on the beads. Alternatively, as long as thorough negative



selections are performed, a soluble antigen incubation as in the method described by Yeung and Wittrup can be utilized to increase stringency. Once FACS-detectable (nM) binders have been isolated via rounds of bead selection with increasing stringency, affinity maturation can proceed via FACS. Figure 5.4.6 presents a schematic diagram of the process for generating high affinity binders with high efficiency from naïve libraries.

Overall, by allowing multivalent presentation of the target antigen locally on a particle surface, the bead selection method described here is able to sort large populations and quantitatively isolate even weak binders in a highly rapid and efficient manner.

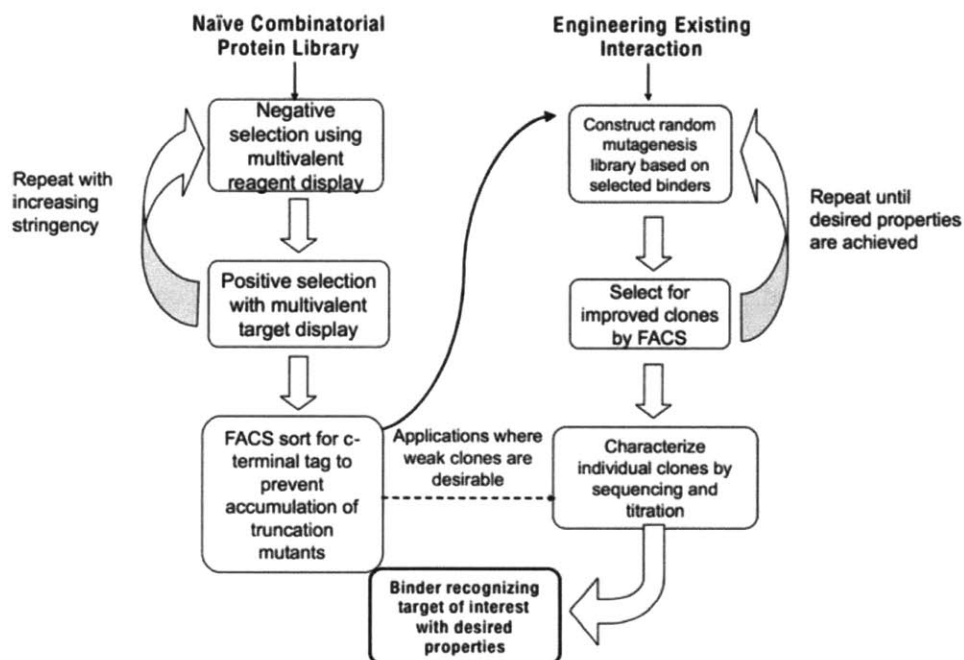


**Figure 5.4.6: Selection Profile for Successful Molecular Evolution:** A flow diagram for successful molecular evolution showing the complementary roles of bead-based and FACS-based selections in the isolation of proteins with desired binding properties.

#### 5.4.7 Recommended quality control steps for *de novo* selections

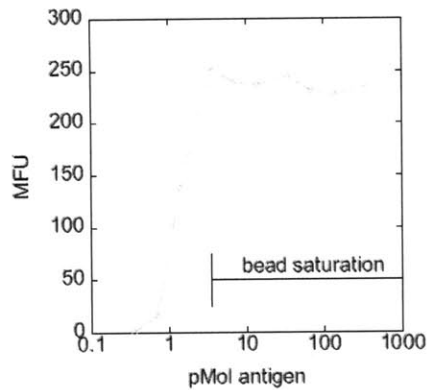
For *de novo* selections, several quality control steps are recommended for best results. First, in order to ensure that even low affinity clones can be reliably selected, care must be taken to ensure that maximum valency between yeast and beads can be reached. This end is achieved in two ways: first, the yeast must be induced to a high expression level; and second, the beads must be saturated with the target antigen in order to ensure the selection pressure is solely against the intended target, and not against either empty streptavidin, or biotin:streptavidin complexes, and provides the opportunity to achieve the highest degree of valency. Provided the antigen is multiply biotinylated, a small dilution (1  $\mu$ l) of beads may be incubated with varying amounts of the antigen overnight, and then beads can be labeled with streptavidin-PE to allow the formation of avidin sandwiches. The labeled beads can then be analyzed on a flow cytometer, and the PE signal determined. This signal is proportional to the antigen coating density. The investigator should ensure that the bead coating conditions used fall into the fully saturated region, as depicted in Figure 5.4.7a. Conversely, if the target antigen is singly biotinylated, then coated beads can be labeled with biotin:FITC and a lack of signal indicates bead saturation. Additionally, one must remove any free biotin from the preparation of biotinylated target protein, as free biotin will both decrease the surface density of the target protein and increase the likelihood of isolating binders to biotin:streptavidin.

Second, care should be taken in properly setting the stringency of each round. Initial rounds of selection can be carried out without washing the beads. If early washes are performed, the duration of the wash should be extended, as the wash period largely

functions to allow rebinding after disruption of yeast:bead complexes due to resuspension. Means to increase stringency include increasing the number of washes or temperature of incubation, decreasing the yeast display level, decreasing the antigen coating density, or performing an incubation with soluble antigen followed by a brief incubation with beads as described in the protocol of Yeung et al <sup>22</sup>. However, most of these strategies greatly increase the likelihood of isolating streptavidin binders, and should be used only after multiple negative selections. Additionally, with the exception of Yeung's method, these strategies are still more highly dependent on the valency than on affinity, but will gradually enrich higher affinity clones.

Lastly, dilutions of both the negatively and positively selected populations should be plated in order to compare the number of yeast binding to streptavidin beads versus target-coated beads, as well as to assess the theoretical diversity of the population. A history of these counts allows the investigator to determine whether progress is being made toward engineering the desired interaction. After several selections, if the colony count for target-coated beads is larger than that for streptavidin beads, then it is likely that progress is being made in isolating a binder to the target of interest, and the population ought to be diversified. Such a plot is presented for the progress of selections against biotin:streptavidin in Figure 5.4.7b.

A



B

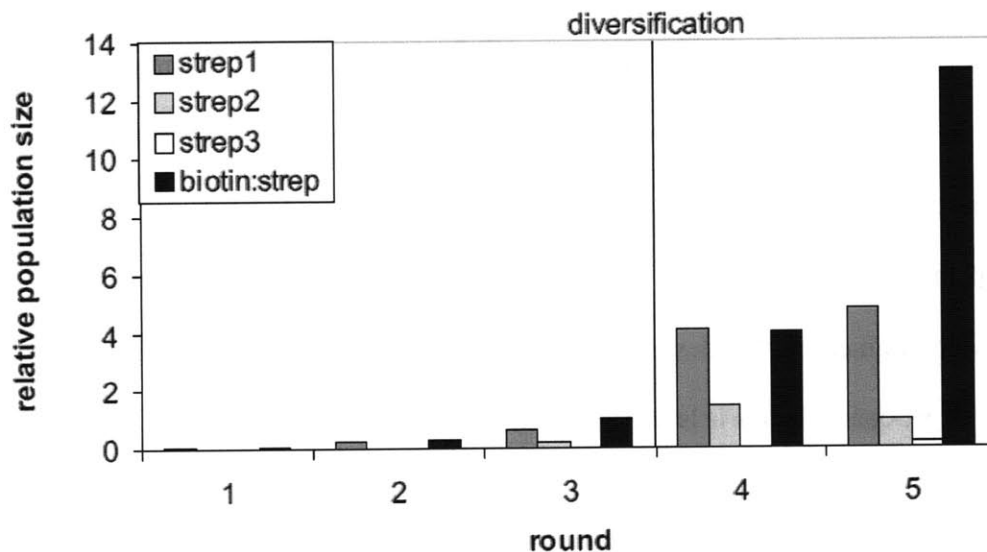


**Figure 5.4.7: Recommended steps for quality control. (a) Ensuring bead saturation:** 1  $\mu$ l of beads was incubated with varying molar quantities of a multiply biotinylated target antigen overnight, followed by detection via streptavidin-PE. The region of maximum fluorescence represents incubation conditions which saturate with the target antigen. **(b) Tracking selection progress:** Beads used in negative (streptavidin alone) and positive (biotin:streptavidin) selections were resuspended in 1 ml PBS-BSA and washed for 15 minutes. The magnet was applied, supernatant removed, and beads were again resuspended in 1 ml PBS-BSA. Dilutions of the resulting bead:yeast mix were plated, and colonies counted. A history of these colony counts over the course of the selections is presented. The population was diversified after 3 selections, and after 5 selections, FACS analysis confirmed that the population contained nM binders to biotin:streptavidin with undetectable affinity to streptavidin alone.

## 5.5 Discussion

Because of their robust protein processing machinery, yeast are an excellent host organism for protein engineering efforts. FACS, while an optimal tool for making fine discrimination among variants<sup>7</sup>, is less well suited for *de novo* selections. Accordingly, we sought an alternative method for early selection rounds that would avoid the limitations posed by FACS. These limitations include the size of the population that can be analyzed, the affinity of binding clone that can be reliably captured, the amount of target antigen needed, and the likelihood of capturing alternative solutions to the selective pressure. Here we have demonstrated a method for capturing rare clones that maintains the advantages of YSD, while avoiding the disadvantages of FACS in isolating *de novo* binders from naïve libraries. Coupling the multivalency of YSD with multivalent target presentation allows screening of billions of yeast in a microcentrifuge tube in an hour and is able to capture even interactions of micromolar affinity.

While previous studies have utilized magnetic beads (MACS) rather than FACS for the first round of library selection, they have done so in order to select from larger sized populations, and not to capture weak interactions, and have thus incubated yeast with soluble antigen rather than pre-coating the magnetic beads. While such a method still possesses some advantages over FACS, such as less time for target dissociation during the selection and the ability to screen a larger population, it remains less suitable for naïve selections than utilizing antigen-coated beads because it requires considerably more antigen, only captures clones of affinities similar to the concentration of antigen achieved in the soluble incubation, and has a high risk of selecting reagent binders.

While the ability to capture weak binders is generally only necessary when no suitably strong binders are present in a population, the additional inclusion of weak clones is likely to provide benefits due to the uneven topology of the sequence-fitness landscape, in which the fittest final solution does not necessarily arise from the fittest initial solution as some sequence variants have a higher inherent capacity for improvement.

Moreover, there are some circumstances in which it may be necessary or beneficial to work with low affinity interactions. For example, when T cell receptors are engineered to interact with specific peptide-MHC complexes, variants with high affinity to the complex often interact with moderate affinity to MHC independent of the presence of the cognate peptide leading to non-specific stimulation, or stimulation when other peptides are present<sup>23</sup>. In order to maintain a requirement for peptide, weak interactions may be necessary. Because such weak interactions are not reliably detectable by FACS, use of the multivalent bead method described here may be advantageous.

Beyond the ability to isolate weak interactions, the use of multivalent beads permits a high local concentration of the target antigen to substitute for a high systemic concentration, decreasing the amount of antigen required for initial selections by almost 2 orders of magnitude. FACS selections often proceed at a 5  $\mu$ M systemic concentration, while beads require far less antigen yet present the target at a mM local concentration—potentially allowing isolation of binders with extremely weak affinities.

While the method described here does require the use of tags and other reagents, isolation of reagent-binding clones can be avoided by the use of bead-based negative selections. This means to scrub populations of reagent binders dramatically increases the

probability of isolating clones capable of interacting with the desired target. In fact, the ability to remove some 99.8% of even extremely weak reagent binders in 4 hours makes the method useful as a negative selection regardless of the method used for positive selections. Such an effective negative screen is in stark contrast with attempts to use FACS as a method for negative selections. Negative selections by FACS are generally ineffective not only because of errors made in droplet sorting, but because the regrowth and subsequent induction required allows reagent-binding clones with low expression during the negative selection a second chance during subsequent re-induction to fall into the sort window. For example, even if negative selections by FACS were able to reliably decrease the prevalence of reagent binders 100-fold, subsequent regrowth and the practice of analyzing a 10-fold excess of library diversity would diminish the effect of the negative selection to a 10-fold reduction in the total number of reagent binders. Given sort windows typically drawn to capture the top 0.1 to 1% of the population, once present, reagent-binders are generally impossible to remove from the library by FACS. Conversely, negative selection by the multivalent bead method described here is able to reduce reagent binders almost 1000-fold in 4 hours, after which a positive selection can be carried out without regrowth—greatly diminishing the chances of enriching these undesirable solutions to the selective pressure.

An improved means to isolate binders from naïve libraries also increases the utility of both alternative scaffold and human scFv libraries, and decreases reliance on immunization of mice or other animals followed by subsequent humanization for initial binding clones. This advance ought to allow isolation of novel binders with greater ease, speed, and higher probability of success than previous techniques.

In conclusion, multivalent antigen presentation on magnetic beads allows microgram quantities of antigen to identify and select even extremely weak binders with high efficiency from populations of billions of yeast. Magnetic bead selection combines the advantages of yeast as a protein engineering host and complements the subsequent use of FACS to isolate variants with improved properties.



## 5.6 Works Cited

1. Gai, S.A. & Wittrup, K.D. Yeast surface display for protein engineering and characterization. *Curr Opin Struct Biol* **17**, 467-73 (2007).
2. Boder, E.T. & Wittrup, K.D. Yeast surface display for screening combinatorial polypeptide libraries. *Nat Biotechnol* **15**, 553-7 (1997).
3. Bowley, D.R., Labrijn, A.F., Zwick, M.B. & Burton, D.R. Antigen selection from an HIV-1 immune antibody library displayed on yeast yields many novel antibodies compared to selection from the same library displayed on phage. *Protein Eng Des Sel* **20**, 81-90 (2007).
4. Piatasi, A. et al. Directed evolution for improved secretion of cancer-testis antigen NY-ESO-1 from yeast. *Protein Expr Purif* **48**, 232-42 (2006).
5. Lipovsek, D. et al. Selection of horseradish peroxidase variants with enhanced enantioselectivity by yeast surface display. *Chem Biol* **14**, 1176-85 (2007).
6. Wittrup, K.D. Protein engineering by cell-surface display. *Curr Opin Biotechnol* **12**, 395-9 (2001).
7. VanAntwerp, J.J. & Wittrup, K.D. Fine affinity discrimination by yeast surface display and flow cytometry. *Biotechnol Prog* **16**, 31-7 (2000).
8. Tanaka, T., Yamamoto, T., Tsukiji, S. & Nagamune, T. Site-specific protein modification on living cells catalyzed by Sortase. *Chembiochem* **9**, 802-7 (2008).
9. Griffiths, A.D. & Duncan, A.R. Strategies for selection of antibodies by phage display. *Curr Opin Biotechnol* **9**, 102-8 (1998).
10. Hackel, B.J., Kapila, A. & Wittrup, K.D. Picomolar affinity fibronectin domains engineered utilizing loop length diversity, recursive mutagenesis, and loop shuffling. *J Mol Biol* **381**, 1238-52 (2008).
11. Crothers, D.M. & Metzger, H. The influence of polyvalency on the binding properties of antibodies. *Immunochemistry* **9**, 341-57 (1972).
12. Klemm, J.D. & Pabo, C.O. Oct-1 POU domain-DNA interactions: cooperative binding of isolated subdomains and effects of covalent linkage. *Genes Dev* **10**, 27-36 (1996).
13. Jung, S.T., Jeong, K.J., Iverson, B.L. & Georgiou, G. Binding and enrichment of Escherichia coli spheroplasts expressing inner membrane tethered scFv antibodies on surface immobilized antigens. *Biotechnol Bioeng* **98**, 39-47 (2007).
14. Richman, S.A. et al. Development of a novel strategy for engineering high-affinity proteins by yeast display. *Protein Eng Des Sel* **19**, 255-64 (2006).
15. Baccarini, M., Bistoni, F. & Lohmann-Matthes, M.L. In vitro natural cell-mediated cytotoxicity against Candida albicans: macrophage precursors as effector cells. *J Immunol* **134**, 2658-65 (1985).
16. Wang, X.X. & Shusta, E.V. The use of scFv-displaying yeast in mammalian cell surface selections. *J Immunol Methods* **304**, 30-42 (2005).
17. Chao, G. et al. Isolating and engineering human antibodies using yeast surface display. *Nat Protoc* **1**, 755-68 (2006).
18. Lubic, S.P. et al. Biodistribution and dosimetry of pretargeted monoclonal antibody 2D12.5 and Y-Janus-DOTA in BALB/c mice with KHJJ mouse adenocarcinoma. *J Nucl Med* **42**, 670-8 (2001).

19. Corneillie, T.M., Fisher, A.J. & Meares, C.F. Crystal structures of two complexes of the rare-earth-DOTA-binding antibody 2D12.5: ligand generality from a chiral system. *J Am Chem Soc* **125**, 15039-48 (2003).
20. Boder, E.T., Midelfort, K.S. & Wittrup, K.D. Directed evolution of antibody fragments with monovalent femtomolar antigen-binding affinity. *Proc Natl Acad Sci USA* **97**, 10701-5 (2000).
21. Nieba, L. et al. BIACORE analysis of histidine-tagged proteins using a chelating NTA sensor chip. *Anal Biochem* **252**, 217-28 (1997).
22. Yeung, Y.A. & Wittrup, K.D. Quantitative screening of yeast surface-displayed polypeptide libraries by magnetic bead capture. *Biotechnol Prog* **18**, 212-20 (2002).
23. Colf, L.A. et al. How a single T cell receptor recognizes both self and foreign MHC. *Cell* **129**, 135-46 (2007).

## Chapter 6: An *in vitro* assay to predict clinical B-cell immunogenicity of therapeutic proteins

### 6.1 Abstract

Protein therapeutics promise systemic exposure with increased specificity of action; and as the fastest growing class of approved drugs, they are beginning to deliver on this promise. However, such biologics pose additional safety concerns due to their immunogenicity, or tendency to be recognized as foreign by the immune system. The resulting adaptive immune response to the therapeutic can lead to both the rapid clearance of drug prior to any pharmacologic benefit, as well as to severe toxicities. Unfortunately, particularly with protein drugs which contain non-human components, there has been no satisfactory pre-clinical means of assessing B-cell, or antibody-mediated immunogenicity—leading to costly late stage failures, and necessitating time consuming and complicated animal and safety studies. Here, we describe an *in vitro* method of assessing the B-cell immunogenicity of candidate drugs utilizing protein engineering tools. By combining a human scFv library with a selection technique capable of isolating extremely weak interactions via avidity, we demonstrate a correlation between scores using our *in vitro* assay and the clinical immunogenicity profile of a wide range of protein drugs.

## 6.2 Background

Beginning with the clinical use of human blood products, organ transplants, and administration of orthologous proteins, it has been recognized that therapeutic proteins have safety considerations beyond the requirements for small molecules. Namely, such biologics must be characterized for their immunogenicity, that is, their tendency to be recognized as foreign and to generate an adaptive immune response. Biologics that induce such an immune response can cause significant toxicities, including inflammation, anaphylaxis, complement mediated cell lysis, as well as to have altered clearance leading to extremely limited efficacy and toxicity. While this is particularly true for proteins originating from non-human species with no human counterpart, it has been observed even with completely native human proteins.

In particular, clinical experience with therapeutic antibodies of murine origin has created an entire industry around the “humanization” of such biologics, in which numerous methods are available to decrease immunogenicity. For antibodies, initial strategies included chimeric fusions, in which whole murine domains were simply replaced by their human counterpart, leaving only the variable domains of murine origin. Subsequently, complementarity determining region (CDR) and specificity determining region (SDR) grafting, in which only a subset of amino acids located in the antigen recognition domains of the antibodies are of non-human origin<sup>1</sup>. Sequence comparisons to germline human antibodies, and computational analysis of residue frequency or rarity at a given position may also be used to minimize the immunogenicity of a therapeutic antibody. Collectively, these tools have led to vast improvements in the safety profile of recombinant antibodies.

But for other biologics, such as those utilizing plant or bacterial toxins or enzymes, which have no human ortholog, there are no similar structural, computation, or comparative tools available to facilitate humanization. Furthermore, there are numerous cases in which even completely human proteins have led to immune stimulation<sup>2,3</sup>. Early efforts at studying immunogenicity have relied on injecting patients or animals with therapeutic and then harvesting reactive T-cells and antibodies, mapping the epitopes they recognize, and then attempting to alter these specific epitopes<sup>4-6</sup>. The limits of these studies are fairly obvious in that they are conducted at a very late stage, and are extremely time-consuming and expensive. Animal studies, including use of mice with humanized immune systems, have been used frequently<sup>7</sup> with notable success. They have been most useful when studying variants of a particular protein, and are generally able to rank the relative immunogenicity between similar proteins<sup>4,8</sup>. Here also, the limits of these strategies are clear as immunogenic epitopes are sometimes conserved across species and sometimes not<sup>9,10</sup>. Better tools, particularly those that can be implemented early in clinical development are clearly needed.

Both arms of the adaptive immune system function in determining the immunogenicity of a therapeutic protein, and though there is sometimes significant overlap between the epitopes recognized by both T and B cells, the best means to assess clinical immunogenicity will involve study of both. Despite having very different mechanisms of action, both T and B cells have a functional diversity that is generated by high levels of genetic recombination, and tempered by deletion of variants that are self-reactive or fail certain checks of quality control<sup>11</sup>.

In the case of T-cells, as the therapeutic protein is taken up by cells, it is degraded into peptides and these fragments are presented on MHC class I and II molecules. T-cells then interact with the peptides bound in the groove of the MHC molecules through their cognate T-cell receptors (TCRs), and depending on fit and other signals at the immunological synapse, are stimulated, triggering a cytotoxic response toward cells displaying this peptide. Several aspects of T-cell biology have made assessments of T-cell immunogenicity a much more tractable problem for *in vitro* prediction. First, T-cell epitopes are linear—allowing simple sequence information to substitute for 3-dimensional crystal structures. Second, MHC structures are known, and computational tools exist for evaluating the fit of various peptide fragments *in silico*<sup>12</sup>. Lastly, the pool of TCRs has a diversity limited enough to be sufficiently covered for testing *in vitro*. Together, these factors have allowed the development of *in vitro* T-cell stimulation assays that are highly predictive of clinical immunogenicity<sup>13, 14, 15</sup>.

T-cell stimulation assays can be carried out by culturing either single donor or pooled T cells with overlapping peptides or whole protein and monitoring stimulation. These procedures can identify T-cell epitopes with great success, and coupled with computational modeling tools allowing the fit of various peptides to MHC to be predicted, have led to excellent ability to remove T-cell stimulatory epitopes from biologics. Now public and private databases which house this information are available and published protocols exist for *in vitro* screens.

However, satisfactory methods for comparable *in vitro* determination of B-cell epitopes do not exist. The computational community has worked to develop prediction tools and databases of mapped linear epitopes, but despite having shown some promise

with test cases, they are not widely utilized in clinical development, as they tend to suffer from insufficient predictive quality<sup>16-18</sup>. The prevalence of conformational, or non-linear, discontinuous epitopes make it a difficult problem to study even by methods which additionally require crystal structure information. Coupled with this difficulty on the epitope side, the particulars of B-cell biology, including the vast diversity of antibodies and their initially low affinity interactions with target antigen, which may be difficult to detect using standard techniques prior to somatic hypermutation and resulting affinity maturation make prediction of B-cell epitopes a significant challenge.

The combined effect of these hurdles has been to effectively limit B-cell epitope determination to being an *in vivo* problem of study, leaving investigators to inject biologic, wait for immune response, pull out antibody, map the binding epitopes, then alter those epitopes somewhat rationally, and repeat—an extremely time consuming, expensive, and in the case of human clinical studies, far from optimal mode of study. This strategy has sometimes been performed in animal models, under the supposition that the same epitopes will be immunogenic in multiple species, but has also been performed directly and painstakingly in human clinical studies. While animal models have been useful in ranking the relative immunogenicity of various constructs, as well as in specifically mapping immunogenic epitopes, the resulting sequence changes have sometimes been better at reducing immunogenicity in animal models than in humans. An *in vitro* means to predict B-cell, or antibody epitopes in humans is clearly needed.

The method described here combines two protein engineering tools: yeast surface display of a human scFv library constructed for protein engineering efforts<sup>19</sup>, and highly avid magnetic beads, capable of isolating extremely weak specific interactions<sup>20</sup>, to score

the B-cell immunogenicity of a given therapeutic candidate. The human scFv library used was generated by cloning out heavy and light chain variable domains from the circulating B-cells in 50 adult volunteers resulting in a library of  $10^9$  sequences. Because B-cells in circulation have already undergone negative selection against self proteins, we theorize that the library will be less reactive toward human proteins than other species. In fact, there has been some discussion as to this library being non-ideal for engineering binding interactions against human targets for this reason. Furthermore, we expect that the diversity of scFv sequences adequately captures the diversity of antibody function *in vivo*, and can therefore be used to predict the relative immunogenicity of proteins, as well as perhaps to identify immunogenic epitopes.

Candidate proteins are biotinylated and immobilized at mM surface densities on magnetic beads, and then incubated with yeast displaying a library of human scFv sequences. Yeast capable of binding to the protein-coated beads are selected and counted. This count provides a means to assess the reactivity of the human antibody repertoire to a given protein. We demonstrate the ability of this assay to consistently score human proteins as lower immunogenicity compared to their orthologs from other species, agreement with clinical immunogenicity for a panel of antibodies used as therapeutics, and differentiation between protein variants that diverge by as few as 2-8 amino acids, or that have been conjugated with polyethylene glycol (PEG) as a means to sterically block interaction with the immune system.



## **6.2 Materials and Methods**

### **Protein production**

9 species of albumin, and 2 IgG's were purchased in high purity from Sigma. Alginate lyase was produced as described (Griswold, manuscript in preparation), and pegylated via site specific maleimide-cysteine chemistry. CEA-binding scFv bearing his<sub>6</sub> tags were cloned into pCT-based vectors and produced in YVH10 yeast as described<sup>21</sup>, and purified using affinity chromatography (Clontech Talon resin). A33 antibodies were a gift of Gerd Ritter at Memorial Sloan Kettering and the Ludwig Institute. The EGFR antibody Ab806 was a gift of Jamie Spangler, Massachusetts Institute of Technology. Immunotoxins were produced as described<sup>22</sup>.

Proteins were biotinylated essentially according to the manufacturer's instructions (Pierce sulfo-nhs-LC-biotin), except for tuning the relative molar amounts of reagent: protein, so as to minimize excessive biotinylation. Free biotin was removed by extensive serial buffer exchange using Amicon spin columns of appropriate molecular weight cutoffs. Successful biotinylation was confirmed by western blot, and can be quantified using the Pierce biotin quantification kit. Target biotinylation levels were between 1-3 biotin groups per molecule.

### **Yeast handling**

The scFv library was grown and induced as described<sup>19,23</sup>. Briefly, yeast were thawed and subcultured twice in SD-CAA before induction in SG-CAA at 20°C for 24 hours. Induction quality was assessed by labeling for c-myc expression (Invitrogen

A21281, A11309) and analysis on a Coulter EPICS flow cytometer for each induced population prior to use.

### **Bead coating**

Biotin binder magnetic beads (Invitrogen 11047) were coated with protein as follows. Approximately  $1 \times 10^7$  beads (25  $\mu$ l) were washed twice with phosphate buffered saline with 0.1% carrier protein (PBS), then incubated with 50  $\mu$ l of biotinylated target protein at a concentration of 100  $\mu$ g/ml, diluted with 500  $\mu$ l PBS and rotated overnight at 4°C. Complete coating was confirmed by incubating beads with differing amounts of target protein, then labeling beads with streptavidin-PE and analyzing on a flow cytometer, as described<sup>20</sup>. A curve of fluorescence versus target protein concentration was generated, and saturating labeling conditions in which an increase in protein concentration did not yield an increase in fluorescence were used. Following coating, beads were washed twice in PBS to remove excess protein.

### **Assay**

For each protein panel,  $4 \times 10^9$  yeast cells were spun down, and in order to deplete the population of streptavidin binding scFvs, were then incubated with 100  $\mu$ l streptavidin beads at 4°C for 1 hour. The yeast:bead slurry was then placed on a magnet for 5 minutes, and unbound yeast were removed using a pipet. In some cases, a second negative selection was also performed against beads coated with a heavily biotinylated irrelevant protein in order to deplete biotin-binding scFvs from the population. The negatively selected yeast were then incubated with pooled beads, each coated

individually with a single protein of interest from the panel being studied for a minimum of 1 hour at 4°C on a rotator. The yeast:bead slurry was again placed on a magnet for 5 minutes, and unbound yeast were removed using a pipet. The remaining beads and yeast were resuspended in 1 ml of PBS, added to 50 mls of growth media, and subsequently induced. This process was repeated a second time with pooled beads, and a 10-fold oversampling of the population bound to beads in the first pass, as determined by optical density measured immediately following the addition of the selected yeast to growth media. Following the second bead selection, truncation mutants were removed by labeling for c-myc expression and collecting all full length (c-myc positive) clones on a FACSAria sorter. Again, a 10-fold oversampling of the population was sorted.

Following these initial selections, yeast were induced, and for each protein in the panel tested,  $10^7$  yeast, representing at least a 10-fold oversampling, were negatively selected for bead and/or biotin binding, then incubated with 10-25  $\mu$ l of beads coated with each antigen individually for at least 1 hour at 4°C on a rotator. The slurry was placed on a magnet for 5 min, after which unbound yeast were removed and discarded. The remaining yeast:bead mixture was resuspended in 1 ml of PBS, and a 50  $\mu$ l aliquot designated wash 1 was removed for serial dilution and plating on SD-CAA to determine the size of the initially bound population. The resuspended yeast and beads were then incubated at 4°C for 15 minutes on a rotator, and then placed on the magnet a second time. Unbound yeast were removed, bound yeast and beads resuspended, and an aliquot designated wash 2 was removed for plating. This process was then repeated a third time, and the final bead-bound population was retained for further analysis.

Plated dilutions were incubated for 2 days at 30°C, and then colonies were counted. Generally, 2 separate dilutions had countable populations (between 5 and 200 colonies), and these counts were averaged.

### **Data analysis**

All data was collected in triplicate. Because total colony counts are greatly dependent on the expression level of the yeast<sup>20</sup>, which can vary significantly from one induction to another, counts between replicates were not compared directly, but counts were ratioed to the mean number of yeast bound in each wash population. Analysis around the mean further allowed the tendency of single high or low counts to greatly skew the entire data set to be minimized. The average and standard deviation of 3 replicates is presented.

### **Follow-up experiments**

For some data sets, the wash 3 yeast populations isolated against specific proteins were grown, induced, and subjected to follow-up study. For the albumin and alginate lyase panel, individually selected populations, as well as clones were subsequently bead-selected against their specific target as well as other targets and binding counts were determined. In other cases, the target protein was multiplexed by incubating with streptavidin-PE, incubated with yeast, and then analyzed by flow cytometry to observe specific binding.

## **Sequencing**

Plasmids were collected from selected yeast populations by zymoprep (Zymo Research D2004), and then transfected into XL-1 blue cells (Stratagene 200130) according to the manufacturer's protocols. Colonies were picked, grown for 10 hours in LB Amp with 10% glycerol, and submitted to Agencourt Biosciences for sequencing using the atermmid primer<sup>23</sup>.

## **6.4 Results**

### **6.4.1 Assay process**

The B-cell immunogenicity assay is schematized in Figure 6.4.1. Briefly, panels of similar proteins were assembled and biotinylated. Streptavidin beads were coated with the proteins of interest, washed twice, combined, and incubated with yeast expressing the Feldhaus human scFv library. After co-incubation at 4°C on a rotator, tubes were placed on a magnet, and unbound yeast removed. Bound yeast were regrown, induced, selected against pooled beads a second time, and then sorted by FACS to remove truncated scFvs. The resulting population was induced and then selected against each protein in the test panel individually, and dilutions of the bead-bound yeast were plated to allow the number of yeast interacting with each protein target to be counted. This basic process was followed in order to minimize divergence between the populations of selected yeast. Because the bead-based selections are highly sensitive to the expression level of the yeast, they were carried out on pooled beads, so that all proteins in the panel were incubated with a single yeast population. Additionally, negative selections were performed to remove bead (streptavidin) and biotin binding clones from the population. These negative selections were performed prior to each positive selection. Only 2 pooled sorts were performed in order to maintain an appropriate balance of selectivity and diversity. Because the bound yeast and beads were not washed, but were simply regrown, a large number of non-binding yeast are carried over each pooled selection. This is likely due to simply being trapped between the wall of the tube and the beads as they migrate toward the magnet. Based on the diversity of clones sequenced after subsequent selection against a single protein target, we concluded that 2 pooled bead

sorts, followed by one selection against a single protein gave an appropriate balance between selectivity and diversity. Furthermore, the sizes of all populations analyzed were maintained such that the number of binding yeast did not exceed the binding capacity of the beads used, which was experimentally determined.

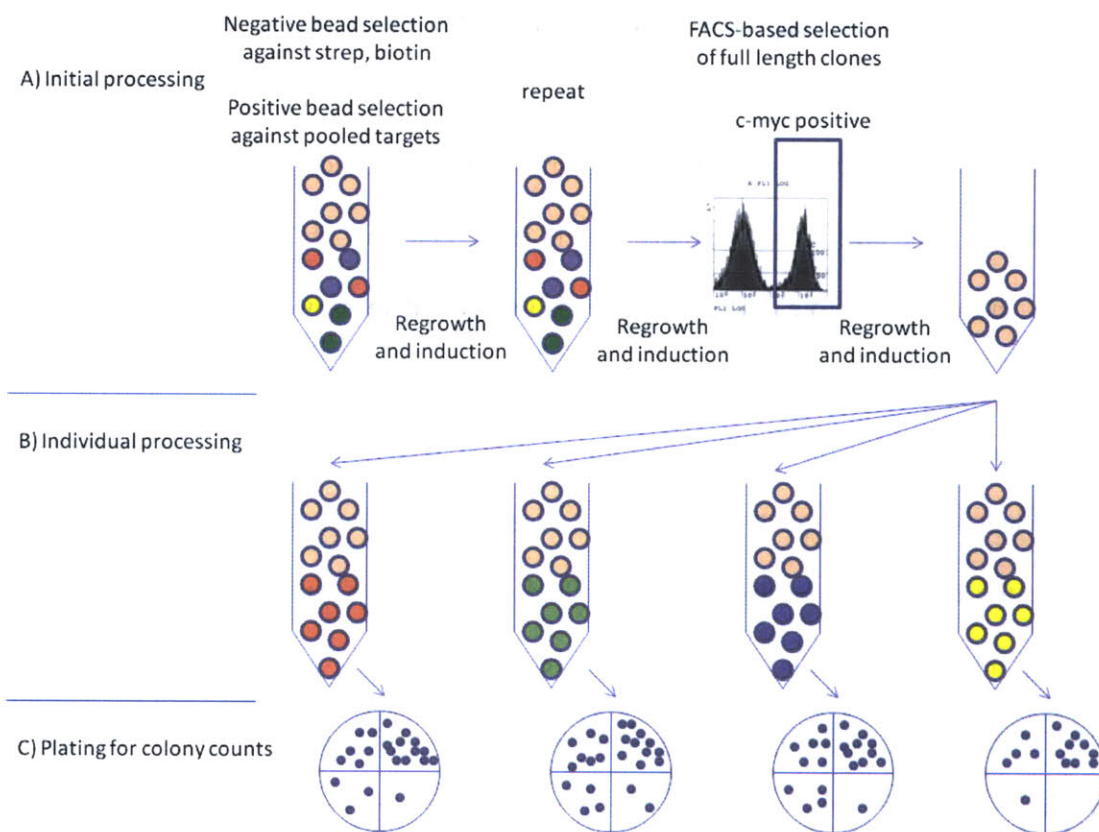


**Figure 6.4.1: Assay process** (a) Initial processing: the scFv library is first depleted of reagent binders by removing yeast that bind magnetic beads and/or biotin, then enriched for yeast which bind the proteins of interest by isolating yeast which bind to protein-coated beads. This process is repeated, and then full length clones are isolated by FACS. (b) In triplicate, the resulting yeast population is then depleted of reagent binders again, and then divided into aliquots which are incubated with beads coated with each protein of interest individually. (c) The bound yeast and bead slurry is washed 3 times, and each wash population is serially diluted and then plated to determine the number of yeast expressing scFVs that interact with each protein.

#### 6.4.2 Assay quality control

Because truncated proteins tend to be misfolded and may consequently have exposed hydrophobic regions, their presence could skew the binding counts via non-specific interactions. Accordingly, a single FACS sort gated on the c-myc tag located at the C-terminus of the displayed scFv was conducted to isolate the full-length clones. Despite the tendency of misfolded truncations to exhibit non-specific sticking, their prevalence was not increased significantly in 2 rounds of bead sorting, and remained at roughly the same level as was initially present in the Feldhaus library (Figure 6.4.2a).

In the single protein selections, beads and bound yeast were washed 0 to 2 times prior to plating. This washing consisted of removal of unbound yeast, resuspension of beads and remaining yeast, followed by a 15 minute incubation at 4°C on a rotator prior to placement on the magnet, and yielded 3 separate colony counts. In general the count before the first wash (wash 1) was very high compared to subsequent counts (Figure 6.4.2b), likely due to the high density of yeast cells present in the incubation mixture prior to washing (100 million/ml), and resulting passive trapping of non-binding yeast by migrating beads. Once the beads were resuspended once, the density was significantly decreased, along with the probability of grossly inflating colony counts via passive trapping. Accordingly, in the analysis of colony counts, wash 1 was excluded, and the data presented consists of the wash 2 and 3 counts averaged over triplicate samples.

Because total colony counts are greatly dependent on the expression level of the yeast<sup>20</sup>, and expression level can vary significantly from one induction to another, counts between replicates were not compared directly, but counts were ratioed to the mean number of yeast bound in the panel for each wash population. This prevents any one



replicate from dominating the analysis due to much higher counts. Similarly, analysis around the mean further allowed the tendency of single high or low counts within a replicate to greatly skew the entire data set to be minimized. The average and standard deviation of 3 replicates is presented.

We determined assay reproducibility by performing 2 separate repeats starting from the initial library and followed through final plate counts independently. This was done for both bovine and human albumin (Figure 6.4.2c) and murine and human IgG (Figure 6.4.2d). Binding counts were centered around the average number of binders for each wash, and the average number of binders across each triplicate was determined for each protein. In all analyses, the count for the human protein variant was assigned a score of one, and the ratio of binding to other targets was calculated. In independent assays, bovine albumin scored as approximately 3 times more reactive to the scFv library as human, and murine IgG scored as approximately 6 times more reactive than human. Across independent tests, there was very good agreement between these values.

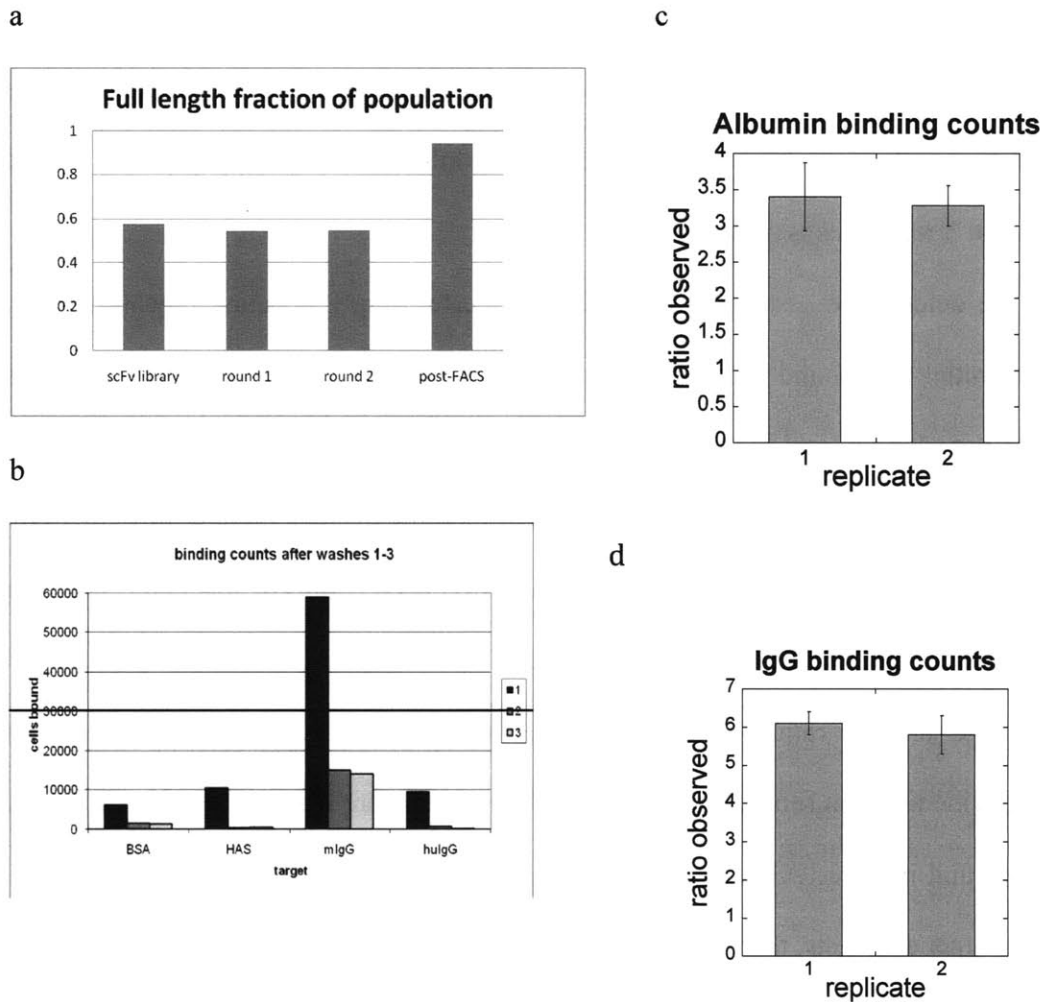


**Figure 6.4.2: Assay quality control.** (a) Initial library composition: the naïve library, populations singly and doubly selected against pooled beads, and following the FACS sort were labeled for c-myc expression, demonstrating no strong trend toward selection of truncation mutants, and their complete removal following FACS. (b) Effect of washes on binding counts: wash 1, 2, and 3 binding counts against 4 targets of interest, demonstrating the trends observed for binding count over the course of 3 washes. The initially high binding counts are likely due to the high density of yeast cells present in the incubation mixture prior to washing. (c) Assay reproducibility: ratio of yeast binding to bovine:human albumin in 2 separate replicates starting from the initial library and followed through final plate counts independently. (d) Assay reproducibility: ratio of yeast binding to murine:human IgG in 2 separate replicates starting from the initial library and followed through final plate counts independently.

### 6.4.3 Panels of human and orthologous proteins

Next, we tested a panel of albumin from 8 different species, and human albumin produced from recombinantly in yeast (Figure 6.4.3a). As would be expected given the de-selection against self-antigens, the scFv library reacts to the lowest extent against human albumin, yeast-produced recombinant human albumin, and baboon albumin, which would be predicted to have a high degree of sequence homology. All other species ranked as more immunogenic. Interestingly, these scores did not directly agree with phylogenetic similarity to human albumin.

A panel of antibodies were tested, including both a human polyclonal, and 3 antibodies that have been used in the clinic: muA33 and huA33, murine and humanized antibodies to the A33 antigen, and Ab806, a human antibody which recognizes the epidermal growth factor receptor<sup>24</sup>. Murine anti-A33 (muA33) was highly immunogenic<sup>25</sup>, leading to its humanization (huA33). Unfortunately, huA33 retained a considerable degree of immunogenicity, and 63% of patients treated with huA33 developed an immune response characterized by significant titers of anti-huA33 antibodies<sup>26,27</sup>. Figure 6.4.3b presents the ratio observed of yeast binding to muA33, huA33, Ab806 and huIgG to huIgG. These ratios agree strongly with clinical experience, in which murine antibody is highly immunogenic, Ab806 has been safe<sup>28</sup>, and huA33 has been significantly more immunogenic than many other humanized antibodies.

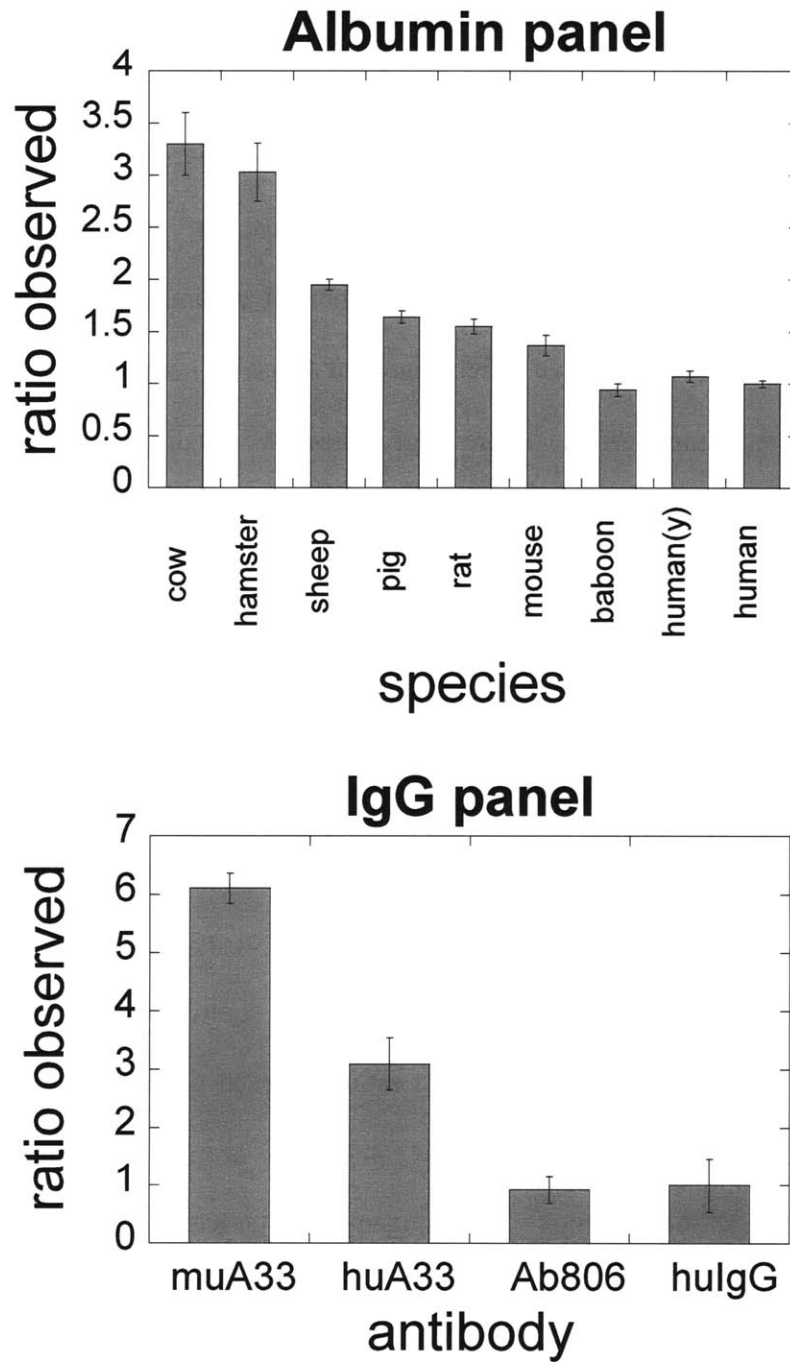


**Figure 6.4.3: Assay results for albumin and IgG.** (a) Ratio observed of yeast binding to muA33, huA33, Ab806 and huIgG to huIgG. Ratios agree with clinical experience. (b) Ratio observed of yeast binding to each species of albumin relative to binding to human albumin. Human albumin, human albumin produced in yeast (y), and baboon score lowest, as would be predicted based on homology arguments.

#### 6.4.4 Fine discrimination between protein variants

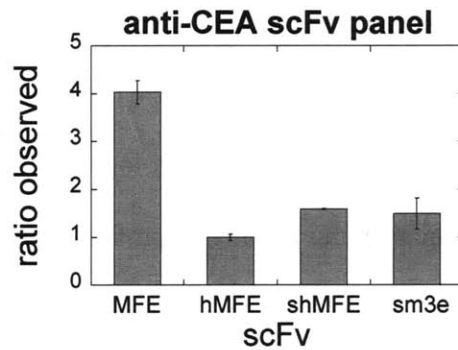
Because the antibodies and albumin variants tested are rather dissimilar, we next looked at whether the assay was able to capture differences between proteins with only a few point mutations. For this, a panel of carcinoembryonic antigen (CEA) binding scFvs were produced, include a murine scFv (MFE)<sup>29</sup>, humanized MFE (hMFE)<sup>30</sup>, a stabilized version of the humanized construct (shMFE)<sup>21</sup>, and a high affinity mutant (sm3e)<sup>21</sup>. These scFvs diverge by 4 to 28 amino acids, and the humanized scFv was generated using the tools available for antibody humanization described previously. As would be expected, MFE, the murine scFv scored highest in the immunogenicity assay, and hMFE, the humanized scFv scored lowest (Figure 6.4.4a). The stability and affinity engineered clones scored slightly higher than hMFE. It remains to be seen whether these engineered variants are clinically more immunogenic than hMFE. However, because the assay is conducted at 4°C in PBS, it is likely that the stabilizing mutations were not beneficial in our analysis. If the assay were conducted at 37°C in serum, it is possible that shMFE and sm3e would have scored lower despite having 4 mutations from its humanized counterpart due better stability and folding at body temperature.

A simple way to reduce immunogenicity is to sterically block interaction of antibodies with the protein of interest by incorporating a polyethylene glycol (PEG) moiety<sup>31</sup>. Therefore, we also tested a highly immunogenic bacterial enzyme, alginate lyase (AL), with (AL-PEG) and without PEG conjugation at a single, genetically controlled site (Figure 6.4.4b). It is important to note that the protein content of these 2 constructs is identical except for a single point mutation to allow control of the PEGylation reaction. Therefore, the difference in binding counts represents the effect

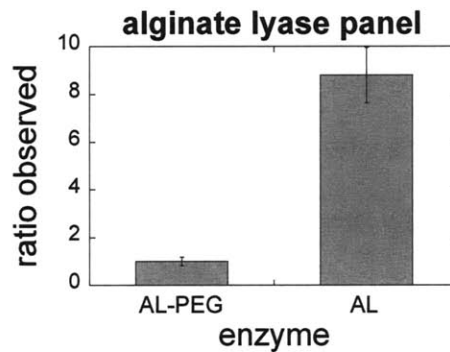
that PEG has on sterically blocking existing immunogenic epitopes, as none of those epitopes have been altered. As is observed clinically, PEG conjugation significantly reduces immunogenicity in our assay.

Lastly, a panel of immunotoxins, consisting of an anti-CD22 scFv fused to pseudomonas exotoxin A (HA22)<sup>32</sup> and a de-immunogenized variant (HA22-8x)<sup>6,33</sup>, which diverges by 8 amino acids were tested. The immunogenic epitopes on the exotoxin were identified by immunizing mice with immunotoxin, and isolating and epitope mapping the sites these antibodies recognized. In general, immunogenic epitopes were altered by the substitution of large hydrophilic residues with glycine or alanine. In mouse models, HA22-8x had significantly reduced immunogenicity<sup>33</sup>, and in human patients, immunogenicity was reduced relative to HA22, but not as significantly (unpublished data, Pastan and Hansen). In good agreement with the human clinical results, our assay reported that HA22 was twice as reactive toward human scFvs as HA22-8x (Figure 6.4.4c).

a



b



c

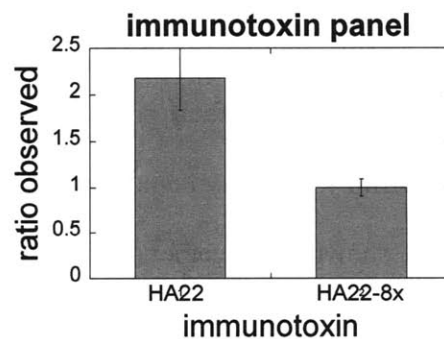


**Figure 6.4.4: Fine discrimination between protein variants.** (a) CEA-scFv panel: 4 anti-CEA scFv's were screened, a murine scFv (MFE, 28 amino acids diverged from hMFE), humanized scFv (hMFE), stabilized humanized scFv (shMFE, 4 amino acids diverged from hMFE), high affinity mutant (sm3e, 6 amino acids diverged from hMFE). (b) Alginate lyase panel: alginate lyase enzyme with (AL-PEG) and without (AL) a single 20,000 kDa PEG molecule site-specifically attached. (c) Immunotoxin panel: HA22 anti-CD22 scFv-pseudomonas exotoxin A fusion (HA22) and de-immunogenized variant HA22-8x (8 amino acids diverged from wild-type immunotoxin).

#### 6.4.5 Diversity and specificity of selected clones

Results thus far have indicated that our *in vitro* immunogenicity assay which counts interactions between clones in a human scFv library and a protein of interest can capture the difference between human and orthologous proteins (albumin, IgG, and scFv), recapitulates the clinical immunogenicity profile of a panel of therapeutic IgGs, captures the steric effects of PEGylation as a means to reduce immunogenicity, and scores the immunogenicity of an immunotoxin in good agreement with human clinical data.

As a follow up to the colony count-based scores, clones isolated in wash 3 were sequenced, and their diversity analyzed. Up to 20 clones isolated against a single target were sequenced, and no duplicate sequences were found, indicating that the assay protocol is not so stringent as to eliminate diversity (data not shown). Selectivity was checked by the induction of single clones isolated from the wash 3 population and then competition against non-expressing yeast to verify binding to protein-coated beads. All clones tested demonstrated specific binding to protein-coated beads (Figure 6.4.5) as determined by their enrichment relative to their prevalence before selection, and some clones bound with sufficient affinity that they demonstrated FACS-detectable binding to their target protein (data not shown). Together, these results indicate that we have achieved selectivity while maintaining diversity.



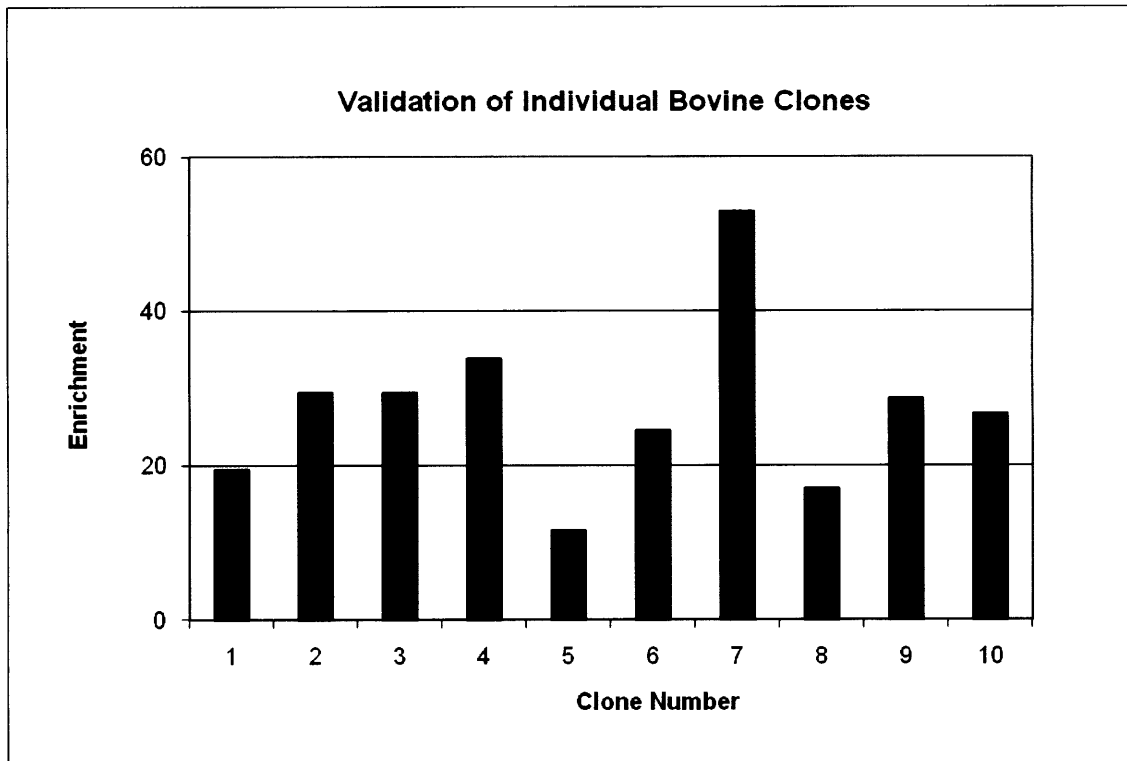


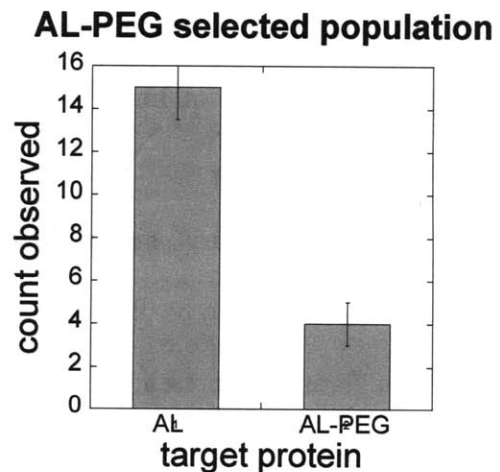
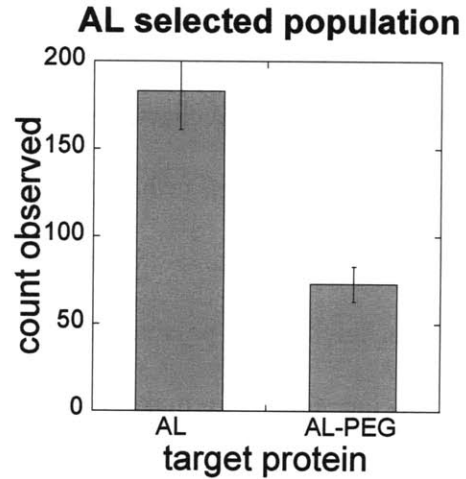
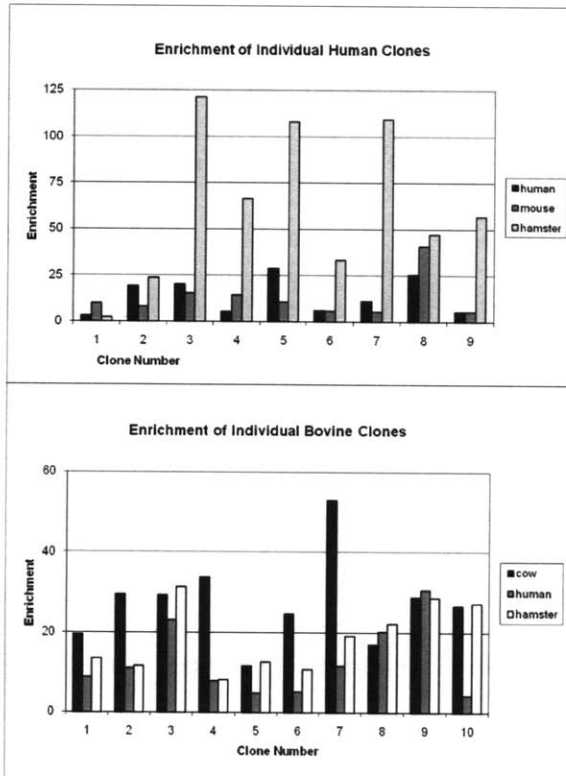
**Figure 6.4.5 Diversity and specificity of selected clones:** 10 clones from the wash 3 population selected against bovine albumin were grown, induced and competed against non-expressing EBY100 yeast for binding to bovine albumin-coated beads. All clones were enriched, indicating that all have a specific interaction with bovine albumin.

#### **6.4.6 Cross-reactivity of selected clones and populations**

Lastly, the cross-reactivity of clones was analyzed. Clones isolated to different species of albumin were tested for their cross-reactivity to albumin from other species. Bovine, human, and hamster-selected clones, were induced and bead selected against bovine and human albumin-coated beads, and a number of cross-reactive clones were identified, as demonstrated by their relative binding counts (Figure 6.4.6a). Interestingly, the clones isolated against human albumin tended to bind better to albumin from other species, whereas the clones isolated against albumin from other species tended to bind best to that species relative to others, particularly human (Figure 6.4.6b). This result, again, is consistent with the de-selection of scFv sequences that bind human targets in the initial Feldhaus library.

As a final test, the wash 3 populations that were isolated against alginate lyase enzyme, with and without PEGylation, were tested for their cross-reactivity. Because all of the same immunogenic epitopes are present in both constructs, and some are simply blocked by the PEG moiety, cross-reactivity testing demonstrates the difference in accessibility of the immunogenic epitopes due to PEGylation. The population isolated against AL had reduced binding to AL-PEG, indicating that the presence of the PEG group limited the interaction between some binding clones to their epitopes (Figure 6.4.6c); and similarly, the population isolated against AL-PEG interacted more strongly with AL (Figure 6.4.6d), indicating that we have not isolated PEG binding scFvs, but have in fact demonstrated that the incorporation of a PEG group simply diminishes the likelihood of interaction between existing immunogenic sites, and the scFv displayed on the surface of yeast. These results agree with animal studies in which subsequent

injection with AL-PEG following an initial injection of AL, resulted in a 44% decrease in reactive antibody titers relative to 2 injections of AL (unpublished data, Griswold).



**6.4.6 Cross-reactivity of selected clones and populations:** (a) Clones from the wash 3 human selection were tested for their enrichment against human, mouse, and hamster albumin. For all clones tested, reactivity to at least one of the orthologous albumins was stronger. (b) Clones from the wash 3 bovine selection were tested for their enrichment against cow, human, and hamster albumin. For half of the clones tested, reactivity toward cow albumin was strongest. In only one case was reactivity against human albumin strongest. Binding of AL (c) and AL-PEG (d) selected clones against AL and AL-PEG. The presence of PEG decreases binding interactions for AL-binding clones, and the removal of PEG increases binding interactions for AL-PEG binding clones.

## 6.5 Discussion

The B-cell immunogenicity assay described here provides a convenient *in vitro* means to assess the clinical safety profile of protein therapeutics using simple colony counts to measure reactivity between a yeast-displayed human scFv library and a protein of interest. We have demonstrated that our assay scores human proteins as less immunogenic than their orthologs, agreement with clinical immunogenicity for a panel of antibodies including a humanized antibody with anomalously high clinical immunogenicity, the passive effects of PEGylation in decreasing immunogenicity, as well as the ability to make fine discriminations between protein variants that have relatively few amino acid substitutions. This last result indicates that not only does this method capture global immunogenicity differences, but could be used to precisely identify and alter immunogenic epitopes without the need for animal studies. Furthermore, the use of highly avid magnetic beads eliminates the need for affinity maturation, and allows rapid screening.

The scFv library used in these studies is a key variable, as it must adequately capture *in vivo* antibody diversity. The technique is predicated on the premise the Feldhaus library is representative of the antibody repertoire *in vivo*. Because the library was constructed from circulating adult B-cells, it indeed ought to reflect the result of negative selection against self-reactive antibody sequences. However, because one of the mechanisms by which auto-reactive antibodies are resolved is by changing the pairing of heavy and light chains, and the means of construction for this library shuffled chain pairings, it is possible that the newly generated pairings restore auto-reactivity. Another shortcoming of this library is that it does not exhibit the same antibody subtype

distribution as native diversity. For example, class 6 variable heavy chain domains are over-represented. Despite these limitations, immunogenicity counts generated using this library correlate well with expectations based on sequence homology and human clinical studies. Perhaps this is not surprising as immunogenicity reductions can translate across species and between individuals. That is, despite the sequence diversity of the antibody repertoire, the same sites seem to frequently act as immunogenic hotspots. Interestingly, there are some indications that there is significant overlap between B and T cell epitopes and that decreasing reactivity toward one arm of the adaptive immune system results in reduced overall immunogenicity—a result that makes sense given the interconnectedness of B and T-cell stimulation.

Factors such as formulation, storage, stability at 37°C, and interactions with plasma proteins also have significant effects on immunogenicity<sup>34</sup>, but are not taken into account by this method. Some alterations to the protocol, such as conducting selections at higher temperature or in human serum could address these added variables. It is likely that no single technique for determining immunogenicity will suffice, but that in combination with T-cell epitope analysis, stability and formulation studies, and monitoring in animal and early human trials, this *in vitro* method for assessing B-cell immunogenicity could help to eliminate the serious side effects and clinical failures caused by immunogenicity.

Future study, perhaps using an scFv library expressly designed for immunogenicity prediction, might allow investigation into trends among self-reactive sequences and immunogenic epitopes, as well as to permit epitope mapping, and allow the generation of databases of immunogenic epitopes to facilitate development of

improved *in silico* methods. Additionally, this study supports the use of antibody libraries that have not been negatively selected against self antigens in protein engineering efforts.

As more biologics come to market, there is a need for increased safety information not required for small molecule therapies. Improved methods for determination of immunogenicity in preclinical models will facilitate drug development and improve the safety of biologics. By combining a human scFv library with a selection technique capable of isolating extremely weak interactions via avidity, we have demonstrated a correlation between scores using our *in vitro* assay and the clinical immunogenicity profile of a wide range of protein drugs, and open the possibility for identification and removal of immunogenic B-cell epitopes from protein therapeutics prior to clinical study.

## 6.6 Works Cited

1. Gonzales, N.R., De Pascalis, R., Schlom, J. & Kashmiri, S.V. Minimizing the immunogenicity of antibodies for clinical application. *Tumour Biol* **26**, 31-43 (2005).
2. Peces, R., de la Torre, M., Alcazar, R. & Urrea, J.M. Antibodies against recombinant human erythropoietin in a patient with erythropoietin-resistant anemia. *N Engl J Med* **335**, 523-4 (1996).
3. Zang, Y.C. et al. Immunoregulation and blocking antibodies induced by interferon beta treatment in MS. *Neurology* **55**, 397-404 (2000).
4. Keil, W. & Wagner, R.R. Epitope mapping by deletion mutants and chimeras of two vesicular stomatitis virus glycoprotein genes expressed by a vaccinia virus vector. *Virology* **170**, 392-407 (1989).
5. Spencer, D.I. et al. A strategy for mapping and neutralizing conformational immunogenic sites on protein therapeutics. *Proteomics* **2**, 271-9 (2002).
6. Onda, M. et al. Characterization of the B cell epitopes associated with a truncated form of Pseudomonas exotoxin (PE38) used to make immunotoxins for the treatment of cancer patients. *J Immunol* **177**, 8822-34 (2006).
7. Wierda D, S.H., Zwickl CM. Immunogenicity of biopharmaceuticals in laboratory animals. *Toxicology* **158**, 71-74 (2001).
8. Zwickl, C.M. et al. Comparison of the immunogenicity of recombinant and pituitary human growth hormone in rhesus monkeys. *Fundam Appl Toxicol* **16**, 275-87 (1991).
9. Milich, D.R. & Leroux-Roels, G.G. Immunogenetics of the response to HBsAg vaccination. *Autoimmun Rev* **2**, 248-57 (2003).
10. Roscoe, D.M., Pai, L.H. & Pastan, I. Identification of epitopes on a mutant form of Pseudomonas exotoxin using serum from humans treated with Pseudomonas exotoxin containing immunotoxins. *Eur J Immunol* **27**, 1459-68 (1997).
11. Nemazee, D. Receptor selection in B and T lymphocytes. *Annu Rev Immunol* **18**, 19-51 (2000).
12. Brusic, V., Bajic, V.B. & Petrovsky, N. Computational methods for prediction of T-cell epitopes--a framework for modelling, testing, and applications. *Methods* **34**, 436-43 (2004).
13. Walden, P. T-cell epitope determination. *Curr Opin Immunol* **8**, 68-74 (1996).
14. Stickler, M.M., Estell, D.A. & Harding, F.A. CD4+ T-cell epitope determination using unexposed human donor peripheral blood mononuclear cells. *J Immunother* **23**, 654-60 (2000).
15. Warmerdam, P.A. et al. Elimination of a human T-cell region in staphylokinase by T-cell screening and computer modeling. *Thromb Haemost* **87**, 666-73 (2002).
16. Roggen, E.L. Recent developments with B-cell epitope identification for predictive studies. *J Immunotoxicol* **3**, 137-49 (2006).
17. Blythe, M.J. & Flower, D.R. Benchmarking B cell epitope prediction: underperformance of existing methods. *Protein Sci* **14**, 246-8 (2005).
18. Saha, S. & Raghava, G.P. Prediction of continuous B-cell epitopes in an antigen using recurrent neural network. *Proteins* **65**, 40-8 (2006).

19. Feldhaus, M.J. et al. Flow-cytometric isolation of human antibodies from a nonimmune *Saccharomyces cerevisiae* surface display library. *Nat Biotechnol* **21**, 163-70 (2003).
20. Ackerman, M. et al. Highly avid magnetic bead capture: an efficient selection method for de novo protein engineering utilizing yeast surface display. *Biotechnol Prog* **25**, 774-83 (2009).
21. Graff, C.P., Chester, K., Begent, R. & Wittrup, K.D. Directed evolution of an anti-carcinoembryonic antigen scFv with a 4-day monovalent dissociation half-time at 37 degrees C. *Protein Eng Des Sel* **17**, 293-304 (2004).
22. Kreitman, R.J. et al. Cytotoxic activity of disulfide-stabilized recombinant immunotoxin RFB4(dsFv)-PE38 (BL22) toward fresh malignant cells from patients with B-cell leukemias. *Clin Cancer Res* **6**, 1476-87 (2000).
23. Chao, G. et al. Isolating and engineering human antibodies using yeast surface display. *Nat Protoc* **1**, 755-68 (2006).
24. Mishima, K. et al. Growth suppression of intracranial xenografted glioblastomas overexpressing mutant epidermal growth factor receptors by systemic administration of monoclonal antibody (mAb) 806, a novel monoclonal antibody directed to the receptor. *Cancer Res* **61**, 5349-54 (2001).
25. Welt, S. et al. Phase I/II study of iodine 125-labeled monoclonal antibody A33 in patients with advanced colon cancer. *J Clin Oncol* **14**, 1787-97 (1996).
26. Ritter, G. et al. Serological analysis of human anti-human antibody responses in colon cancer patients treated with repeated doses of humanized monoclonal antibody A33. *Cancer Res* **61**, 6851-9 (2001).
27. Welt, S. et al. Phase I study of anticolon cancer humanized antibody A33. *Clin Cancer Res* **9**, 1338-46 (2003).
28. Scott, A.M. et al. A phase I clinical trial with monoclonal antibody ch806 targeting transitional state and mutant epidermal growth factor receptors. *Proc Natl Acad Sci U S A* **104**, 4071-6 (2007).
29. Chester, K.A. et al. Phage libraries for generation of clinically useful antibodies. *Lancet* **343**, 455-6 (1994).
30. Boehm, M.K. et al. Crystal structure of the anti-(carcinoembryonic antigen) single-chain Fv antibody MFE-23 and a model for antigen binding based on intermolecular contacts. *Biochem J* **346 Pt 2**, 519-28 (2000).
31. Molineux, G. Pegylation: engineering improved biopharmaceuticals for oncology. *Pharmacotherapy* **23**, 3S-8S (2003).
32. Salvatore, G., Beers, R., Margulies, I., Kreitman, R.J. & Pastan, I. Improved cytotoxic activity toward cell lines and fresh leukemia cells of a mutant anti-CD22 immunotoxin obtained by antibody phage display. *Clin Cancer Res* **8**, 995-1002 (2002).
33. Onda, M. et al. An immunotoxin with greatly reduced immunogenicity by identification and removal of B cell epitopes. *Proc Natl Acad Sci U S A* **105**, 11311-6 (2008).
34. Schellekens, H. Bioequivalence and the immunogenicity of biopharmaceuticals. *Nat Rev Drug Discov* **1**, 457-62 (2002).



## Chapter 7: *In vitro* protein-protein fusion catalyzed by sortase A

### 7.1 Abstract

Chimeric proteins boast widespread use in areas ranging from cell biology to drug delivery. Post-translational protein fusion using the bacterial transpeptidase sortase A provides an attractive alternative when traditional genetic level fusion fails. We describe optimization of conditions for this *in vitro* protein ligation and report the successful fusion of 10 pairs of protein domains with preserved functionality - demonstrating the robust and facile nature of this reaction.

## 7.2 Background

The ability to incorporate disparate modular domains within multi-functional chimeric proteins has revolutionized both the basic and applied biological sciences. While genetic fusion remains the gold-standard for chimera production, a given pair of protein domains may fail to express in tandem either in reasonable yield, or with proper folding and function—thereby limiting the diversity of domains that can be combined. Fusion protein expression can be particularly difficult when working with recombinant proteins originating from different hosts.

Post-translational protein fusion would allow native expression of the individual fusion partners—permitting expression of each domain in the optimum host, as well as allowing modular pairing and assembly of component domains after expression—effectively circumventing the diversity-limiting cloning steps of tandem genetic fusion. A number of systems for protein-protein fusion have been explored, including native chemical ligation<sup>1</sup>, intein and enzyme based strategies<sup>2,3</sup>, and residue specific chemistries relying on cysteines or unnatural amino acids<sup>4</sup>. Unfortunately, these solutions tend to be technically challenging, residue rather than site specific, or necessitate the inclusion of whole additional protein domains to mediate fusion.

Sortase A is a bacterial transpeptidase that covalently attaches proteins to the bacterial cell wall by cleaving between threonine and glycine at an LPXTG recognition motif to generate an acyl-enzyme intermediate which then reacts with an N-terminal glycine, regenerating a native amide bond<sup>5,6</sup>. This chemistry has been increasingly exploited to site-specifically link proteins displaying the C-terminus LPETG motif to a

range of substituents<sup>7</sup> possessing a triglycine motif, including fluorophores<sup>8,9</sup>, photoaffinity probes<sup>8</sup>, peptide nucleic acids<sup>10</sup>, sugars<sup>11</sup>, polymers<sup>12</sup>, solid supports<sup>12-14</sup>, and lipid-modified oligoglycine peptides<sup>15</sup>. Conjugation of GFP to cell surfaces<sup>9</sup> and to make GFP multimers has been demonstrated under reducing conditions<sup>7,12</sup>. These reports reveal the broad applicability of sortase A catalyzed addition reactions, and motivated this study of its use in producing complex fusion proteins.

We describe here tractable *in vitro* conditions for the site-specific assembly of diverse, multi-functional fusion proteins. Sortassembly requires only 2 short peptide tags: a C-terminal LPETGX<sub>n</sub> tag on one partner, usually incorporated as LPETG-His<sub>6</sub> to facilitate downstream separation, and a complementary N-terminal triglycine (GGG) motif on the other domain (Figure 7.2.1). These domains are small and generally unobtrusive to protein production, yet allow site and stoichiometric control of the fusion reaction. Furthermore, a suite of proteins may be expressed with these tags allowing for modular pairing of diverse domains without additional molecular cloning effort.

## 7.3 Materials and Methods

### Protein Expression and Purification

Sortase-His6 enzyme was expressed essentially as described previously<sup>12</sup>. Briefly, BL21 e. coli (Invitrogen, Carlsbad, CA) transformed with pHTT27 (a gift of Dr. Olaf Schneewind, University of Chicago) were induced with 1 mM IPTG for 4 hours after reaching an OD<sub>600</sub> of 0.4. Sortase was extracted with B-per reagent (Pierce, Rockford, IL) from pelleted cells that had been frozen overnight. The lysate was purified on Talon resin (Clontech, Mountainview, CA), and buffer exchanged into 50 mM Tris, 150 mM NaCl, pH 8 using a 10,000 MW cutoff spin filter (Pierce, Rockford, IL), yielding approximately 100 mg of purified enzyme from a 1 L culture.

A33 antigen extracellular domain bearing a His6 tag (A33-LPETG-His6) and all IgG constructs were produced in HEK293 cells (Invitrogen, Carlsbad, CA) after PEI transfection with gWIZ plasmids (Genlantis, San Diego, CA) according to the manufacturer's instructions. Secreted protein was purified by Protein A chromatography (Pierce, Rockford, IL), or by affinity chromatography using Talon resin (Clontech, Mountainview, CA).

GGG-GFP was produced in BL21 e. coli as described<sup>12</sup>.

GGG-Gelonin, GGG-Fab, and GGG-albumin were kind gifts from Christopher Pirie, Mike Schmidt, and Kelly Davis Orcutt.

## **Reaction Optimization**

The ligation reaction was optimized using A33-LPETG-His6 and GGG-GFP. Briefly, 20  $\mu$ l test reactions were conducted under a variety of conditions. Each reaction consisted of LPETGXn and GGG reactants, sortase A, in storage buffer (50 mM Tris, 150 mM NaCl, pH 8) and 10x reaction buffer (60 mM CaCl<sub>2</sub> in 1x storage buffer). Reactant concentrations ranged from 5 to 50  $\mu$ M, while enzyme concentrations were varied from 50 nM to 250  $\mu$ M. The gradient function of a thermocycler was used to vary reaction temperature, and reaction time was varied by removing aliquots of a large reaction mix at set intervals, chilling to 4°C, and adding EDTA to a final concentration of 10 mM to stop the reaction. The resulting samples were analyzed by running at 200 V on 12% bis-tris or Tris-acetate gels (Invitrogen, Carlsbad, CA) according the manufacturer's protocol after the addition of 4x sample dye and 10x reducing agent (Invitrogen, Carlsbad, CA), as appropriate, before being boiled for 10 min. The fusion product, approximate MW 70 kDa, was visualized after staining with Simply Blue Safestain (Invitrogen, Carlsbad, CA).

## **Fusion Pair Tests**

A33-LPETG-His6 and IgG-LC-LPETGGS at micromolar concentrations were reacted with each of the following: GGG-GFP, GGG-Fab, GGG-IgG, GGG-gelonin, and GGG-albumin (also at micromolar concentrations). Reactions were allowed to proceed for 2 hours at 37°C after addition of 10x reaction buffer and 100 nM sortase enzyme.

## **Western Blotting**

For western blots, gels were transferred onto nitrocellulose at 50 V in Invitrogen transfer buffer and blocked in 5% milk in phosphate buffered saline with 0.1% Tween-20. An anti-human light chain-HRP conjugate (AbD Serotec, Raleigh, NC) was used to detect the light chain in the IgG-LC-LPETG fusions, and a murine anti-human A33 antigen (gift of Gerd Ritter, Ludwig Institute, New York) and goat anti-mouse-HRP (Sigma, St. Louis, MO) were used to detect A33 antigen before and after sortase reaction in order to quantify the reaction yield. Bands were detected using ECL reagents (Pierce, Rockford, IL), and where appropriate, quantified using ImageJ (NIH, Bethesda, MD).

## **Functional Testing**

For functional tests of A33-IgG fused to GFP, 1  $\mu$ l of biotin binder magnetic beads (Dyna, Invitrogen, Carlsbad, CA) was washed twice in phosphate buffered saline, 0.1% bovine serum albumin (PBSA), and incubated with 250  $\mu$ l of 850 nM biotinylated A33 antigen (biotinylation reagent, Pierce, Rockford, IL) in PBSA at 4°C overnight on a rotator. After beads were washed twice in PBSA to remove free antigen, 10  $\mu$ l of A33-IgG-GFP sortase reaction mixture was added to the A33-antigen coated beads. The reaction mix and beads were incubated overnight at 4°C on a rotator, then washed twice before being analyzed for GFP signal by flow cytometry on a coulter counter epicsXL (Beckman Coulter, Fullerton, CA). Bare beads and a mock reaction mix excluding sortase were run as negative controls, and the binding of A33-IgG-GFP was specifically competed using an excess of soluble A33-IgG. Because both A33-IgG and GFP are

conformationally sensitive, these tests demonstrate function and proper folding of both domains.

The functional tests of CEA IgG fused to A33 antigen, a similar protocol was followed utilizing biotinylated CEA (antibody, Fitzgerald Industries, Concord, MA; biotinylation, Pierce, Rockford, IL) to coat beads, and an Alexa-488 labeled anti-A33 IgG (antibody gift of Gerd Ritter, Ludwig Institute, New York; Alexa labeling, Molecular Probes, Invitrogen, Carlsbad, CA) to detect A33 antigen. Binding of fusion product was specifically competed using an excess of soluble CEA-IgG.

### Example Purification

The A33-GFP fusion was separated from unreacted A33-LPETG-His6 and sortase enzyme by purification on Talon resin according to the manufacturer's protocol, and various fractions were subjected to SDS-PAGE analysis and western blotting as previously described.

### Sequences of LPETGX<sub>n</sub> and GGG-containing Proteins

A33-LPETG-His6  
 ISVETPQDVLRASQGKSVTLPTCYHTSTSSREGLIQWDKLLLTHTERVVIWPFNSKNYIHGELYKNR  
 VSISNNAEQSDASITIDQLTMADNGTYECSVSLMSDLEGNTKSRVRLLVLPVPPSKPECGIEGETIIGN  
 NIQLTCQSKEGSPTPQYSWKRYNILNQEQLAQPASGQPVSLKNISTDTSGYYICTSSNEEGTQFCNI  
 TVAVRSPSMNGGGGSGGGGSLPETGGSGHHHHH

Anti-A33	IgG	LC	LPETG	—
SELQMTQSPSSLSASVGDRTITCLASEFLFNGVSWYQQKPGKVPKFLIYGASNLESGVPSRFSGSG				
SGTDFTLTISSLQPEDVATYYCLGGYSGSSGLTFGGGKVEIKRTVAAPSVFIFPPSDEQLKSGTASV				
VCLLNIFYPREAKVQWKVDNALQSGNSQESVTEQDSKDYSLSTLTLTKADYEEKHKVYACEV				
THQGLSSPVTKSFNRGECGGGGSGGGGSLPETGGSG				

Anti-A33	IgG	HC	—
EVQVMESGGGLVKPGGSLRLSCAASGIGFSHYGISWVRQAPGKGLEWVAYITPNYGSVDYASSV			
NGRFTISLDNAQNSLYLQMNSLRAEDTAVYFCARDRGYYSGSRGTRLDLWGQGLTVTVSSASTK			
GPSVFPLAPSSKSTSGGTAALGCLVKDYFPEPVTVSWNSGALTSGVHTFPAVLQSSGLYSLSSVVT			
VPSSSLGTQTYICNVNHKPSNTKVDKKEPKSCDKTHTCPPCPAPELGGPSVFLFPPKPKDTLMIS			
RTPEVTCVVVDVSHEDPEVKFNWYVDGVEVHNAKTKPREEQYNSTYRVVSVLTVLHQDWLNGK			

EYKCKVSNKALPAPIEKTISKAKGQPREPQVYTLPPSRDELTKNQVSLTCLVKGFYPSDIAVEWES  
NGQPENNYKTPPVLDSDGSFFLYSKLTVDKSRWQQGNVFCFSVMHEALHNHYTQKSLSLSPGK

GGG-GFP

GGGLNDIFEAQKIEWHEMVSKGEELFTGVVPILVELDGDVNGHKFSVSGEGEGDATYGKLTCLKFI  
CTTGKLPVPWPTLVTTLTYGVQCFSRYPDHMKQHDFFKSAMPEGYVQERTIFFKDDGNYKTRAE  
VKFEGDTLVNRIELKGIDFKEDGNILGHKLEYNYNSHNVYIMADKQKNGIKVNFKIRHNIEDGSVQ  
LADHYQQNTPIGDGPVLLPDNHYLSTQSALS KDPNEKRDMVLEFVTAAGITLGMDELYKLEHH  
HHHH

Anti-CEA

GGG-IgG

LC

GGGGGSENVLTQSPSSMSVSVGDRVTIACSASSVPYMHWLQKPKGKSPKLLIYLTSLNLASGVPS  
RFGSGSGTDYSLTISSVQPEDAATYYCQQRSSYPLTFGCGTKLEIKATVAAPSVFIFPPSDEQLKSG  
TASVVCLLNNFYPREAKVQWKVDNALQSGNSQESVTEQDSKDYSLSSLTLSKADYEKHKVY  
ACEVTHQGLSSPVTKSFNRGEC

Anti-CEA

GGG-IgG

HC

GGGGGSQVKLEQSGAEVVKPGASVKLSCKASGFNIKDSYMHWLRQGPQCLEWIGWIDPENGD  
TEYAPKFKQKATFTTDSANTAYLGLSSLRPEDTAVYYCNEGTPTPYFDYWGQGLTVTVSSPS  
TKGPSVFPLAPSSKSTSGGTAALGCLVKDYFPEPVTVSWNSGALTSGVHTFPAVLQSSGLYSLSSV  
VTVPSSSLGTQTYICNVNHKPSNTKVDKKVEPKSCDKTHTCPPCPAPELLGGPSVFLFPPKPKDTL  
MISRTPEVTCVVDVSHEDPEVKFNWYVDGVEVHNAKTKPREEQYNSTYRVVSVLTVLHQDWL  
NGKEYKCKVSNKALPAPIEKTISKAKGQPREPQVYTLPPSRDELTKNQVSLTCLVKGFYPSDIAVE  
WESNGQPENNYKTPPVLDSDGSFFLYSKLTVDKSRWQQGNVFCFSVMHEALHNHYTQKSLSLSP  
GK

Anti-CEA

GGG-Fab

LC

GGGGGSENVLTQSPSSMSVSVGDRVTIACSASSVPYMHWLQKPKGKSPKLLIYLTSLNLASGVPS  
RFGSGSGTDYSLTISSVQPEDAATYYCQQRSSYPLTFGCGTKLEIKATVAAPSVFIFPPSDEQLKSG  
TASVVCLLNNFYPREAKVQWKVDNALQSGNSQESVTEQDSKDYSLSSLTLSKADYEKHKVY  
ACEVTHQGLSSPVTKSFNRGEGSHHHHHH

Anti-CEA

GGG-Fab

HC

GGGGGSQVKLEQSGAEVVKPGASVKLSCKASGFNIKDSYMHWLRQGPQCLEWIGWIDPENGD  
TEYAPKFKQKATFTTDSANTAYLGLSSLRPEDTAVYYCNEGTPTPYFDYWGQGLTVTVSAGT  
KGPSVFPLAPSSKSTSGGTAALGCLVKDYFPEPVTVSWNSGALTSGVHTFPAVLQSSGLYSLSSVV  
VTVPSSSLGTQTYICNVNHKPSNTKVDKKVEPKSNASGWSHPQFEK

GGG-gelonin

GGGISEFGSSRVLDLQGLDTSFSTKGATYITYVNFNLNLRVVKLKEGNSHGIPLLRKKCDDPGKCF  
VLVALSNDNGQLAEIAIDVTSVYVVGYYQVRNRSYFFKDAPDAAEGLFKNTIKTRLHFGGSYPSLE  
GEKAYRETTDLGIEPLRIGIKLDENAIIDNYKPTIEASSLLVVIQMVSEAAARFTFIENQIRNRFQRRR  
PANNTISLENKWGKLSFQIRTSGANGMFSEAVELERANGKYYVTAVDQVKPKIALLKVFVDK  
DPKAS

GGG-albumin

GGGGGSDAHKSEVAHRFKDLGEENFKALVLIIFAQYLQCPFEDHVKL VNEVTEFAKTCVADES  
AENCDKSLHTLFGDKLCTVATLRETYGEMADCCAQEPERNECFLQHKDDNPNL PRLVRPEVDV  
MCTAFHDNEETFLLKYLIEIARRHPYFYAPELFFAKRYKAAFTECCQAADKAAACLLPKLDEL RD  
EGKASSAKQRLK CASLQKFGERAFKAWAVARLSQRFPKAEFAEVSKLVDTLTKVHTECCHGDL L  
ECADDRDLAKYICENQDSISSKLEKCEKPLEKSHCIAEVENDEMPADLPSLAADFVESKDVCK  
NYAEAKDVFLGFLYIEYARRHPDYSVVLRLAKTYETTLKCCAAADPHECYAKVFDEFKPLV  
EEPQNLIKQNCLEFELGEYKFNALLVRYTKKVPQVSTPTLVEVSRNLGKVGSKCCKHPEAKRM  
PCAEDYLSVVLNQLCVLHEKTPVSDRVTKCTTESLVNRRPCFSALEVDETYVPKEFNAETFTFHAD  
ICTLSEKERQIKKQTALVELVKHKPKATKEQLKAVMDDFAAFVEKCKADDKETCF AEEGKKLV  
AASQAALGL

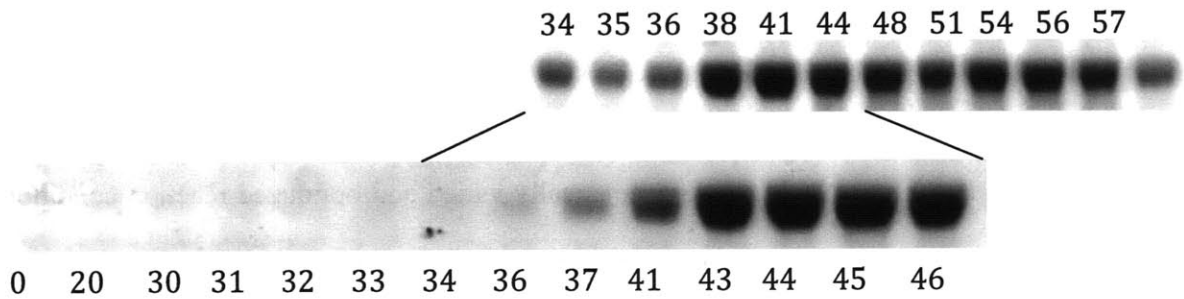


## 7.4 Results

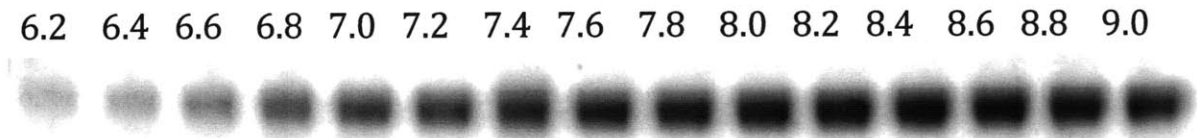
### 7.4.1 and 7.4.2: Sortassembly reaction and optimization.

The reaction is typically carried out in pH 8.2 buffered Tris containing 6 mM  $\text{CaCl}_2$  and 150 mM NaCl. We systematically varied and optimized reaction conditions using A33 antigen as a model LPETG-containing substrate and triglycine-GFP as its fusion partner. This optimization was done in reaction volumes as low as 20  $\mu\text{l}$  before determination of ideal conditions to be used in large scale reactions. Overall, the reaction was robust and there was good fusion product yield under a broad range of conditions, permitting the stability and sensitivities of the proteins being ligated to determine reaction conditions rather than a narrow catalytic window. Briefly, ligation product was maximal under slightly alkaline conditions with high substrate concentrations in a reaction at 42°C for 1-4 hours with dilute sortase A. Perhaps surprisingly, as sortase A natively functions at 37°C, higher temperatures can produce a greater yield of fusion product (Figure 7.4.1a), and are recommended as long as the proteins being fused are not thermolabile. For proteins with pH sensitive conformations, the pH of the reaction may be varied between 7.0 and 9.0 while maintaining high yields (Figure 7.4.1b). High concentrations of reactants ought to be used (Figure 7.4.1c) and the reaction may be pushed toward completion by adding an excess of either fusion partner (Figure 7.4.2b). At a 1:1 molar ratio of reactants, typical fusion protein yields range from 40-75% of the maximum theoretical yield, while with a 20-fold excess of one reactant, the reaction can proceed to approximately 85% yield (Figure 7.4.2 c,d).

**Figure 7.4.1 Optimization of sortassembly reaction conditions (a)** Yield of fusion product at different reaction temperatures. Optimal temperature is between 37 and 46°C.



**(b)** Yield of fusion product at different reaction pH values.



**(c)** Yield of fusion product in reactions with 55 uM total reactants at differing ratios of A33-LPETGXn and GGG-GFP. High concentrations of each reactant leads to higher yield of fusion product.

reactants (uM)	55	55	55	55	55	55	55
GGG-GFP	1	1	1	1	2	5	10
A33-LPETGX	10	5	2	1	1	1	1
Fused A33-GFP							

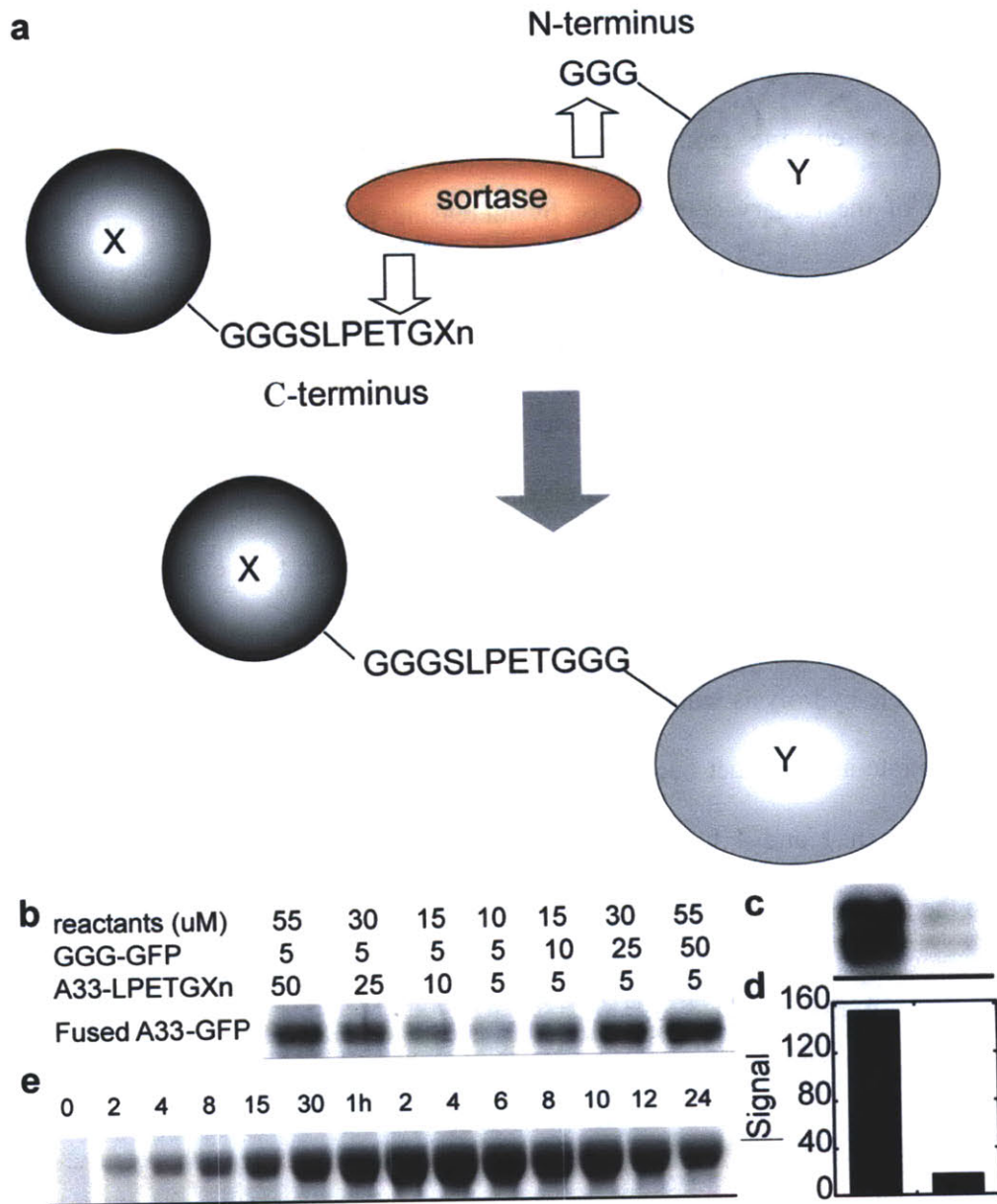


**Figure 7.4.2: Sortase-mediated reaction and optimization.** (a) Schematic illustration of sortase A mediated reaction fusing two proteins. (b) Gel of fusion product demonstrating that excess of either reactant pushes reaction toward completion. Western blot (c) and quantification (d) showing amount of unreacted LPETGXn substrate before (left) and after (right) reaction. (e) Coomassie gel of fusion product at various reaction times.

### 7.4.3 Optimization of sortase concentration

Care must be taken, however, in tailoring the concentration of sortase enzyme, as adding excess enzyme reduces the amount of fusion product either by inhibiting formation of the ternary complex, or by increasing the overall rate of an irreversible hydrolysis reaction of the LPETG motif, which releases LPET as a terminal product. For equimolar fusion partners, a 0.1 molar equivalent of enzyme gave optimal fusion product yield (Figure 7.4.3a)—though this fraction changes as the ratio of reactants is varied (Figure 7.4.3b). Similarly, this hydrolysis reaction impacts the time allowed for the reaction to proceed. Because the LPETG motif is present in the desired fusion product, the enzyme will continue to react with fusion product, and over extended periods of time the irreversible hydrolysis reaction will outweigh any marginal increases in product yield as all substrate and product becomes hydrolyzed. Experimentally, the optimal reaction time is between 1 and 4 hours (Figure 7.4.2e), after which EDTA may be added to quench the reaction.

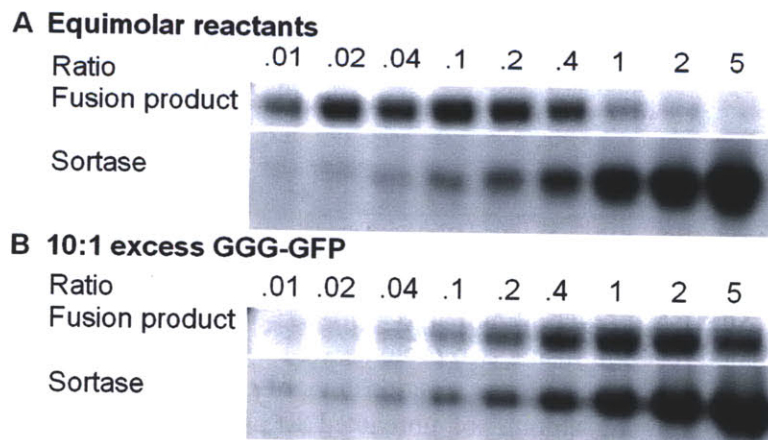


**Figure 7.4.3 Optimization of enzyme quantities:** The ratio of sortase enzyme to total reactants (25  $\mu$ M) was varied under conditions with equimolar A33-LPETGXn and GGG-GFP (**a**), and with a 10-fold excess of GGG-GFP (**b**) in order to identify conditions with maximal fusion product yield.

#### 7.4.4 Separation of product and reactants

For separation of product from reactants and enzyme, a His<sub>6</sub> tag can be incorporated both after the LPETG motif and on the sortase enzyme, allowing unreacted substrate and enzyme to be removed simply by passing over an affinity column (Figure 7.4.4). Product may then be separated from the tri-glycine reactant by methods such as size exclusion or ion exchange chromatography or through the inclusion of a second tag on the LPETG reagent. In optimized reactions we have been able to achieve 85% yields of fusion protein, with reagents and enzyme undetectable after downstream separations.

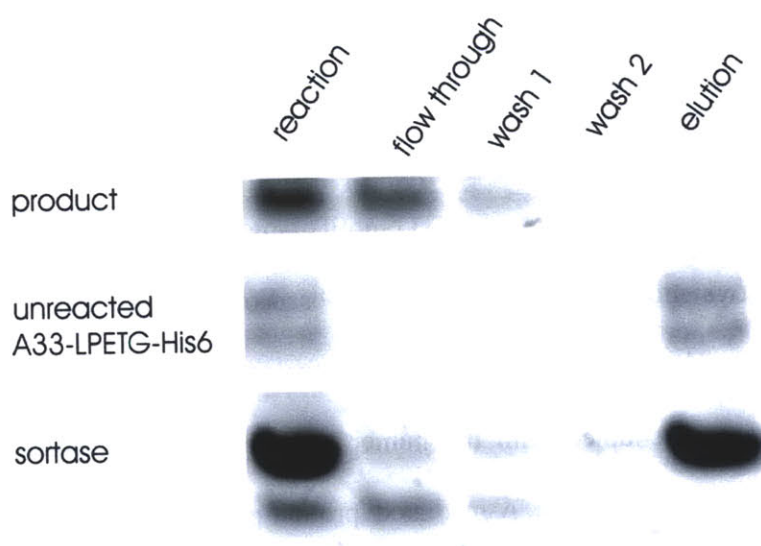


**Figure 7.4.4:** Example purification step demonstrating efficient removal of sortase enzyme and unreacted A33-LPETG-His6 from a reaction mixture following affinity chromatography.

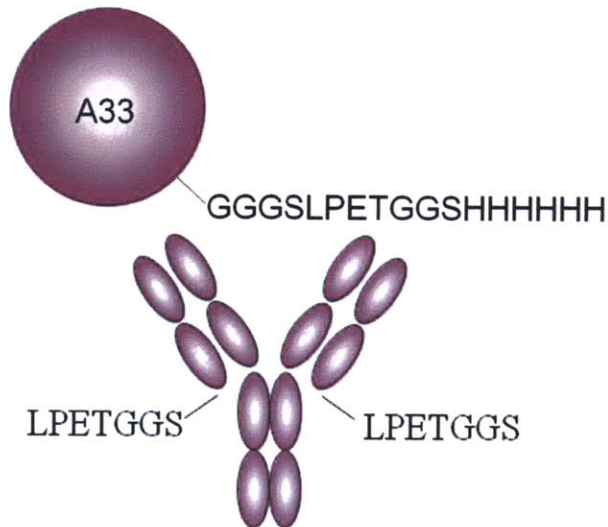
#### **7.4.5 and 7.4.6 Structures of sortassembled domains, reactions, and functional testing**

To assess the diversity of pairings that could be produced through sortase-catalyzed fusion reactions, we generated GGG- and LPETGX<sub>n</sub> derivatives of a variety of representative modular domains, including enzymes (gelonin), antibodies (IgG, Fab), fluorescent protein (GFP), and cell surface and blood proteins (A33 antigen and albumin) (Figure 7.4.5), produced in a range of hosts, including *e.coli*, yeast, and mammalian cells. All reactions yielded fusion proteins of the appropriate molecular weight with yields ranging from approximately 30-85%. (Figure 7.4.6a,b) Particularly important was the successful ligation of whole antibodies without disruption of the associations between their heavy and light chains or constant domains, and the fusion of multiple triglycine reactants to substrates with multiple LPETG motifs—most notably the fusion of 3 whole IgG to form a covalently bonded molecule composed of 12 individual protein domains (Figure 7.4.6a,c). These results demonstrate the fusion of complex disulfide stabilized protein domains, and coupled with the numerous pairings tested, greatly expand the practical applicability of sortase A-mediated protein-protein fusion from the original method carried out under reducing conditions and reported by Mao et al<sup>7</sup>.

## LPETGXn Proteins

A33-LPETG-His6

IgG-LC-LPETG-GS



## Triglycine (GGG-X) Proteins

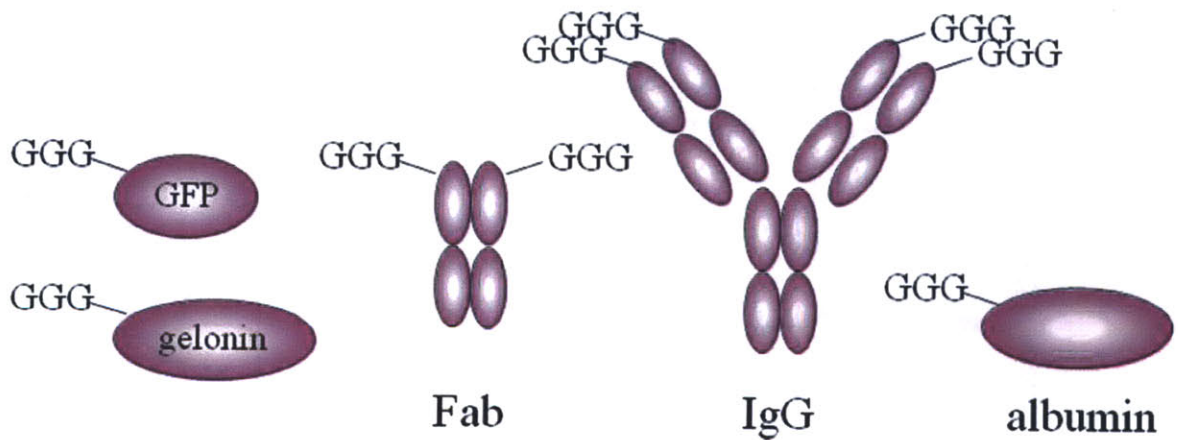


**Figure 7.4.5: Structures of constructs used for fusion tests**

To demonstrate the preserved function of sortase-assembled fusion proteins, magnetic beads were coated with antigen and then incubated with reaction mixtures containing IgG-based fusion proteins: A33 IgG fused to GFP, and CEA IgG fused to A33

antigen. The protein fused to the IgG was then detected by flow cytometry either directly due to inherent fluorescence (detection of GFP), or by incubation with a conformation-specific antibody-fluorophore conjugate (detection of A33 antigen). In both cases, high signal intensity was observed, and signal was decreased in the presence of specific competitor (Figure 7.4.6d,e), indicating that the conformation and functionality of both fusion partners remained intact following sortassembly.

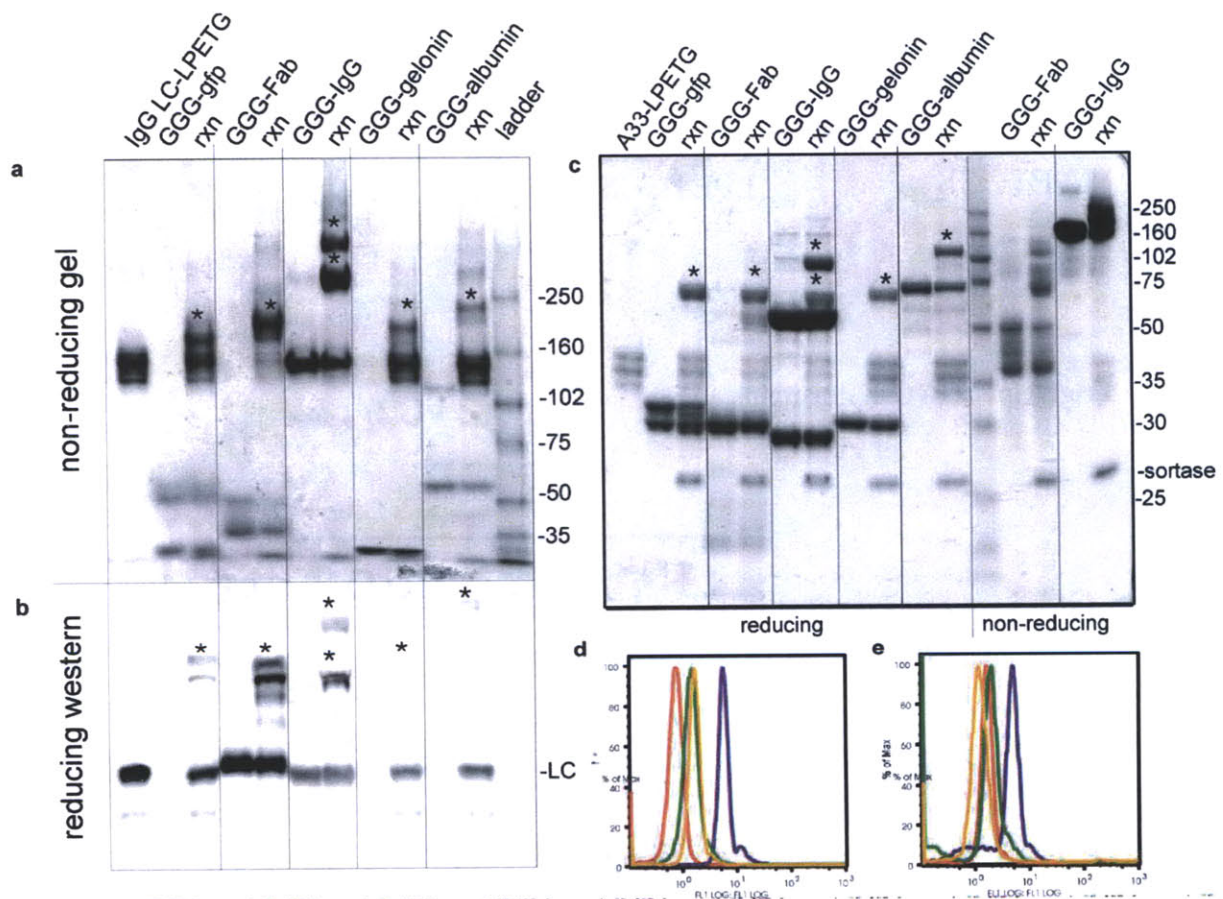


**Figure 7.4.6: Sortassembled products and functional testing.** Nonreduced gel (a) and reduced western blot (b) demonstrating the shift in molecular weight of an IgG light chain-LPETGXn following fusion with 5 different triglycine partners. (c) Gel demonstrating shift of A33 antigen-LPETGXn following fusion with 5 different triglycine partners. Fusion products are marked with an asterisk. (d,e) Functional tests of A33 IgG fused to GFP (d), and CEA IgG fused to A33 antigen (e). Blue trace represents reaction mix, remaining traces represent bare beads, reaction mix without sortase enzyme, and reaction mix with competitor IgG.



## 7.5 Discussion

Post-translational protein fusion allows native expression of the individual fusion partners—permitting expression of each domain in the optimum host, as well as allowing modular pairing and assembly of component domains after expression—effectively circumventing the diversity-limiting cloning steps of tandem genetic fusion. Alternative solutions, including native chemical ligation<sup>1</sup>, intein and enzyme based strategies<sup>2,3</sup>, and residue specific chemistries relying on cysteines or unnatural amino acids<sup>4</sup> tend to be technically challenging, residue rather than site specific, or necessitate the inclusion of whole additional protein domains to mediate fusion.

Previous reports reveal the broad applicability of sortase A catalyzed addition reactions, and motivated this study of its use in producing complex fusion proteins. We have described tractable *in vitro* conditions for the site-specific assembly of diverse, multi-functional fusion proteins, requiring only 2 short peptide tags: a C-terminal LPETGX<sub>n</sub> tag on one partner, and a complementary N-terminal triglycine (GGG) motif on the other domain. These domains are small and generally unobtrusive to protein production, yet allow site and stoichiometric control of the fusion reaction. Furthermore, a suite of proteins may be expressed with these tags allowing for modular pairing of diverse domains without additional molecular cloning effort, after being expressed a single time.

By decoupling protein expression and fusion, and allowing native amide bonds to be formed through inclusion of short peptide tags with site and stoichiometric control, sortassembly promises to increase the diversity and ease of producing fusion proteins.

## 7.6 Works Cited

1. Dawson, P.E. & Kent, S.B. Synthesis of native proteins by chemical ligation. *Annu Rev Biochem* **69**, 923-60 (2000).
2. Blaschke, U.K., Silberstein, J. & Muir, T.W. Protein engineering by expressed protein ligation. *Methods Enzymol* **328**, 478-96 (2000).
3. Jackson, D.Y. et al. A designed peptide ligase for total synthesis of ribonuclease A with unnatural catalytic residues. *Science* **266**, 243-7 (1994).
4. Ayers, B. et al. Introduction of unnatural amino acids into proteins using expressed protein ligation. *Biopolymers* **51**, 343-54 (1999).
5. Bentley, M.L., Lamb, E.C. & McCafferty, D.G. Mutagenesis studies of substrate recognition and catalysis in the sortase A transpeptidase from *Staphylococcus aureus*. *J Biol Chem* **283**, 14762-71 (2008).
6. Mazmanian, S.K., Liu, G., Ton-That, H. & Schneewind, O. *Staphylococcus aureus* sortase, an enzyme that anchors surface proteins to the cell wall. *Science* **285**, 760-3 (1999).
7. Mao, H., Hart, S.A., Schink, A. & Pollok, B.A. Sortase-mediated protein ligation: a new method for protein engineering. *J Am Chem Soc* **126**, 2670-1 (2004).
8. Popp, M.W., Antos, J.M., Grotenbreg, G.M., Spooner, E. & Ploegh, H.L. Sortagging: a versatile method for protein labeling. *Nat Chem Biol* **3**, 707-8 (2007).
9. Tanaka, T., Yamamoto, T., Tsukiji, S. & Nagamune, T. Site-specific protein modification on living cells catalyzed by Sortase. *Chembiochem* **9**, 802-7 (2008).
10. Pritz, S. et al. Synthesis of biologically active peptide nucleic acid-peptide conjugates by sortase-mediated ligation. *J Org Chem* **72**, 3909-12 (2007).
11. Samantaray, S., Marathe, U., Dasgupta, S., Nandicoori, V.K. & Roy, R.P. Peptide-sugar ligation catalyzed by transpeptidase sortase: a facile approach to neoglycoconjugate synthesis. *J Am Chem Soc* **130**, 2132-3 (2008).
12. Parthasarathy, R., Subramanian, S. & Boder, E.T. Sortase A as a novel molecular "stapler" for sequence-specific protein conjugation. *Bioconjug Chem* **18**, 469-76 (2007).
13. Chan, L. et al. Covalent attachment of proteins to solid supports and surfaces via Sortase-mediated ligation. *PLoS ONE* **2**, e1164 (2007).
14. Clow, F., Fraser, J.D. & Proft, T. Immobilization of proteins to biacore sensor chips using *Staphylococcus aureus* sortase A. *Biotechnol Lett* **30**, 1603-7 (2008).
15. Antos, J.M., Miller, G.M., Grotenbreg, G.M. & Ploegh, H.L. Lipid Modification of Proteins through Sortase-Catalyzed Transpeptidation. *J Am Chem Soc* **130**, 16338-43 (2008).

Margaret Pawlowski Ackerman

9 Fairfax St #1, Dorchester, MA 02124  
mack7@mit.edu

---

Education	<b>Massachusetts Institute of Technology</b> Ph.D. Candidate, Department of Biology Thesis research conducted in Wittrup Lab, Departments of Chemical and Biological Engineering	Cambridge, MA, 2004-present
	<b>Brandeis University</b> MS in Biochemistry BS in Chemistry, BS in Biochemistry Conferred <i>summa cum laude</i>	Waltham, MA, 1999-2003
Research Experience	<b>Massachusetts Institute of Technology</b> Advisor: K. Dane Wittrup •Thesis: Immunotherapy of Cancer – Targeting the Tight Junction	Cambridge, MA, 2004-present
	<b>Brandeis University</b> Advisor: Chan Fulton •Thesis: The Role of the Pentose Phosphate Pathway in Thiamin Depletion-Induced Apoptosis Determined effect of redox state on thiamin-depletion induced apoptosis using assays to monitor apoptosis and measurements of reduced and oxidized molecules.	Waltham, MA, 1999-2003
	<b>Dartmouth Medical School</b> Advisor: Alexandra Howell Developing protocols to purify HIV-related proteins for use in vaccine development	Hanover, NH, Summer 2000
Teaching Experience	<b>College of Charleston</b> <u>Department of Chemistry</u> , Adjunct Instructor Taught general and organic chemistry lab lecture and lab to both chemistry major and non-majors, emphasizing quantitative thinking and problem solving.	Charleston, SC, 2003-2004
	<b>Trident Technical College</b> <u>Department of Chemistry</u> , Adjunct Instructor Taught general chemistry lecture as well as general chemistry lab and lab lecture	Charleston, SC, 2004
	<b>Massachusetts Institute of Technology</b> •Teaching Assistant, Introductory Biology, 7.012 •Teaching Assistant, Principles of Human Disease, 7.27	Fall 2005 Spring 2008
Advising Experience	<b>Massachusetts Institute of Technology</b> •Supervised and trained high school (through the Research Science Institute-RSI program), undergraduate, and post-BS students in work leading to publication and numerous awards in international and national science competitions.	Cambridge, MA, 2004-present
	Priyanka Jain      ChemE, MIT <i>Fibronectin Engineering</i> Lucy Lin          ChemE, MIT <i>Antibody Fragment Engineering</i> Greg Johnson    ChemE, MIT <i>Fibronectin Engineering</i> Gabriel Tobon    MechE, MIT <i>De Novo Engineering Selection Methods</i> Emmanuel Quiroz    Biological Eng, MIT <i>Bispecific Antibody Construction</i> Jennifer Lai      Biology, MIT <i>Immunogenicity Prediction</i>	

---

David Levary	RSI; Physics, Harvard	<i>De Novo Engineering Selection Methods</i>
Ananth Ram	RSI	<i>Matlab Modeling of Immunotherapy</i>
Vivek Raman	RSI	<i>Turnover of A33 Antigen</i>
Jenny Sul	RSI	<i>In vitro protein fusion</i>
Nisarg Shah	ChemE, BE, Johns Hopkins	<i>Therapeutic Protein Engineering</i>

---

Honors and Scholarships	Goldwater Scholar	Howard Hughes Summer Fellowship
	Schiff Fellowship	Phi Beta Kappa
	Richter Fellowship	Justice Brandeis Scholar
	Nathan O. Kaplan Prize in Biochemistry	Pfizer Summer Fellowship
	MIT-Portugal Fellow	

---

- Presentations**
- Ackerman, M.** and Wittrup, K. D., "A33 Antigen Displays Persistent Surface Expression" Conference on Cancer Therapy with Antibodies and Immunoconjugates, Parsippany, NJ, Oct 2006.
- Ackerman, M** and Wittrup, K. D., "A33 Antigen Displays Persistent Surface Expression, a Desirable Property for Immunotherapeutic Targeting" Keystone Symposia, Antibodies as Drugs, Lake Louise, AB, Feb 2007 (poster).
- Ackerman, M** and Wittrup, K. D., "Effect of Antigen Turnover Rate and Expression Level on Antibody Penetration into Tumor Spheroids" IBC Antibody Engineering, San Diego, CA, Dec 2007 (poster).
- Ackerman, M.,** Levary, D., and Wittrup, K. D., "A Highly Efficient Selection Method for de novo Protein Engineering" American Chemical Society, Philadelphia, PA, Aug 2008 (poster).
- Ackerman, M.,** Levary, D., and Wittrup, K. D., "Sortassembly: sortase A catalyzed in vitro assembly of fusion proteins" American Institute of Chemical Engineers, Society for Biological Engineering, International Conference on Biological Engineering, Santa Barbara, CA, Jan 2009 (poster).

- 
- Publications**
- Ackerman ME,** Chalouni C, Schmidt MM, Raman VV, Ritter G, Old LJ, Mellman I, Wittrup KD. "A33 Antigen Displays Persistent Surface Expression" *Cancer Immunol Immunother* (2008) 57:1017-1027.
- Ackerman ME,** Pawlowski DJ, Wittrup KD, "Effect of Antigen Turnover Rate and Expression Level on Antibody Penetration into Tumor Spheroids" *Mol Cancer Ther* (2008) 7(7):2233-40.
- Ackerman ME,** Levary D, Tobon G, Hackel BJ, Orcutt KD, Wittrup KD, "Highly avid magnetic bead capture: an efficient selection method for *de novo* protein engineering utilizing yeast surface display" *Biotech Prog* (accepted)